Apatite (U-Th-Sm)/He thermochronology of the Eastern Arctic Rim: Evolution of the north-central Baffin Island rifted margin.

Sean Yaehne

Submitted in Partial Fulfilment of the Requirements
for the Degree of Bachelor of Science, Honours
Department of Earth Sciences
Dalhousie University, Halifax, Nova Scotia
March 11, 2008

DALHOUSIE UNIVERSITY
Inspiring Minds

Department of Earth Sciences
Halifax, Nova Scotia
Canada B3H 4J1
(902) 494-2358
FAX (902) 494-6889

DATE: April 24, 2008

AUTHOR: Sean Yaehne

TITLE: Apatite (U-Th-Sm)/He thermochronology of the Eastern Arctic Rim: Evolution of the north-central Baffin Island rifted margin

Degree: B.Sc. Honors Convocation: May Year: 2008

Permission is herewith granted to Dalhousie University to circulate and to have copied for non-commercial purposes, at its discretion, the above title upon the request of individuals or institutions.

Signature of Author

ABSTRACT

Along the eastern margins of Labrador and Baffin, Devon, and Ellesmere Islands an extensive highland surface (1300-2000m) divides a narrow, coastal lowland from a series of upland plateau and lowland surfaces that decline in elevation as well as relief to the west. This extensive linear feature is known as the Eastern Arctic Rim and its geomorphologic similarity to other high elevation passive margins suggests that it formed as a result of rifting of Greenland from the North American Craton. This study presents (U-Th-Sm)/He thermochronologic data from north-central Baffin Island to supplement already existing geologic, geophysical and geomorphic interpretation in order to evaluated the evolution of the passive margin since late Cretaceous rift flank uplift altered the islands topographic character.

Interpretations from two sampling transects are presented from the north-central Baffin Island region, (i) a vertical transect within the Davis Highlands, and (ii) an isolated elevation horizontal transect oriented SW-NE perpendicular to the rifted margin.

On the horizontal transect, a systematic trend is observed with the youngest He ages occurring in a narrow region adjacent to the Baffin Bay margin (~200 Ma), oldest ages in the high elevation Davis Highlands and Baffin Uplands (300 – 350 Ma), and moderately young ages occurring in the west near the Foxe Basin (~250 Ma). This pattern of He ages indicates that the margin has been evolving in a manner closely resembling the pinned divide model described by Gallagher et al., (1998). There is also some evidence that the rift scarp is retreating, following Gallagher et al.'s (1998) other end member model, but down wearing of the elevated margin appears to be the dominant exhumation force. This evidence of the pinned divide model supports the notion that the Baffin Island crustal block has been tilted westwards and that the uplifted margin formed as a result of rift flank uplift.

From the vertical transect a late Paleozoic period of accelerated cooling is observed, but uplift that affected the margin during the late Cretaceous is buried well below sea level. This indicates that the region has been undergoing significantly low exhumation rates, and therefore the exact timing and cause of flank uplift can not be determined.

TABLE OF CONTENTS

APPENDICES

TABLE OF FIGURES

TABLE OF TABLES

Table

Acknowledgements

I would like to express my sincerest gratitude to everyone that helped me out through out this project. First of all I would like to thank my supervisor, Dr. John Gosse for his enthusiasm, support, as well as criticism of my work on this project. Without John this thesis would not be possible. I would like to thank Canada Nunavut Geoscience Office and Geological Survey of Canada for their part in collecting the north-central Baffin Island samples. I would also like to thank everyone from the Dalhousie Geochronology Center namely Jose Luis Antinao, Keith Taylor, Guang Yang, and Debra Wheeler for their help in dating the samples, as well as Daniel Stockli from the University of Kansas for his U-Th-Sm work. Last but definitely not least I would like to thank Daniel Utting and Mike Young for their suggestions and guidance in the interpretation of the data.

1 INTRODUCTION

1.1 Introduction

Baffin Island makes up the southeast portion of the Canadian Arctic Archipelago. Ellesmere, Devon, and Baffin Islands as well as Labrador are separated from Greenland by Baffin Bay and Labrador Sea rifted basins which are believed to have been initiated in the late Mesozoic –Paleogene (Fig 1.1; Balkwill et al., 1990). Topography along Canada's eastern margin bordering these basins is a highly elevated (1500 – 2100 m) mountain range that can be traced over 1250 km (Bird, 1967). This linear feature is referred to as the Eastern Arctic Rim and it extends from Torngat Mountains of Labrador, north to Ellesmere Island. Along this discontinuous range a generally asymmetric topographic profile perpendicular to the margin reveals coastal lowlands and interior elevated plateau surfaces divided by highlands with a relief >1500 m (Fig. 1.1). Such topography can be observed in many elevated passive margins worldwide that have formed as a result of rift flank uplift (Southeast Australia, Persano et al., 2002; Southwestern Africa, Brown et al., 2000; Eastern United States of America, Spotila et al., 2004; northern Labrador, Centeno, 2005).

Elevated passive margins form in response to the temporary increase in thermal activity associated with rifting, as well as more static forces such as isostasy in response and crustal underplating of volcanic material in extensional environments. Erosion in a basinward direction results in isostatic compensation that ensures a long life span of uplifted rift margins. As extension is facilitated by normal faulting, uplift results in the exposure of the scarp face or escarpment. Many studies have been focused on rift flank margins in order to better understand the sequence of events that is involved in continental extension and basin

formation, as well as the evolution of these features in response to denudation (Persano et al., 2002; Brown et al., 2000; Spotila et al., 2004; Centeno, 2005).

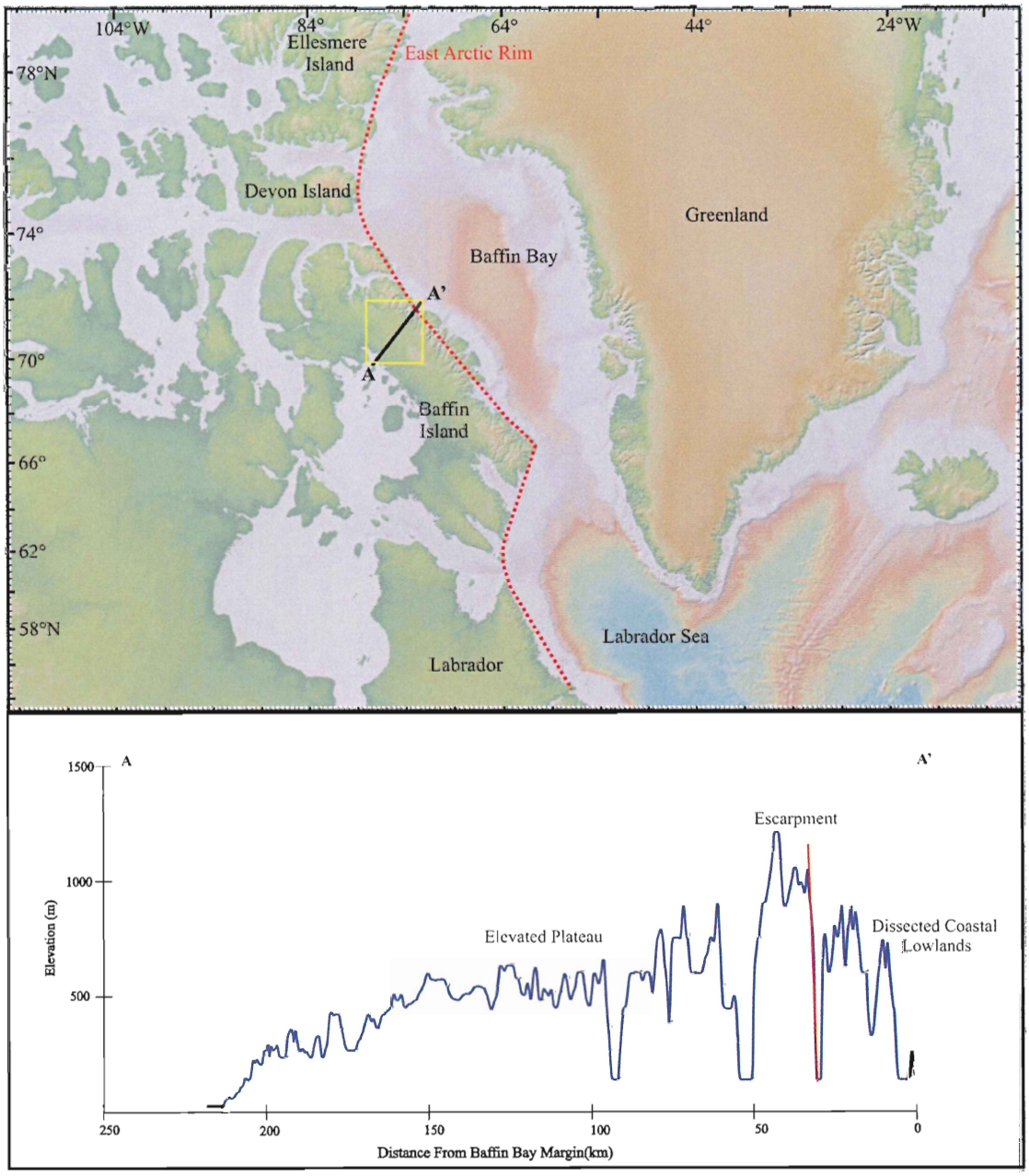

Figure 1.1: *Map of the Canadian Arctic Archipelago, Greenland and the Cretaceous rifted basins that separate them. The extent of the Eastern Arctic Rim is displayed as a dashed red line. Topographic profile from A'-A is displayed below the map, in which the present escarpment and high elevation mountain range separates the highly dissected coastal lowlands and interior elevated plateau. Characteristics of this topographic profile are common in many elevated passive margins and are considered indicative of rift flank uplift. The north-central Baffin Island Study area is marked as a yellow square (§ 1.2)*

The most recent studies focused on the evolution of rifting and rift flank uplift have been strongly reliant on low-temperature thermochronology in order to attain quantitative data to compliment geological and geomorphological observations. Low-temperature thermochronometers such as apatite (U-Th-Sm)/He record the time when rock masses cool through closing temperatures (~75 °C) and radiogenic He begins accumulating within the apatite crystal. With average geothermal gradients of 25 °C/km, this low temperature corresponds to the upper 3-4 km of the earths crust, and therefore can be used to provide age constraints on processes that shape the earth's surface and the thermal character of the shallow crust, and the rates at which these forces occur. For this reason these techniques have become widely used in quantitative analysis of the evolution of geomorphic features such as the retreating of an elevated passive continental margin.

1.2 North-central Baffin Island study area

This study utilizes apatite (U-Th-Sm)/He thermochronology in the north-central region of Baffin Island, Nunavut, Canada, in order to better understand the timing and chronology of processes that formed the contemporary landscape (Fig 1.1). Thermochronologic study was viable because the region exhibits sufficiently high relief (>1500m), a relatively straight rift margin, uniform lithologies across the entire surface, and lack of thermal activity that may have reset the radiometric clock. Access to the area and pre-determined sample sites was made possible by GSC and C-NGO field camps as well as fixed wing and helicopter support in 2005 and 2007, during geological projects conducted by these two organizations. Sampling was conducted (i) along a horizontal transect from the Foxe Basin at Steensby Inlet

(77° 7'W, 70° 16'N) to Baffin Bay (73 ° 42'W, 71 ° 44'N) at a relatively constant elevation of 400 m; (ii) along a horizontal transect parallel with the rift margin at an isolated elevation of 600 m; (iii) along a 1200 m vertical transect below an ice free high relief surface within the Bruce Mountains (73 ° 44'W, 71 ° 9'N); and (iv) randomly throughout the region, as opportunity afforded by other mapping and sampling objectives throughout the field season, in order to provide information in order to constrain He 3D diffusion models away from the linear transects (Fig. 1.2). For the purposes of this study samples from the Bruce Mountains vertical and SW-NE, 400 m isolated elevation sampling transects were processed, analyzed for (U-Th-Sm)/He, and the results have been interpreted.

The central objective of this thesis is to establish an explanation for the evolution of the north-central Baffin Island landscape, within the broader scope of the eastern Arctic Rim. The primary means of establishing this is a comprehensive analysis of exhumation and uplift history using (U-Th-Sm)/He thermochronology. One horizontal and one vertical transect have been documented in order to achieve this objective (Fig. 1.2). The horizontal transect used in this study is roughly perpendicular to the rift margin and Eastern Arctic Rim in the region. Using thermochronology on samples collected at an isolated elevation crossing Baffin Island perpendicular to the rift margin is intended to observe exhumation trends across the rift shoulder, with younger measured He ages reflecting increased amounts of exhumation. This transect also strategically crosses major SW dipping White Bay, Central Borden, and Nina Bang normal faults with the intention of documenting any fault displacement that may be responsible for the elevated plateau surfaces of Baffin Island. In using thermochronology on samples collected from a vertical transect, it is hoped that the period of accelerated uplift is observed. This would be observed as a segment of the transect

covering a significant vertical distance with similar He ages, indicating a large amount of exhumation occurred in response to a rapid increase in elevation.

1.3 Hypothesis

Two hypotheses will be tested in this study. The first hypothesis is that the elevated features of the Eastern Arctic Rim in the north-central Baffin Island region were formed as a consequence of continental rifting from Greenland. A very similar apatite (U-Th-Sm)/He thermochronologic study from southern extension of the Eastern Arctic Rim, the Torngat Mountains of northern Labrador observed a period of rapid uplift occurring ~145 Ma, which corresponds closely with to the oldest rift basalts and syn-rift sediments in the Labrador Sea (Balkwill et al., 1990). Rigid plate models show that Baffin Bay opened shortly after the Labrador Sea, and the oldest rift sediments are of mid-Cretaceous, so it is suggested that the region underwent marginal uplift during the mid - late Cretaceous (Balkwill et al., 1990).

Following the hypothesis that the elevated Baffin Island margin is the result of rift flank uplift, the second hypothesis tested is that the rift scarp has been exhuming by processes consistent with the pinned divide model described by Gallagher et al. (1998) (§ 2.1). The majority of escarpments that have been studied using low-temperature thermochronometry have been down wearing as the pinned divide model describes (Southeast Australia, Persano et al., 2002; Western Africa, Brown et al., 2000; Labrador, Canada, Centeno, 2005). Also, the regional drainage divide of the study area is located closer to the interior than the present location of the escarpment, and appears to be eroding both the interior and coastal sections of the rifted margin as described by the pinned divide model, so this is the model is the most probable (Fig 1.3).

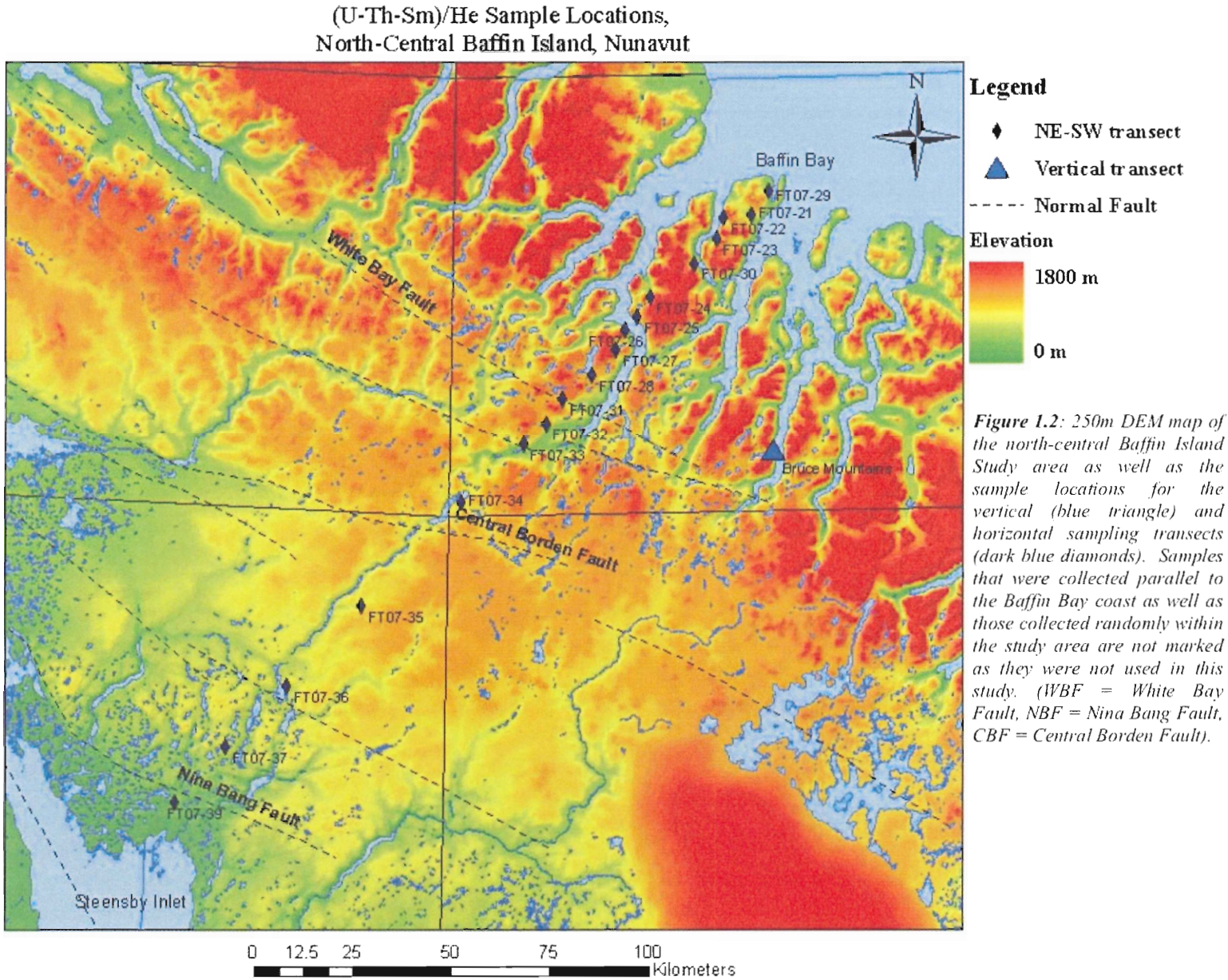

***Figure 1.2**: 250m DEM map of the north-central Baffin Island Study area as well as the sample locations for the vertical (blue triangle) and horizontal sampling transects (dark blue diamonds). Samples that were collected parallel to the Baffin Bay coast as well as those collected randomly within the study area are not marked as they were not used in this study. (WBF = White Bay Fault, NBF = Nina Bang Fault, CBF = Central Borden Fault).*

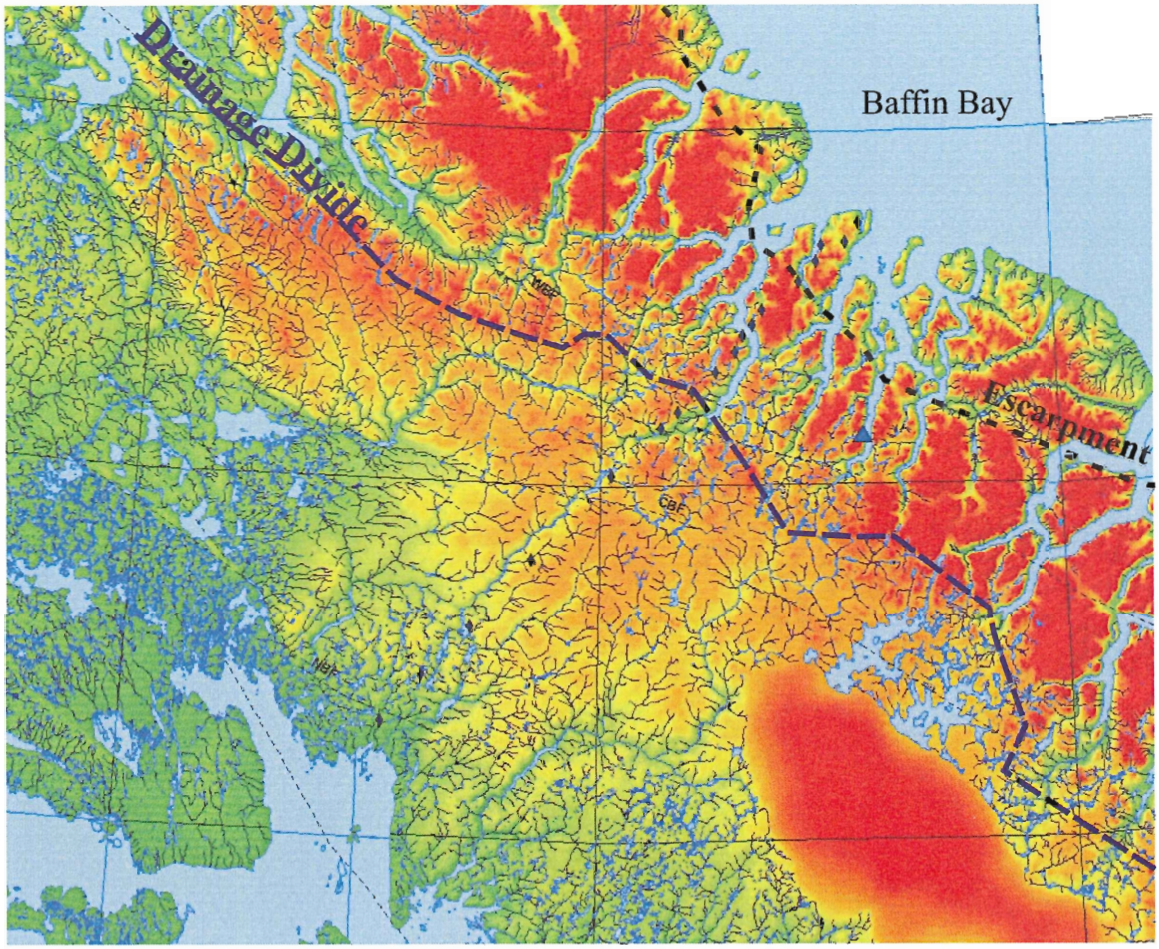

***Figure 1.3**: 250m DEM of the north-central Baffin Island study area with streams and rivers displayed. The approximate location of the regional drainage divide (blue dashed line) is within the interior of the island, dictating that erosion wears away both the low relied surfaces of the interior, as well as the escarpment (black dashed line) and coastal region of the island. (WBF = White Bay Fault, NBF = Nina Bang Fault, CBF = Central Borden Fault).*

1.4 My role within this project

During the many stages of this thesis I was assisted by many people, but a large portion of work was performed by me. Sample collection was conducted by Daniel Utting, and Mike Young of the Canada-Nunavut Geoscience Office, Eric Little of the Geological Survey of Canada, and John Gosse of Dalhousie University. The physical processing of samples involving crushing, grinding, sieving, and separation (density and magnetic) was carried out by Debra Wheeler. Personally, I was responsible for 75% of the physical separation and preparation of apatite crystals for gas extraction and U-Th-Sm analysis, the other 25% completed by Jose-Luis Antinao. Data reduction was also completed by me also, with the final stage being completed with a MatLab program that was also created by Jose-Luis Antinao.

2 BACKGROUND

2.1 Rift Flank Denudation Models

A common characteristic of rifted basins is uplift along its margins as a result of tectonic, isostatic, and thermal forcing. Downthrowing of normal faults that are facilitating extension in continental rifting environments exposes the fault scarp of the footwall. Though the effects of thermal uplift are temporary (~50 Ma), crustal underplating and isostatic rebound in response to denudation of the newly formed rift scarp ensures the long life of these features. The evolution of such coastal features have been studied in many regions world wide including southeast Australia, south and western Africa, eastern United States of America, and Labrador (Persano et al., 2002; Brown et al., 2000; Spotila et al., 2004; Centeno, 2005). Gallagher et al. (1998) suggested three end member models for the landscape evolution of uplifted rift flanks due to denudation that can be identified using low temperature thermochronometers such as the (U-Th-Sm)/He method.

2.1.1 Rift Flank Denudation Models

1. Downwarp Model (Fig. 2.1): Basin subsidence causes the lithosphere to downwarp along the continental margin with minimal faulting occur during extension. A weakness of this model is that it does not take into account isostatic uplift in response to mechanical unloading. Denudation is limited to the crest of the monocline (B), and very low amounts of denudation taking place inland of the escarpment (C). This trend of erosion results in (U-Th-Sm)/He ages that decrease in the coast to crest region (B), but remain old basinward from the coast (A), and inland from the escarpment.

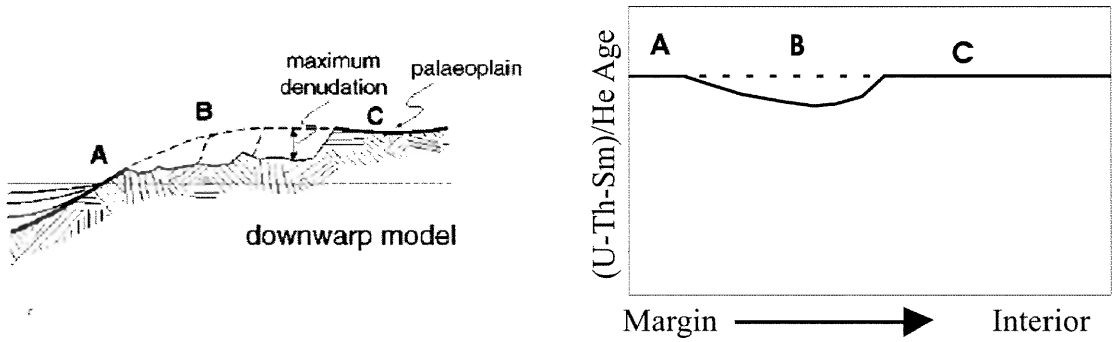

Figure 2.1: *Downwarp model of escarpment evolution. Downwarping of the rifted margin in the direction of the subsiding basin has the results of increased denudation rates in the crest to coastal region of the margin (B) and the youngest He ages are observed across the rift shoulder. Coastal section (A) and inland of the escarpment (B) are both paleo-surfaces that have not been subject to denudation and display the older He ages (figure modified Gallagher et al., 1998).*

2. Scarp Retreat Model (Fig 2.2): Significant erosion takes place on the escarpment facing the newly formed basin (A), where as the interior of the rift shoulder undergoes minimal erosion (B). By far the lowest erosion rates would take place in the interior where slope is the lowest (C). This exhumation pattern would result in the escarpment front continually wearing away towards the interior region. A thermochronologic study that crosses the entire rift shoulder would support this model if it revealed that the oldest (U-Th-Sm)/He ages inland of the escarpment, and youngest ages occurring directly seaward of the scarp. Spotila et al., (2004) observed that the Blue Ridge escarpment of the Appalachians evolved in an escarpment retreat type fashion.

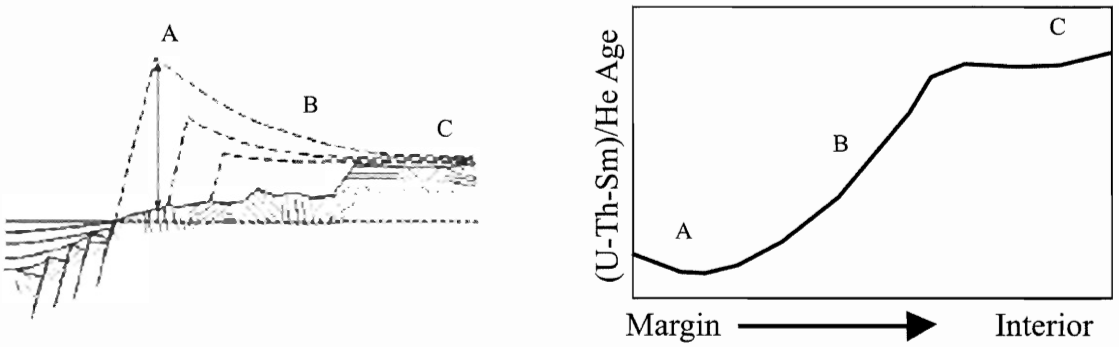

Figure 2.2: *Scarp retreat model for denudational evolution of a permanent rift shoulder. Letters indicate different exhumation regimes; A) Maximum exhumation of the scarp front is displayed from the young (U-Th-Sm)/He Ages, B) Decreasing exhumation towards the interior can be seen from the increasing (U-Th-Sm)/He Ages, C) Minimal exhumation in the interior of the rift shoulder yields the oldest (U-Th-Sm)/He ages (figure from Gallagher et al., 1998).*

3. Pinned Dived Model (Fig. 2.3): Significant erosion takes place on the interior of the rift shoulder (C) as well as the escarpment front (A). This model requires that the regional drainage divide is located within the interior of the rifted margin with respect to the escarpment front. Both surfaces have increased amount of slope due to rift flank uplift. Accelerated fluvial incision would be expected with the increase in slope of the escarpment, in accordance with the stream power law for channel incision rate on bedrock (ε),

$$\varepsilon = KA^{m}S^{n} \qquad (2.1);$$

where S is slope, A is drainage area, K is a constant, and n and m are positive exponents which along with K reflect rock resistance and other environmental attributes of individual rivers (e.g. Stock and Montgomery, 1999). The escarpment front (A) has a much higher increase in slope so it undergoes the most erosion compared to the interior of the rift shoulder (C). The central area containing the regional drainage (B) is subjected to the lowest erosion

rates. This exhumation pattern results in a down wearing of the rift shoulder from the pinned drainage divide. Thermochronologic study across the rift shoulder would display the youngest He ages in the area where the scarp front is being eroded (A), oldest He ages where the drainage dived is located (B), and a slight but progressive younging towards the interior (C). Many elevated rifted margins have been found to evolve as the pinned divide model describes, including southeast Australia, south and western Africa, and Labrador (Persano et al., 2002; Brown et al., 2000; Centeno, 2005).

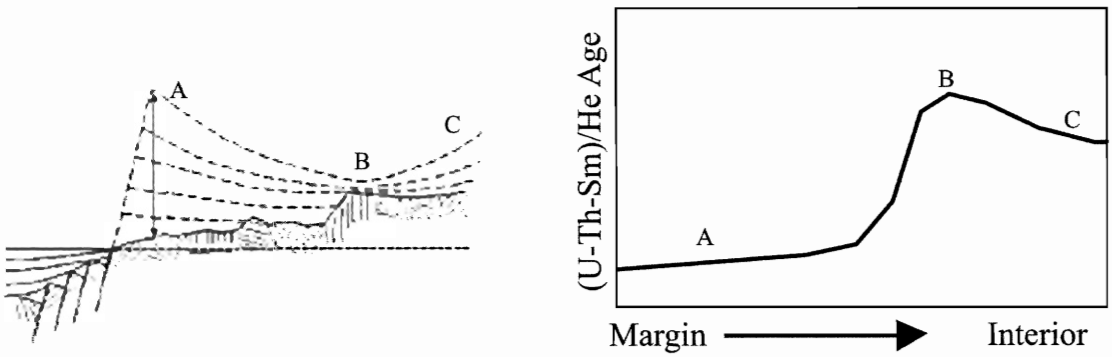

***Figure 2.3**: Pinned divide model for escarpment evolution. Point A) maximum exhumation basinward of the newly formed scarp, evident from the youngest (U-Th-Sm)/He ages across the rift shoulder; B) minimal exhumation in the location of the pinned drainage divide, indicated by the oldest (U-Th-Sm)/He ages across the rift shoulder; C) Some exhumation in the interior section of the rift shoulder due to increase in slope in the region leads to younger ages in this area than that around the pinned drainage divide (figure modified from Gallagher et al., 1998) .*

The north-central Baffin Island portion of the Eastern Arctic Rim appears to have been uplifted due to rifting from Greenland (Fig 2.4). This may be a reasonable hypothesis because area has apparently been tectonically and thermally stable since continental rifting and the current physiography is the product of erosive and isostatic forces. The hypothesis can be tested by thermochronological analysis of the exhumation history of the region, in

concert with paleo-drainage analysis and examination of the offshore sediment record.

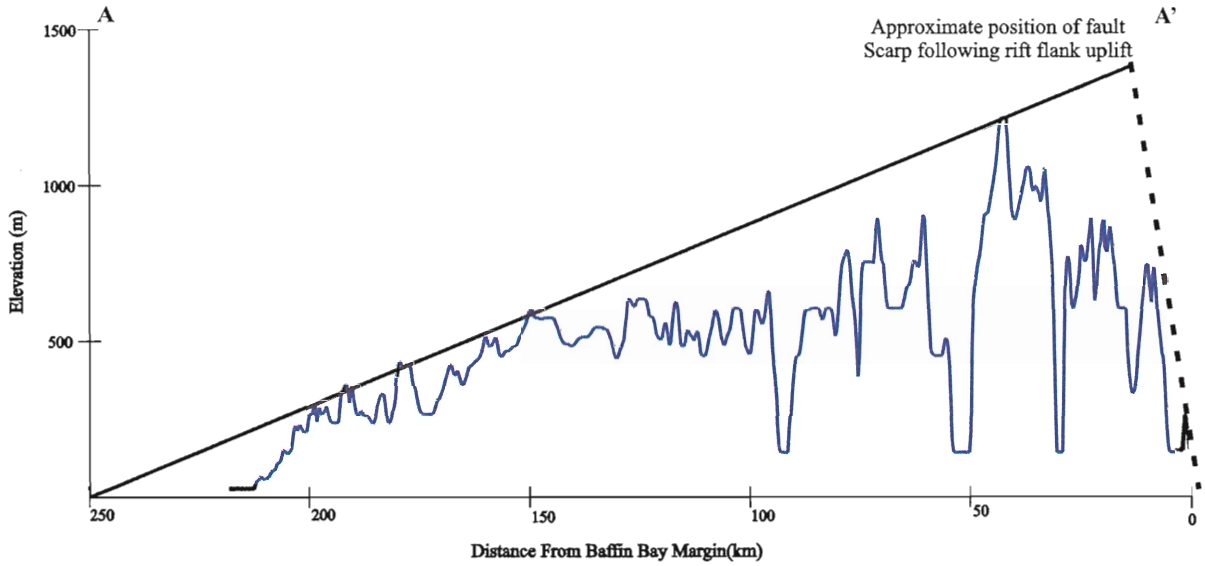

Figure 2.4: *Topographic profile along the SW-NE horizontal sampling transect (A-A' from Fig. 1.1) in north-central Baffin Island study area. Approximated locations of the original fault scarp surface (dashed black line) are displayed as well as an estimated position of the Baffin Island crustal block without erosion (solid black line).*

2.2 Baffin Island Physiography

The north-central Baffin Island terrain is a barren and rugged arctic landscape where topography, ice cover, and lakes are the most important physical attribute at almost all scales. Topographically, Baffin Island varies from high elevation and mountainous near the Baffin Bay margin to very low relief, low elevation surfaces approaching the Foxe Basin (Fig 1.1). Mountainous highland and upland surfaces are common features across Baffin Island as well as the rest of the Islands that comprise the Eastern Arctic Rim. North-central Baffin Island has been divided into a number of physiographic provinces that make up the rift shoulder and interior surfaces based on elevation and relief. Three major NW-SE striking normal faults

(White Bay, Central Borden, and Nina Bang Faults) further aid in marking divisions between physiographic provinces. The study area from NE-SW comprises the coastal lowlands, Davis Highlands, Baffin Upland Surfaces, Lancaster Plateau and Foxe Plain physiographic provinces which will be discussed (Fig 2.5) (Bird, 1967; Staiger et al., 2005).

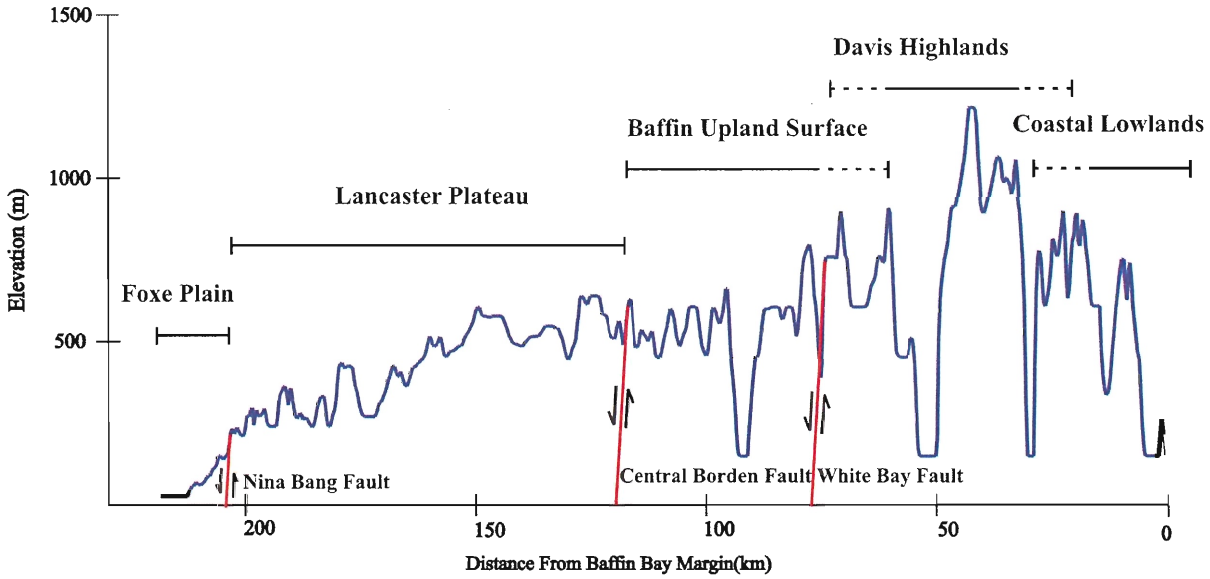

***Figure 2.5**: Topographic profile (A – A', Fig. 1.1) depicting the physiographic provinces and major fault locations (red lines) of the north-central Baffin Island study area. Dashed lines indicate rough boundaries between two physiographic provinces.*

The eastern margin of Baffin Island consists of the coastal lowlands and Davis Highlands. Coastal lowlands make up a narrow (~30 km) section directly adjacent to Baffin Bay. Its small width may be indicative of the youthful nature of the rifted margin or the resistive Precambrian lithologies that comprise the Baffin surface geology, or both. This narrow lowland quickly gives rise to the Davis Highlands, a mountainous highland surface comparable to the Penny Surface of south Baffin Island. Elevations within the highland

surface reach over 1500 m, and relief can exceed 1700 m due to deep fiord incision (Staiger et al., 2006). North central Baffin Island's regional drainage divide is located within this highly elevated province.

A decrease in elevation roughly marked by the White Bay fault zone, as well as a decrease in relief occurs in a SW direction from the Davis Highlands. Adjacent to the Davis Highlands is the Baffin Upland Surface, a high elevation but lower relief, dissected plateau that is divided by a series of SW dipping normal faults. This surface gradually slopes to the SW, decreasing in elevation from >900 m to <300 m in the deepest valleys, with a portion of the declining elevation facilitated by normal fault displacement, supported by steep cliff faces defining fault or fault line scarps (Bird, 1967). Relief of the Baffin Surface reaches over 300 m in the highest elevated regions, but decreases to <60 m at mid range elevations indicating it has undergone an extensive period of subaerial denudation as well as far less fiord dissection compared to the Davis Highlands (Bird, 1967; Staiger et al. 2006). The Central Borden Fault divides the core of the Baffin Upland surface from the Lancaster Plateau. Within the study area the Lancaster Plateau is a low relief surface at roughly 600-300 m elevation, but to the north, the Central Borden fault defines a graben structure containing unmetamorphosed Paleozoic carbonate and siliclastics.

The SW margin of Baffin Island is further segmented by the Nina Bang Fault, defining the border to the Foxe Plains physiographic Province. At near horizontal attitude and very low amounts topographic relief, the Foxe Plain is generally below 100m elevation (Dawes and Christie, 1991). Within the Foxe Basin Ordovician carbonates and sediments of the Foxe Plain unconformably overly the Archean-Proterozoic basement that makes up much of the upland and highland surfaces (Dawes and Christie, 1991). All physiographic provinces

within the study area consist of similar metamorphic and igneous lithologies that are strongly resistant to weathering (lithologic details in §2.3).

The general low relief of upland and lowland surfaces as well as evidence of normal fault displacement has led to the assumption that these upland surfaces were once all eroded to the same elevation (peneplanation), and significant fault movement during the Tertiary brought them to their current elevation (Bird, 1967). They may on the other hand be pedeplain surfaces in which they were uplifted, weathered, and subaerial erosion was controlled by regional weathering rate, not sea level. Interpretations of drainage patterns prior to the formation of Baffin Bay by Bird (1967) indicate that northern north-central Baffin Island was roughly the location of a drainage divide, dividing flow between the Sverdrup Basin to the northwest, and river drainage southeast to the Atlantic (Fig. 2.6). This interpretation would imply that some degree of topography existed in the region prior to rifting of Baffin Island from Greenland, and the surface present are not peneplains.

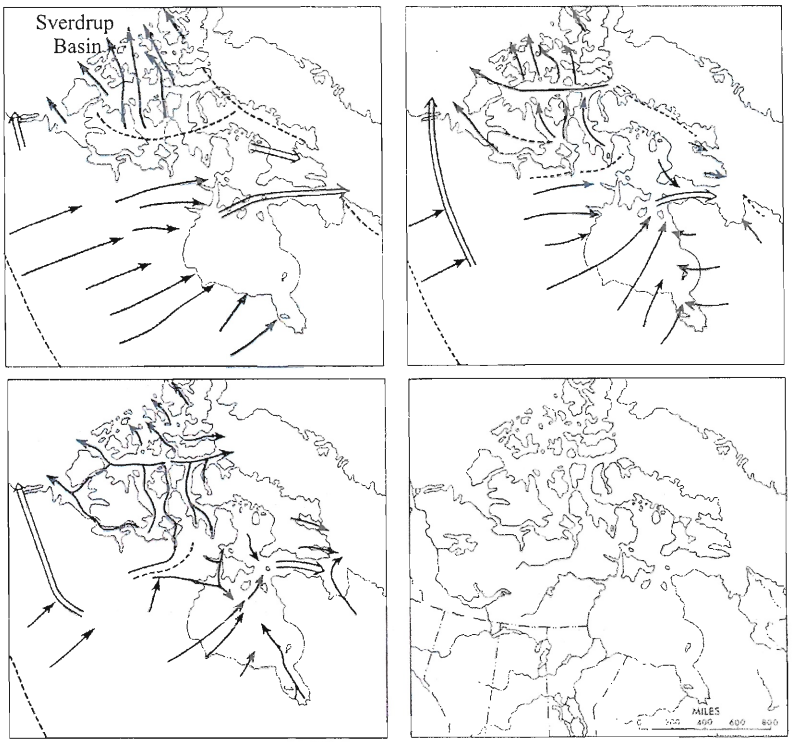

***Figure 2.6**: Drainage pattern from the Paleozoic to present. Paleozoic drainage (Top two diagrams) was directed to the NW towards the Sverdrup basin, and SE to the Atlantic Ocean and north-central Baffin Island was likely near the regional drainage divide at the time. Following the formation of Baffin Bay much of the drainage shifted towards the east (bottom left diagram) (Figure from Bird, 1967).*

2.3 Geology of Study Area

The major lithologies of the study area consist of Precambrian granitic orthogneiss of greenschist to granulite facies metamorphism, and to a lesser extent slightly metamorphosed supracrustal sedimentary units. With the vast majority of the Baffin Island surficial geology consisting of granitic lithologies, apatite can be found widespread making this area a prime target for the utilization of apatite (U-Th-Sm)/He thermochronologic study. Unmetamorphosed Paleozoic of the Arctic platform is present as a discontinuous cap unit to the southeast in Foxe Basin and northwest in Lancaster Plateau. Northern Baffin Island lies

within the 3.0 - 2.5 Ga Committee Belt, which has been slightly overlain and overprinted by the Baffin orogen that lies largely in the southern region of the island (Fig. 2.7). During the Baffin Orogeny (1.8 Ga.) northwest directed thrusting of the Isortoq fault zone and subsequent southeast extension resulted in the burial and exhumation of high grade metamorphic rocks of the Dexterity Granulite Belt. The Committee Belt is a part of the Northern Rae Province, which extends from Nunavut northwest into Greenland, covering a distance of over 2000 km (Jackson and Berman, 2000). Geology of the Northern Rae province is characterized by mainly Achaean and Early Proterozoic granitic orthogneiss and NE – N trending greenstone belts (Fig 2.8; Young et al. 2004). There are few examples of Late and post-Proterozoic lithologic units occurring regionally within northern Baffin Island, but due to significant fluvial and glacial erosion surficial lithologies mainly consist of Archean-Proterozoic basement units. There is however Paleozoic carbonates and siliclastics located on the Lancaster Plateau just northwest of the study area, as well as Paleocene Lake sediments that have been identified on the Lancaster Plateau near the Barnes Ice Cap.

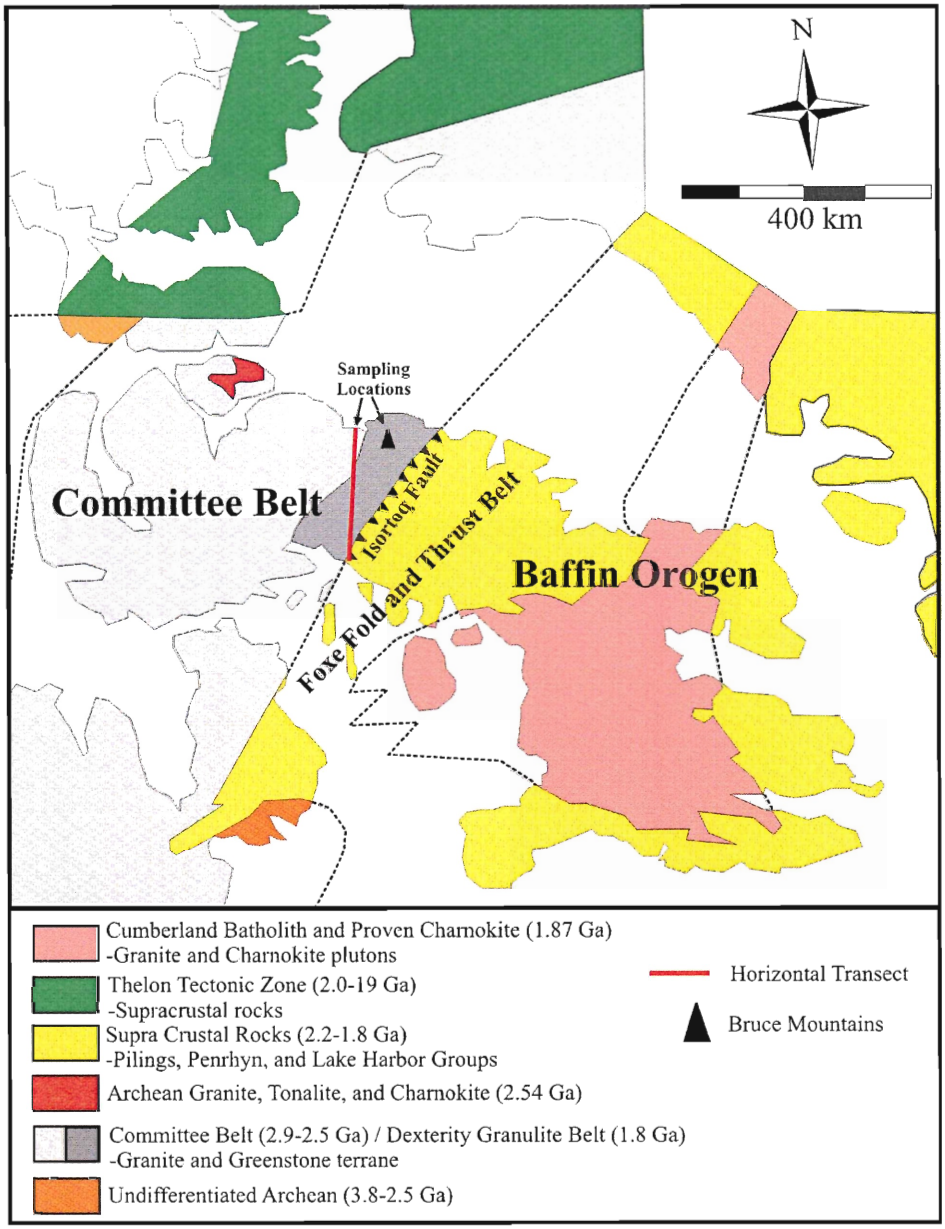

***Figure 2.7**: General lithologic and tectonic terranes of Baffin Island and immediately surrounding islands. Sampling location largely lies within the Dexterity Granulite Belt and Committee Belt, but also extends across Isortoq Fault into the Foxe Fold and Thrust Belt of the Baffin Orogen (Figure modified from Jackson and Berman, 2000).*

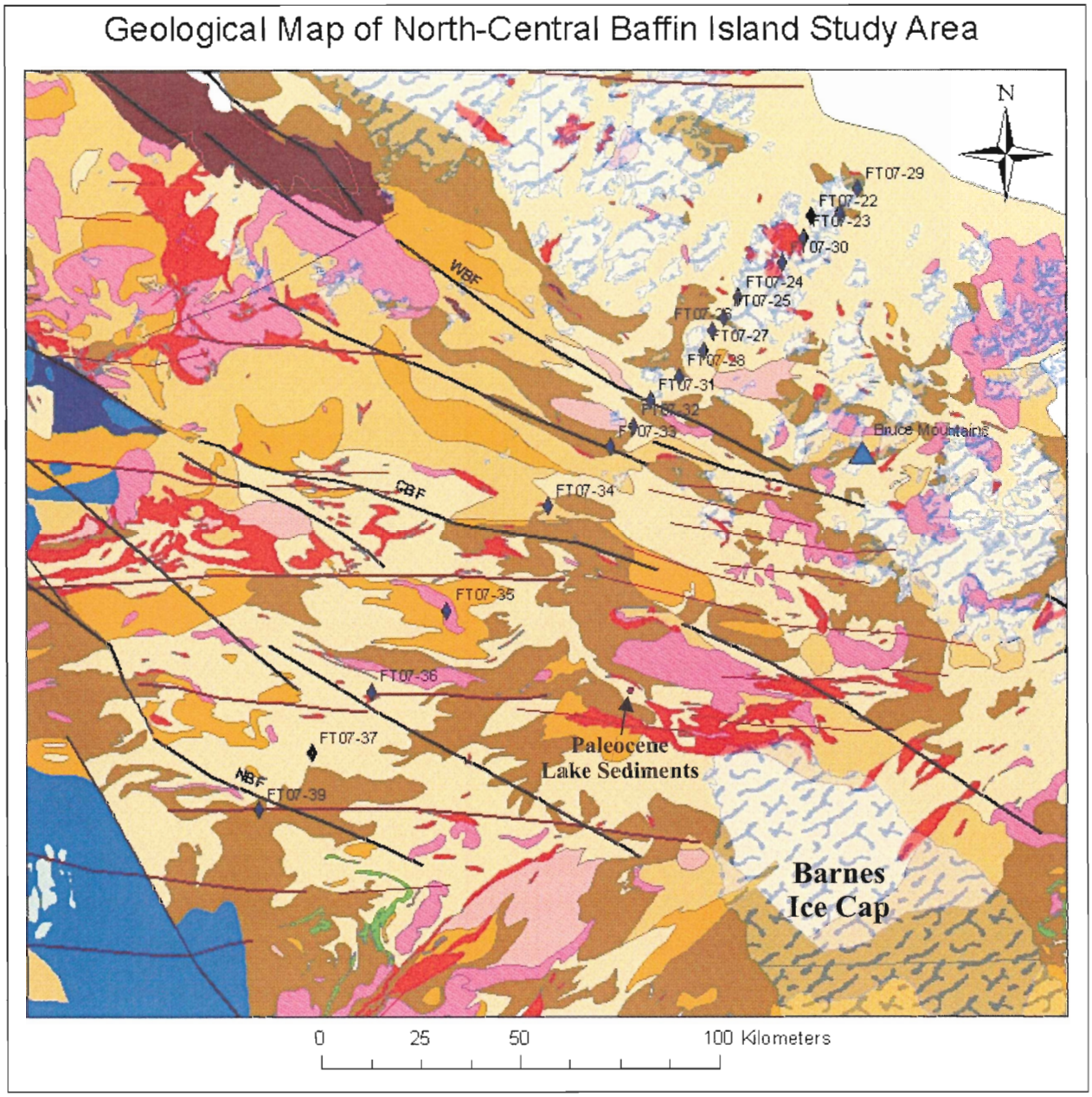

Figure 2.8 *(Legend on following page): Detailed Geologic Map of study area with samples plotted. The vast majority of surface lithologies are composed of granite, granodiorite, monzogranite, gneiss, and migmatite. (WBF = White Bay Fault, CBF = Central Borden Fault, NBF = Nina Bang Fault)*

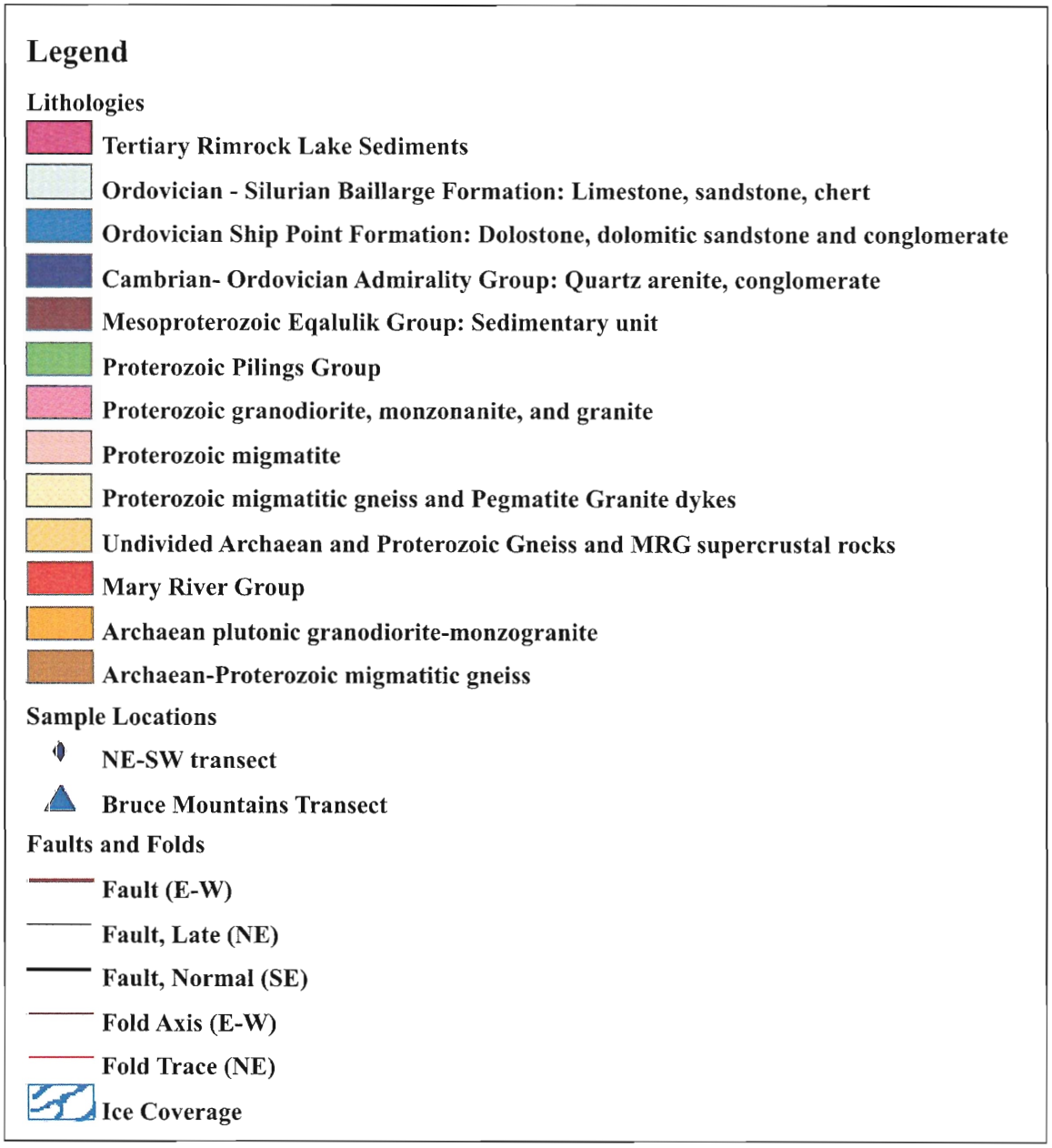

Archean to Proterozoic rocks are the oldest and by far the most abundant units in the study area. The main lithologies present are granitic – granodioritic gneiss and migmatite, as well as plutons that consist of granite subtypes such as granodiorite-granite, syenogranite, tonalite, charnokite, and monzogranite (Young et al. 2004; Jackson and Berman, 2000). Charnokite plutonic intrusions are also present near the Isortoq fault zone associated with extension during the late stages of the Trans Hudsonian Orogeny. Supracrustal rocks of the

Mary River Group (MRG, ~2.7 Ga) occur as isolated, elongate greenstone belts within NE trending folds of orthogneiss basement (Young et al. 2004). Greenstone belts show minor variation but in general display a sequence consisting of mafic-intermediate volcanics, banded iron-formation, intermediate-felsic volcanic rocks, and slightly metamorphosed sedimentary units (Johns and Young, 2006; Bethune and Scammel, 2003)). Metamorphic grade across Northern Baffin Island varies from greenschist to amphibolite facies, with granulite facies occurring mainly within the Dexterity Granulite Belt. The wide spread abundance of mainly igneous and metamorphic Pre-Cambrian lithologies forms a surface that is very resistive to erosion.

There are very few examples of post-Proterozoic strata to be observed in the north-central Baffin Island study area. Cambrian-Ordovician carbonates and sedimentary strata can be found within a downthrown graben underlying the Foxe Basin extending north to the Brodeur Peninsula unconformably overlying the Precambrian basement (Dawes and Christie, 1991). The youngest lithology located in the study area is a brown limy mudstone and conglomerate discovered by Andrews et al. (1972) (Fig. 3.1). This carbonate-cemented siltstone-conglomerate is found non-conformably within fractures of the granitic gneiss basement in an isolated location near Rimrock Lake northwest of the Barnes ice cap (70°36.6'N, 75°20'W). Microfossil analysis by Andrews et al. (1972) and unpublished results from a replicate study in 2005 by the Geological Survey of Canada (D. Utting, personal communication, 2007) indicate that the limy mudstone was deposited in a warm fresh-water swamp or marginal marine marsh environment during the Paleocene. The known distribution of the Paleocene unit, which remains nameless, is limited to the upper third of a hill south of Rim Rock lack, with an aerial extent of approximately 1 km^2 and outcrop

thicknesses of cm to dam. The critical significance of this outcrop, situated approximately 120 m above the surrounding Baffin Upland surface, will become clearer in Chapter 5 when it will help establish the rates and styles of exhumation of the study area during and since rifting.

2.4 Proterozoic Structural Elements

There is strong indication of multiple episodes of Achaean-Proterozoic deformation within the granitic gneiss and Mary River Group metamorphosed rocks (Fig. 2.8). The most extensively observable tectonomorphic event can be attributed to the Trans-Hudson Orogeny (~1.8 Ga.) that resulted in greenschist-amphibolite facies metamorphism of the supracrustal sequences (Young et al., 2004). Strong NE-SW trending fabrics are observed from this event, most notable are tight kilometer scale northwest verging folds and the SE dipping Isortoq fault zone (Young et al., 2004). Within the Dexterity Granulite Belt gneissosity intensity and metamorphic grade are observed to increase in the vicinity of fault zone, implicating the responsibility of Isortoq fault zone activity for these features (Fig. 2.7) (Jackson and Berman, 2000).

The structural elements of particular interest to this study are the laterally extensive NW trending, brittle normal faults: Nina Bang, Central Borden, and White Bay (Fig. 1.2). The three faults dip to the SW and run semi-parallel to Baffin's eastern coast and rift margin in the area. These fault systems help define the boundaries of the previously discussed physiographic provinces (Fig. 2.5) and have therefore controlled the relief and denudational trends. The faults are known to have formed during the Proterozoic and little is known of

their evolution since (Jackson and Berman, 2000). Thermochronologic transects across these faults could document post - Proterozoic reactivation of these faults and help understand their role in the evolution of the Baffin Island landscape.

2.5 Continental Rifting and Offshore Geology

Following the Trans-Hudsonian Orogeny, rifting of Greenland from the North American Craton was the next major tectonomorphic event to influence Baffin Island. Continental rifting and basin development initiated in the Labrador Sea, which subsequently extended north to form Baffin Bay through the shallow Davis Straight. The timing of actual seafloor spreading has been a subject of much debate, but most recent interpretation of linear magnetic anomalies and the position of the ocean-continent boundary indicates that spreading began within the Labrador Sea during Chron 27 (61 Ma) and ceased by Chron 13 (33 Ma)(Chalmers and Pulvertaft, 2001). The lack of magnetic anomalies within Baffin Bay has made deciphering when initial spreading began difficult, but it is assumed to have began between Chron 27 and Chron 24 based on rigid plate models (Chalmers and Pulvertaft, 2001).

Interpretation of linear magnetic anomalies within the Labrador Sea also identified a re-orientation of the spreading axis from N27W to N40W occurring before chron24 (55.9-53.3Ma) and corresponding to the initiation of sea floor spreading between Greenland and Europe (Srivastava, 1978; from Chalmers and Pulvertaft, 2001). Opening of Baffin Bay and the Labrador Sea after chron25 resulted in transpression of Greenland and Ellesmere Island during the Eurekan Orogeny (Grist and Zentilli, 2005). The amount of sinistral strike slip

fault displacement occurring within the Nares Strait is estimated between 120 – 300 km based on rigid plate reconstructions, and 0-50 km based off onshore geologic features (Saalmann et al., 2005).

The process of continental extension to seafloor spreading spanned many millions of years beginning in the Labrador Sea (Balkwill et al., 1990). Early Cretaceous extension within Labrador Sea was first evident from rift related basalts of the Alexis Formation (>131 Ma) and syn-rift sediments of the Bjarni Formation (130-99 Ma) present under the current Labrador shelf (Balkwill et al., 1990). Though volcanics are not present in northern Baffin Bay, syn-rift equivalents of the Bjarni Formation are represented in the Hassel Formation, within the Eclipse Trough near Pond Inlet (Balkwill et al., 1990). The Hassel Formation consists of fluvial sandstones and coal seams of Albian – Cenomanian age (112 - 93 Ma), unconformably overlying Proterozoic or Paleozoic basement (Balkwill et al., 1990). Similar aged, or younger, sediments within the Eclipse Trough to those found on the Labrador shelf indicate that sea floor spreading occurred simultaneously or shortly afterwards within Baffin Bay.

Though volcanic material associated with rifting is not found in northern Baffin Bay similar to the Alexis formation in Labrador Sea, there are basalts located on SE Baffin Island and SW Greenland adjacent to the Davis Straight. Located near Cape Dyer on Baffin Island and adjacent on Western Greenland, basalts were extruded during chron27n/26r (~60 Ma) and have been associated with the Icelandic mantle plume (Skaarup et al., 2006). The relationship between volcanic flows and marine breccias indicates that the area has undergone approximately 400-500 m of post-volcanic uplift (Dawes and Christie, 1991). The existence of these basalts has contributed to the evidence that has been used to classify

Baffin Island's margin from 69-63°N as a volcanic margin (Skaarup et al., 2006). These margins also display high velocity volcanic lower crust with high amplitude magnetic anomalies, seaward dipping reflectors, and a varying amount of volcanic material located offshore as well as onshore (Skaarup et al., 2006). It is believed that volcanic crustal underplating and isostatic response within the Davis Straight is the cause of shallower depths that restrict deep water circulation through the Baffin Bay and Labrador Sea (Skaarup et al., 2006). Though volcanics are not present in the study area the increased thermal activity associated with the Icelandic Plume and crustal underplating may have some responsibility for rift flank uplift along the northern Baffin margin.

The remaining portion of Arctic rim, like the rest of Canada's Atlantic margin is classified as non-volcanic. North of Davis Straight within Baffin Bay, crustal extension and thinning has been facilitated by normal faulting trending in a NW-SE orientation, roughly parallel to Baffin Island's east coast and the Eastern Arctic Rim (Skaarup et al. 2006). Faulting within non-volcanic portions of Baffin Bay is far more laterally extensive then that observed within the volcanic region, forming elongate fault bound grabens down-thrown to the east (Skaarup et al. 2006). These graben structures on the Baffin shelf form Precambrian basement highs and narrow basins, filled with Cretaceous rift related sediments visible in seismic and aeromagnetic data (Skaarup et al., 2006). Considering these faults that formed during the Cenozoic are essentially parallel to those that had formed during the Proterozoic, it is very likely that re-activation of major NW-SE faults occurred in response to rifting.

Post-rifting uplift has also been observed during the Neogene in many passive margins of the North Atlantic. Of particular interest are uplifts that have been documented along the conjugate margin to northern Labrador on southwest Greenland. Two separate cooling

periods have been documented following major Paleocene cooling during the mid to late Neogene using fission track and vitrinite reflectance data down bore holes in SW Greenland (Japsen et al., 2005). It is possible that the north-central Baffin Island study area also underwent renewed uplift during the Neogene.

2.6 Thermochronologic Studies of the Eastern Arctic Rim

The amount of thermochronologic study along the Eastern Arctic Rim is limited. Centeno (2005) carried a similar apatite (U-Th-Sm)/He study within the Torngat Mountains of Labrador using vertical sampling transects as well as margin-parallel and margin-perpendicular sampling transect (Fig. 2.11). In the southern section of the Eastern Arctic Rim a period of accelerated cooling occurring at ~150-140 Ma was observed, attributed to increased erosion rates in response to rift flank uplift (Fig. 2.9 A.). This is coeval with the deposition of the Alexis Formation syn-rift deposits and Bjarni volcanics. During this 10 Ma duration, an erosion rate of ~30 m/Ma was observed, followed by a rate of <11 m/Ma for the remaining section of the vertical transect. Centeno, (2005) also suggested that the margin perpendicular sampling transect (Fig. 2.9B) displayed a trend that closely resembled that of the pinned divided model. The data supports the idea that the Eastern Arctic Rim formed as a result of crustal root accelerated rift flank uplift. However geophysical data suggesting that Labrador has a deep crustal root feature is not available for Baffin Island (Funck and Louden, 1999). The north-central Baffin Island area may not be supported by a root, in which case the two locations will have differed thermal histories. A unique crustal root in beneath Labrador may have been largely responsible for an accelerated rate and increased magnitude

of uplift in the southern region of the Eastern Arctic Rim compared to the rest of the margin.

A fission-track and (U-Th-Sm)/He study conducted by Grist and Zentilli (2005) in the Canadian Arctic Archipelago surrounding the Sverdrup Basin gives some insight into the evolution of the Eastern Arctic Rim (Fig.2.11). Cooling ages of fission-track data suggest that the areas surrounding the Sverdrup Basin underwent late Paleozoic – Mesozoic cooling, relating to the formation and subsidence that followed during the formation of the Sverdrup rift basin. Grist and Zentilli (2004) also present fission-track models to explain the cooling trends observed in the region (Fig. 2.10). Modeling of fission-track data suggested that areas distal to the Sverdrup Basin such as Kap Trautwine, Greenland underwent an early accelerated cooling event during the Permian (Fig. 2.10). This accelerated cooling in distal regions was attributed to increased erosion rates during the rifting of the Sverdrup basin and uplift of its marginal flanks. Fission-track cooling models from more proximal regions to the Sverdrup Basin, such as the Inglefeild field Uplift of Devon Island, underwent accelerated cooling during the early Mesozoic (Fig. 2.10). It was suggested that this more localized increased rate of erosion was due to subsidence of the Sverdrup Basin subsequent to the rifting event. It is possible that the north-central Baffin Island also underwent accelerated erosion during the late Paleozoic – Mesozoic as fission-track data from these areas displayed, considering its proximity to the Sverdrup Basin and suggested drainage patterns prior to the formation of Baffin Bay (Fig. 2.6).

A sample collected from Devon Island at an elevation of 80 m was also dated using apatite (U-Th-Sm)/He thermochronometry, yielding an age of ~110 Ma. This is the approximate time that rift flank uplift is expected to have occurred within northern Baffin Bay, based on the mid-late Cretaceous deposition of the Hassel Formation. Fission-track

models suggest that this age reflects a period of increased thermal activity associated with the onset of rifting with Baffin Bay during the late Cretaceous (Grist and Zentilli, 2004).

Grist and Zentilli (2005) also calculated average erosion rates from these two locations using fission-track ages from samples from collected at different elevations (700 m, 444 m, and 80 m from Devon Island and 665 m, and 0 m from Kap Trautwine). The average erosion rates during the Paleozoic to Mesozoic were found to be ~19 m/Ma for eastern Devon Island and ~9 m/Ma for northwest Greenland. These average erosion rates as well as those observed within Labrador should indicate a reasonable range for erosion rates within north-central Baffin Island region. Fission-track models from these areas also estimated cooling rates of 5 °C/Ma for Devon Island and 3 °C/Ma for Greenland as well as average geothermal gradients following the Paleozoic of 22 - 25 °C/km and 36 - 38 °C/km respectively. For this thesis a constant geothermal gradient of 25 °C will be assumed because of the proximity of Devon Island to the study area.

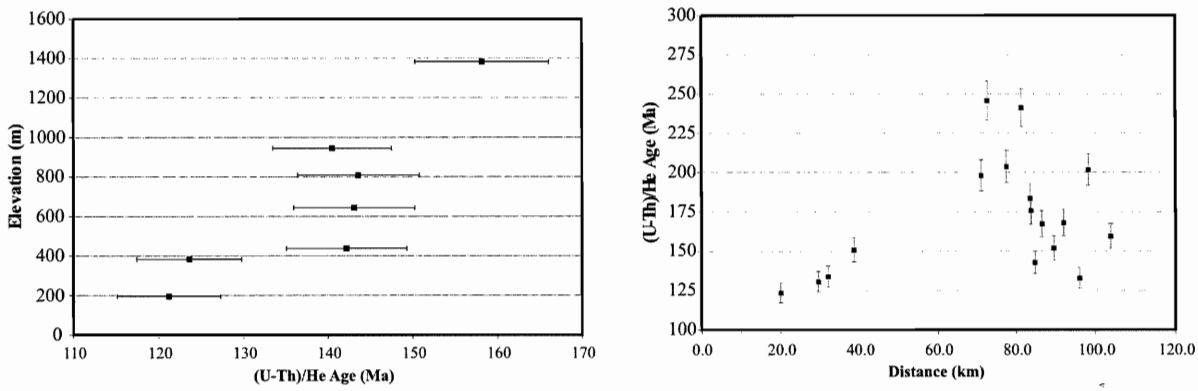

***Figure 2.9**: Results from Centeno, (2005) (U-Th-Sm)/He study conducted within the Torngat Mountains of northern Labrador. The vertical sampling transect (left) displays a trend of accelerated cooling suggested to reflect rift flank uplift occurring ~140-150Ma The horizontal coast perpendicular sampling transect (right) displays a trend in ages similar to that suggested for Gallagher et al. (1998) (figures from Centeno, 2005).*

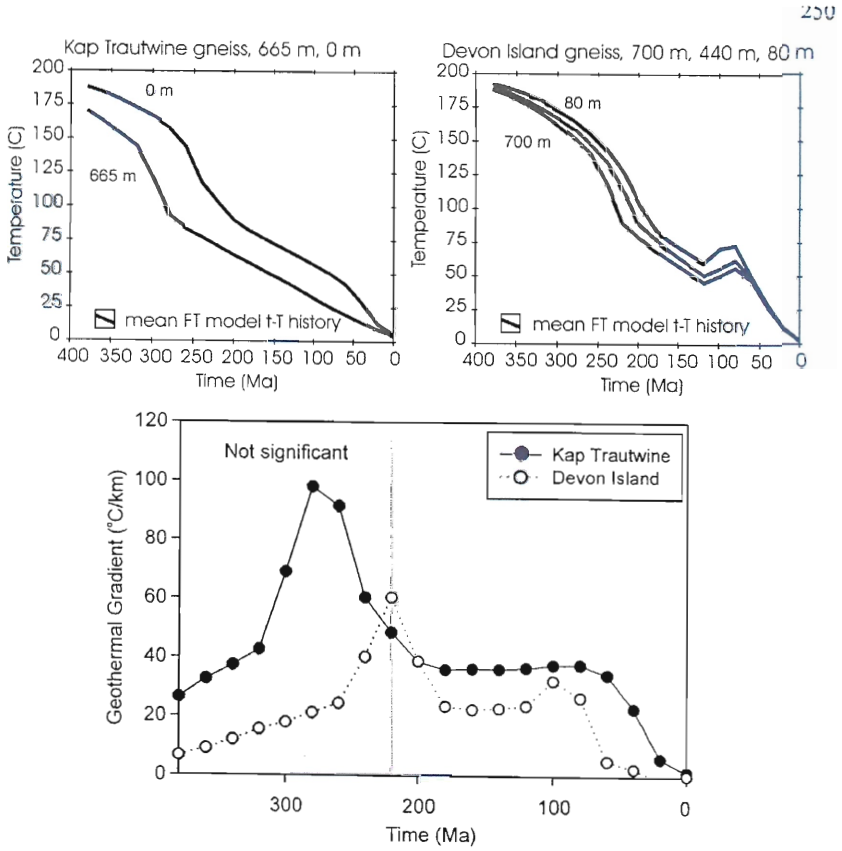

Figure 2.10 *Mean thermal histories for fission-track models from Devon Island and Kap Trautwine, Greenland. Kap Trautwine displays an accelerated cooling period during the Permian, where as Devon Island displays a cooling period during the Triassic and Paleogene (Note: Devon Island cooling rate has (U-Th-Sm)/He data to constrain cooling histories below 75* °C). *Paleo-geothermal gradients from model results are shown below. Gradient before 220 Ma is insignificant because samples had been above apatite partial annealing zone (PAZ) temperatures (figure from Grist and Zentilli, 2004).*

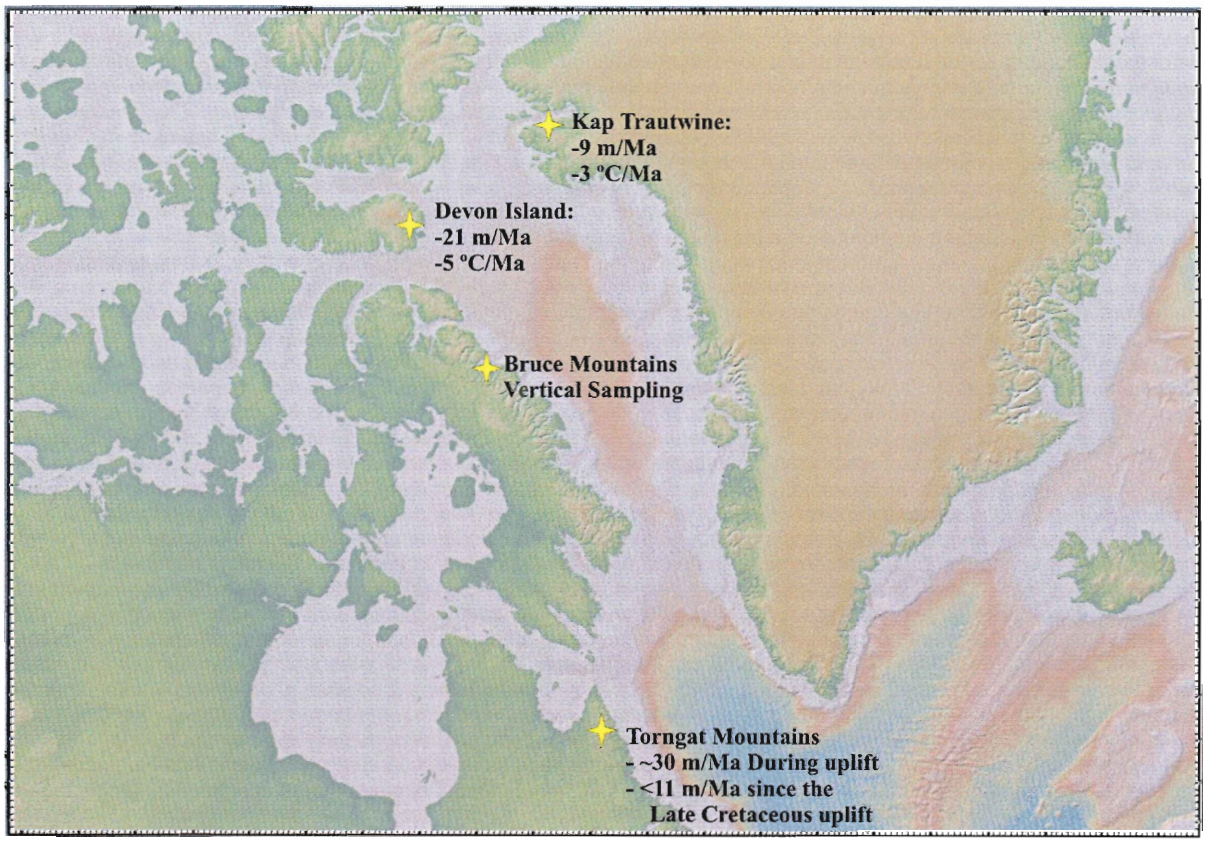

***Figure 2.11**: Locations of observed cooling and erosion from previous low-temperature thermochronologic studies near the study region and along the Eastern Arctic Rim, as well as the location of the Bruce Mountains vertical transect from this study is displayed. (Data from Kap Trautwine, NW Greenland and eastern Devon Island is from Grist and Zentilli, 2004; data from Torngat Mountains of Labrador is from Centeno, 2005).*

3 METHODS

3.1 Sampling Strategy

Sampling for this study was carried out during a 2005 field expedition, as part of cooperation between J. Gosse of Dalhousie University and scientists from the Canada-Nunavut Geoscience Office and the Geological Survey of Canada. Samples of granitic to granodioritic gneiss and migmatite (Fig. 3.1) ranging in mass from 1.5 - 3 kg were collected along two transects in the north-central Baffin Island study area: one vertical and one horizontal SW-NE sampling transect (Fig. 1.2).

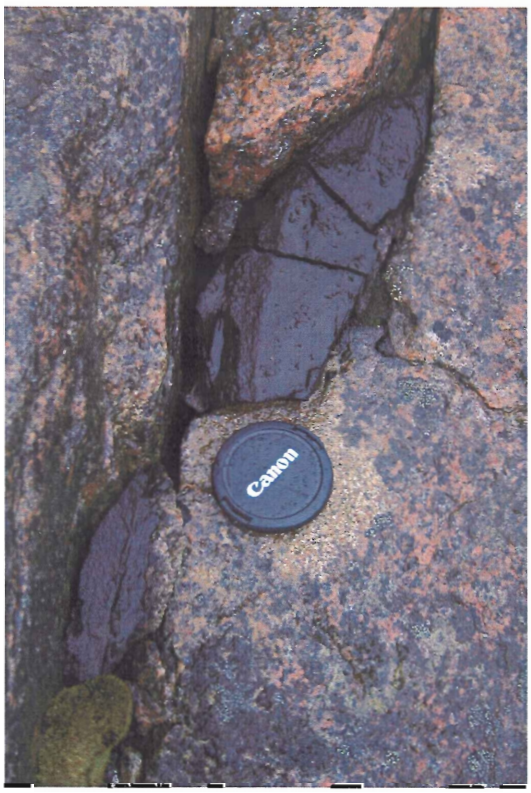

***Figure 3.1**: Photograph of orthogneiss similar to that sampled for (U-Th-Sm)/He analysis. Also seen in photo is Paleocene mudstone found near Rimrock Lake.*

3.1.1 SW-NE Horizontal Sampling Transect

The horizontal transect extends from Steensby Inlet of Foxe Basin, NE to Baffin Bay over a distance of ~230 km (Fig. 1.2). This SW-NE transect is perpendicular to the average strike of the rifted margin and parallel to the dip observed in the north-central Baffin Island region. The horizontal transect was strategically positioned to cross three major NW-SE normal faults (Nina Bang, Central Borden, and White Bay faults). All samples were collected at about 400 m elevation (with one exception, FT07-39) at spacing of 5 km in the northern half of the transect, and 10 km in the southern half. Collection of samples at a uniform elevation was possible by sampling along walls of incised valleys within the high relief provinces of the study area. The principle objective of sampling along a horizontal transect was to document any exhumational variations across Baffin Island, with zones of younger He ages being interpreted as areas with greater exhumation. This transect was also strategically positioned to cross the major NW-SE drainage divide, controlled by topography within the Davis Highlands. The intention of this positioning was to identify a rift flank denudational model that is most suiting for the Eastern Arctic Rim in the north-central Baffin Island region (Pinned -divide, Scarp retreat, or Down warping). Also, the positioning of the horizontal transect across major NW-SE trending faults will allow determination of any post Paleozoic slip in the region.

3.1.2 Bruce Mountains Vertical Sampling Transect

The location of the vertical transect was selected subject to a number of constraints. The vertical transect had to; (i) be free from any fault dissection, (ii) be near both the horizontal transect and the rift margin, and (iii) allow sampling access from near sea level to over 1000 m in order to maximize the potential of capturing thermal signatures that could assist in documenting the timing and rates of cooling of the rift margin. Ten samples were collected in the Bruce Mountains of the Davis Highlands, at increments of approximately 110 m elevation, from roughly sea level (40 m asl) to 1028 m asl (Fig. 3.1). A principle objective of this transect was to relate observed periods of accelerated cooling with periods of rift-related uplift in the north-central Baffin Island area. Regardless of the period of cooling observed from the vertical transect, information from it can be used to calculate a rough erosion rate for the vertical rock column.

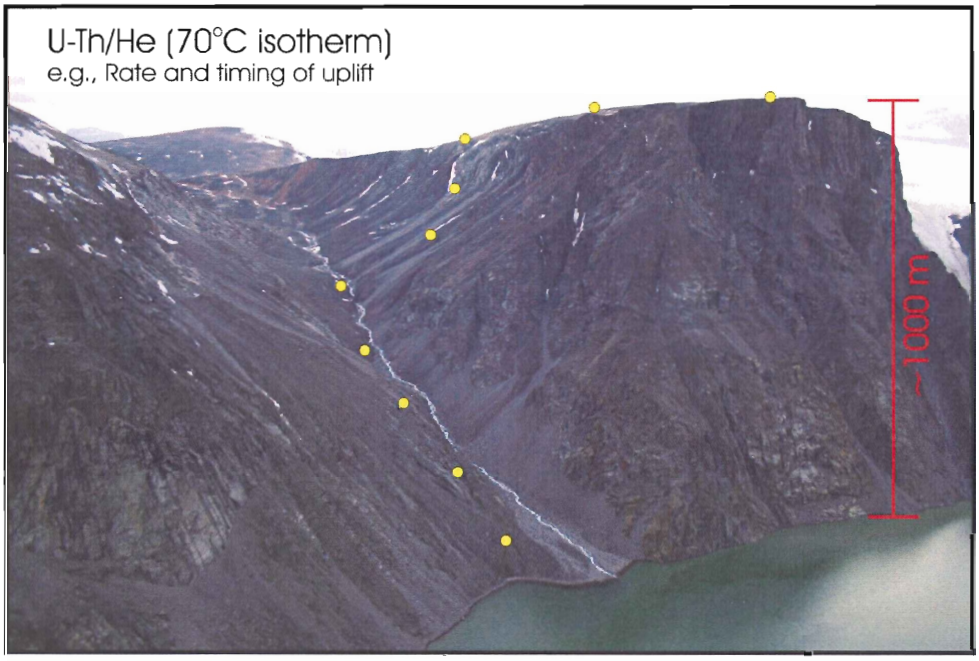

***Fig 3.2**: Vertical transect sample locations at ~100 m intervals up a 1000 m elevation mountain located within the Davis Highlands.*

3.2 (U-Th-Sm)/He Thermochronology

(U-Th-Sm)/He thermochronometry is becoming a widely utilized method for establishing the cooling histories of rocks. This technique is based upon the radioactive decay series of ^{238}U, ^{235}U, ^{232}Th, and ^{147}Sm sequentially producing stable alpha-particles (or ^{4}He nuclei). The amount of time since a mineral cooled through its closing temperature can be calculated using the present day amounts of parent and daughter nuclei within the crystal and the equation:

$$^{4}He = 8\ ^{238}U\ (e^{(\lambda_{238}t)} - 1) + 7\ (^{235}U/137.88)\ (e^{(\lambda_{235}t)} - 1)$$

$$+ 6\ ^{232}Th\ (e^{(\lambda_{232}t)} - 1) + ^{147}Sm\ (e^{(\lambda_{147}t)} - 1)) \qquad (3.1);$$

where λ is the decay constant for the parent atoms ($\lambda_{238} = 1.551 \times 10^{-10}\ y^{-1}$, $\lambda_{235} = 9.849 \times 10^{-10}\ y^{-1}$, $\lambda_{232} = 4.948 \times 10^{-11}\ y^{-1}$, $\lambda_{147} = 6.539 \times 10^{-12} y^{-1}$) and **t** is the time (years) He has been accumulating in the mineral (Farley, 2002).

Many minerals can be used for (U-Th-Sm)/He thermochronometry but apatite has become a popular mineral for (U-Th-Sm)/He dating due to its low closing temperature of ~75°C for Helium diffusion (Ehlers and Farley, 2003). The temperature range between ~75-40°C is referred to as the partial retention zone (PRZ), as only partial diffusion takes place and He concentration no longer remains at zero. Apparent closing temperature is thus largely dependant upon the amount of time spent within the PRZ and radius of the apatite crystal (Farley and Stockli, 2002). A closing temperature of <75°C corresponds to 2 to 4 km of crustal depth depending on geothermal gradient, making apatite (U-Th-Sm)/He thermochronometry of particular interest to dating events and processes that influence local

topography and the thermal character of shallow crust such as uplift, burial, exhumation, and erosion.

These processes that shape the earth's surface also have a strong effect on shallow crustal isotherms. Surface uplift and exhumation processes have an effect of decreasing and increasing the geothermal gradient respectively (Fig. 3.3). The maximum change in geothermal gradient is reached once the system has come to equilibrium by means of advection of heat, which can take over 40 Ma to achieve (Mancktelow and Grasemann, 1997). If an exhumation rate is calculated using low temperature thermochronometry during a period where equilibrium has not yet been reached, the result will be an overestimated rate during exhumation events due to the downward shift of isotherms as crustal material is being exhumed. The opposite of this is an underestimated exhumation rate when measured erosion rates are taken during equilibration to surface uplift. Mancktelow and Grasemann (1997) point out that for exhumation rates < 100m/Ma the effects of exhumation on isotherms can be disregarded due to geologically insignificant error in measured exhumation rates (< 7m/Ma).

It is also important to understand the character of shallow isotherms in response to mountainous and basin and range topography. A common assumption is that upper crustal geothermal gradients are roughly 25˚C/km, meaning that apatite (U-Th-Sm)/He thermochronology records the cooling history of the upper 3 km of the earths crust. At these depths it has been shown that isotherms mimic topography quite closely, resulting in elevated geothermal gradients underlying valleys, and decreased gradients beneath ridges (Fig 3.4) (Mancktelow and Grasemann, 1997). This is clearly an immediate variation from a basic 25 ˚C/km assumed geothermal gradient. Again the effects of equilibration of isotherms to the

formation of topography can be disregarded for exhumation rates below 100m/Ma, but the affect on geothermal gradient must be acknowledged.

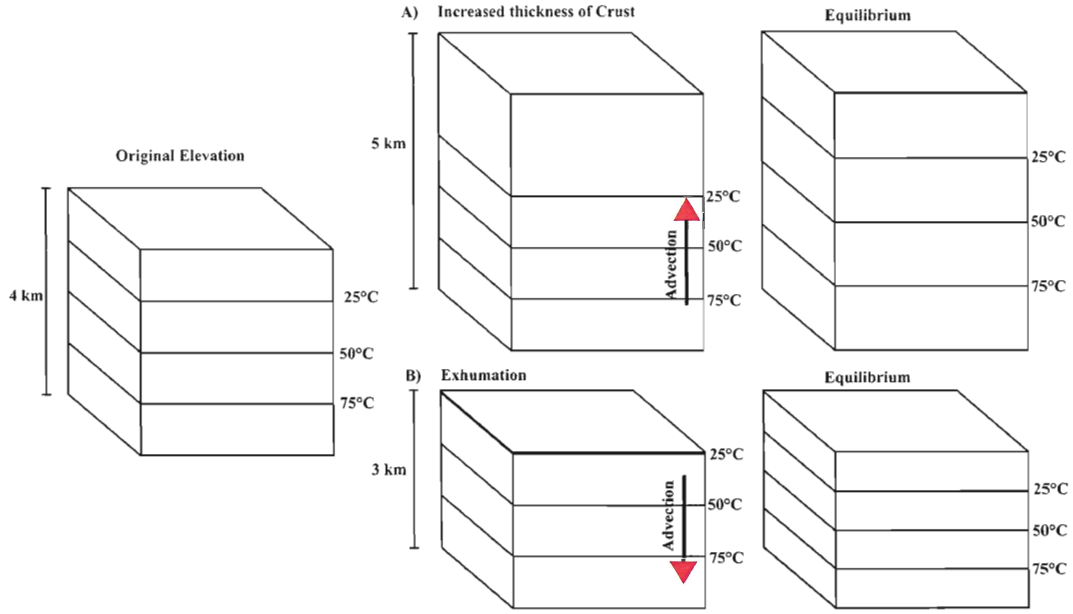

Figure 3.3: *Affects of surface uplift and exhumation on shallow geothermal gradients. A) and B) are both deviations from an original crustal block that has a geothermal gradient of 25˚C/km; A) An immediate increase of 1 km of crustal material (deposition) will reach equilibrium by advection of heat towards the surface from the earth's core. Once the system has equilibrated the geothermal gradient is 20˚C/km. B) Instantaneous exhumation of 1 km results in advection of heat towards the earth's core. The equilibrated system will have a geothermal gradient of 33˚C/km.*

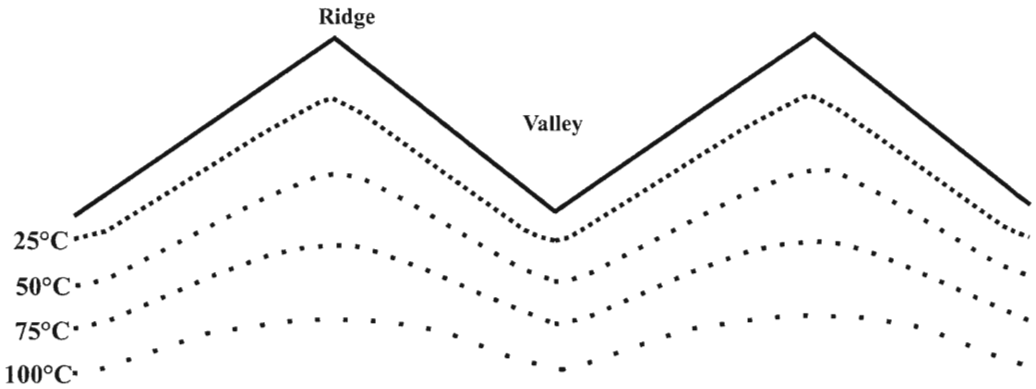

Figure 3.4: *A 2 dimensional view of how local topography affects the shallow thermal character of a region after equilibration to erosion has been reached. Beneath valleys increased geothermal gradients are observed where as beneath ridges a decreased geothermal gradient is observed.*

In a rifted margin environment such as Baffin Island, both factors can influence the shallow thermal character simultaneously (Figure 3.5). This implies that if (U-Th-Sm)/He studies identify a period of accelerated cooling induced by exhumation, factors affecting shallow isotherms must be considered.

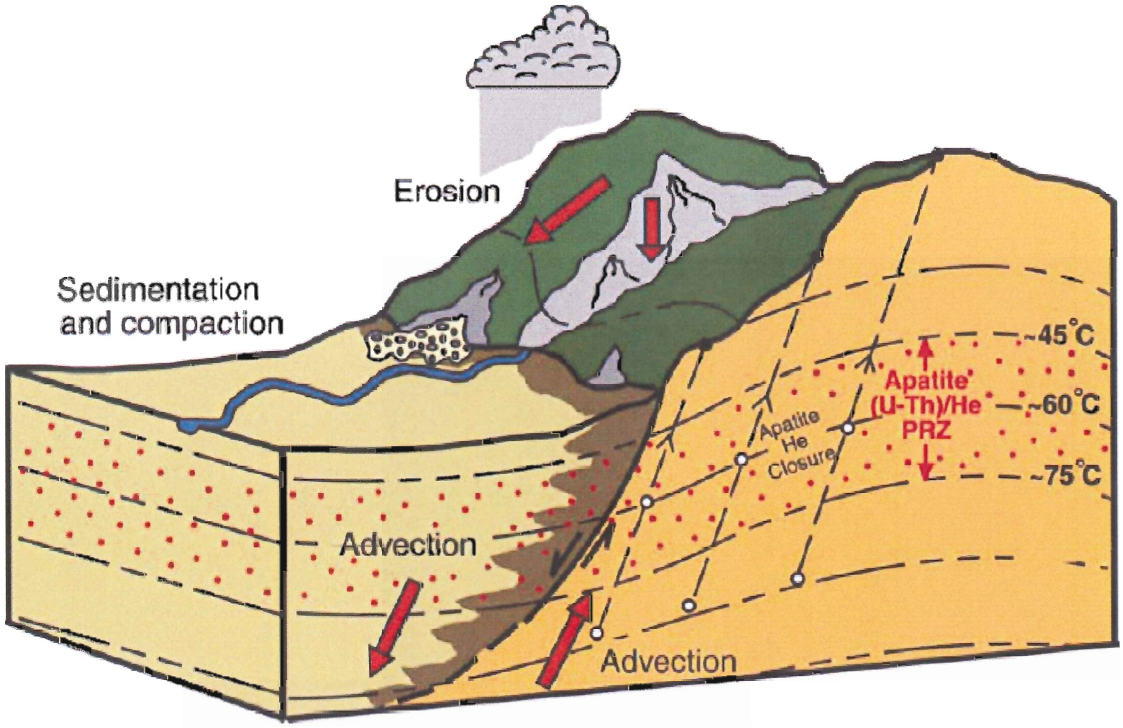

Figure 3.5*: The combination of advection due to uplift and topographic influences on the geothermal gradients of a normal fault environment, such that is present along the Eastern Arctic Rim. Geothermal gradients are decreased on the footwall and increased on the hanging wall, and isotherms closely follow topographic features such as valleys and ridges (figure from Ehlers and Farley, 2003)*

3.3 Physical Processing of Samples

The process of isolating apatite crystals from the samples began with the crushing of approximately 800 g aliquots of the whole rock samples. This process was completed by members of the Dalhousie Geochronology Centre. Samples were crushed, ground, and sieved to isolate grains of sufficient size (>30 μm). The isolated fraction of crushed and ground sample was further separated based on density using heavy liquid separation and on magnetic properties using a Frantz Isomagnetic separator. A minimum of 5 g of non-magnetic heavy phases (primarily zircon and apatite) were isolated from each sample. In a few instances where insufficient apatite was isolated, more of the rock was processed. Three samples from the base of the vertical transect (FT07-08, FT07-09, and FT07-10) did not contain sufficient high quality apatite. Fortunately, in 2007 a GSC-CNGO field party was able to recollect samples along the same vertical transect, but in slightly different locations. These duplicate samples (FT07-73, FT07-74, and FT07-75) contained sufficient apatite for (U-Th-Sm)/He dating.

3.4 Apatite Crystal Selection

Crystal selection is the most important and laborious component of the (U-Th-Sm)/He procedure. The main objective during crystal selection is to isolate grains of high quality apatite from each sample to achieve a sufficiently precise age. Other factors such as F_T correction (described in § 3.7) will also contribute uncertainty (~2-25% error at 1σ) based on the crystal size and dimensions. The desired coefficient of variation about the mean age (σ/μ, σ = Standard deviation and μ = mean) is <5% for ages of individual apatite crystals

from the same sample. To achieve this precision the goal was to collect 5 grains from each sample, in accordance with recommendations from previous studies (Centeno, 2005; Hanson and Reiners, 2006).

The first stage of crystal selection was conducted at low powers of magnification (35.2-105.6X) using a Stemi SV11 Zeiss binocular microscope that allows ample room between the stage and objective lens to maneuver the samples during the first separation process. A major consideration during this stage is the size and general shape of the crystal. The size of the apatite crystal has proved to be an important consideration due to its aforementioned diffusive behavior within the PRZ. Fitzgerald et al. (2006) showed that measured He ages of samples that spent extended periods of time in the PRZ displayed much larger range and poor reproducibility of ages than He ages of crystals that spent relatively short periods of time. Crystal size and symmetry considerations are also necessary in order to minimize the amount of error associated with the alpha particle ejection modeling and F_t Correction (§ 3.7; Ehlers and Farley, 2003). Appropriate crystals have approximately a 2-1 to 3-1 length to width ratio with the largest radius possible. For example a crystal radius of 25 μm yields an F_T correction of 0.51 and a corrected He age uncertainty of 26% (refer to § 3.7 for details on F_T corrections). Crystals with perfectly symmetrical (or close to) hexagonal crystal shape were sought. Measurements of length and width (all three distances between apices) were taken for input into the F_T equation to correct measured Helium ages (Fig 3.6). Grains were also measured and photographed using the binocular microscope and with a PaxCAM and PaxIt software which enables real time calibrated measurement of crystal axes lengths.

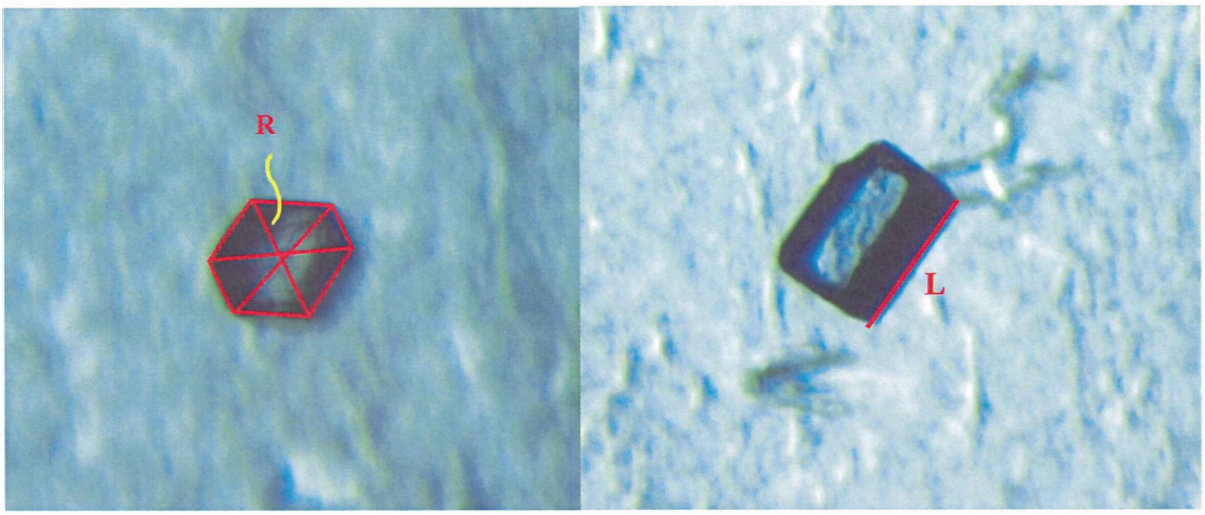

Figure 3.6: *Example of apatite crystal (FT07-28-8) and dimensions that were measured during the crystal selection process indicated in red. Also shown are the R and L dimensions that are used for calculating the crystal's surface area to volume ratio for the F_T correction.*

Apatite crystals with appropriate shape and size were further rejected if imperfections were present. Imperfections such as inclusions or bubbles may be an unwanted source of parent and daughter atoms (Fig. 3.7). Bubbles may contain additional He with an uncertain isotopic ratio. Mineral inclusions such as zircon, and monazite are rich in U-Th-Sm, and can yield an erroneously old (U-Th-Sm)/He age by producing "parentless" He in thermochronologic studies (Vermeesch et al., 2007). The presence of inclusions also incorporates error into the Ft correction calculations due to the non-homogeneous distribution of U-Th-Sm atoms, as homogeneous distribution is a fundamental assumption of the alpha particle emission models (§ 3.7; Vermeesch et al., 2007). In order to thoroughly examine apatite grains for inclusions, higher powers of magnification are necessary to identify microscopic and needle-like inclusions that are not visible under low powers. A Zeiss Axioplan binocular microscope at 44-400X magnification with computer operated stage was used to view 10-14 apatite crystals from each sample location that were considered suitable for testing based on size and crystal geometry. All crystals that were viewed with

this microscope were also photographed for reference (refer to Appendix B). Apatite crystals that that were of appropriate size, symmetry, geometry and void of inclusions were then ready for heating and gas extraction. Each crystal was loaded into platinum crucibles for He gas extraction. Platinum crucibles are hollow, open-ended cylinders about 0.5 mm in diameter by 1 mm length (Fig 3.8). Platinum is ideal for this procedure due to the low hydrogen content, high melting temperature (1768 ˚C) and malleability of the metal, but dissolution of the metal during U-Th-Sm analysis can cause interference on the ^{232}Th (discussed further in §3.6; Evans et al., 2005). Once apatite grains are enclosed within the crucibles, the samples are ready for Helium gas measurement by heating and mass spectrometry.

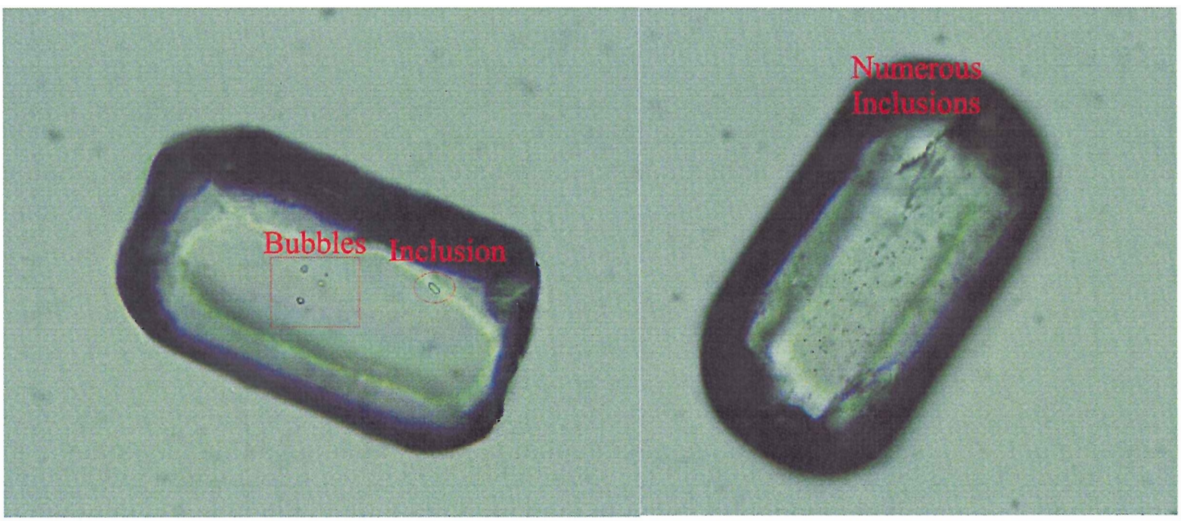

***Figure 3.7**: Two different types of imperfections are presented in this figure of examples of rejected crystals. The grain on the left displays a typical zircon inclusion that may contains high levels of U-Th-Sm, as well as bubbles within the center of the crystal that may contain He. On the right is a crystal with many very small inclusions that can contribute a substantial amount of U and Th. Both types of inclusions were quite common in the apatite from north-central Baffin Island.*

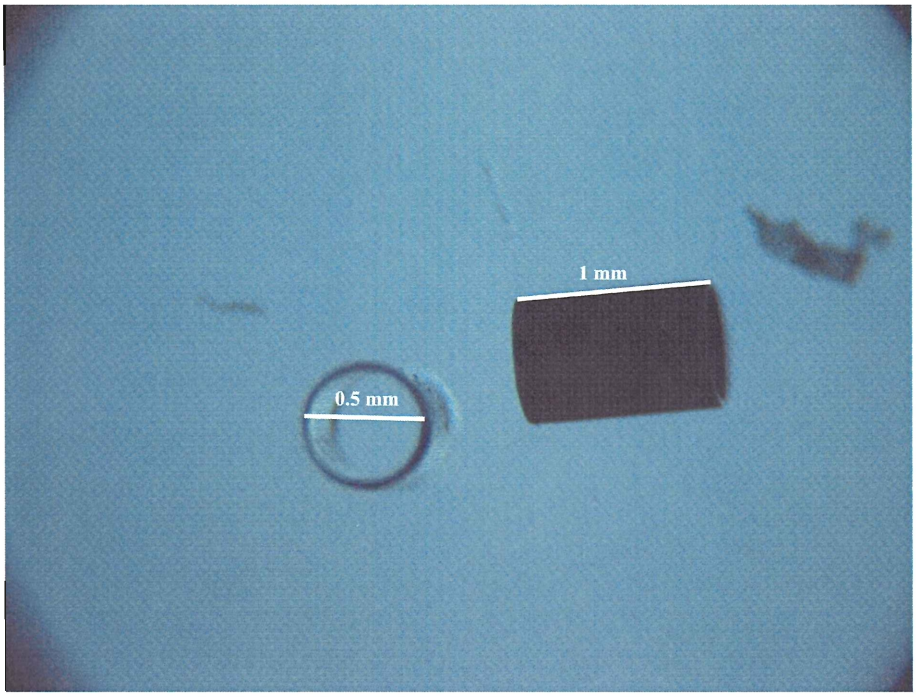

Figure 3.8: *Dimensions of platinum cylinder that apatite crystals are placed in for He extraction. Ends are pinched off once the crystal is inside.*

3.5 Helium Gas Extraction: Mass Spectrometry

The first step towards obtaining a (U-Th-Sm)/He age is the precise measurement of ^{4}He present within the apatite crystals. All He measurements were completed by the He mass spectrometer in the Dalhousie Geochronology Centre - Noble Gas Lab, operated by K. Taylor. The spectrometry involves a process of heating the sample with a laser or furnace, vacuo extraction, purification, spiking with a known ^{3}He spike, and analysis of the $^{3}He/^{4}He$ by a mass spectrometer (Fig. 3.9). For any gas extraction system to obtain accurate results, it is necessary to completely degas all parts of the gas extraction line and mass spectrometer. This is done by vacuum pumping the system with multiple pumps until the amount of ^{4}He within the system is less than 1% of that expected to be released from the apatite crystals during heating. This process of minimizing the amount of Helium within the mass

spectrometry system is termed "swamping the blank", and takes 24-48 hours of pumping to complete. ^{4}He measurements of blank runs were between 0.2 and 0.5 fmol. The apatite samples are placed on a 25-holder disk where they are heated and measured one at time. A measurement of the blank is taken between every apatite sample to ensure He levels are sufficiently low and to prevent contamination from the previous sample. This measured blank is subtracted from the subsequent sample measured. The average blank measurement from this study was 0.38 fmol of ^{4}He.

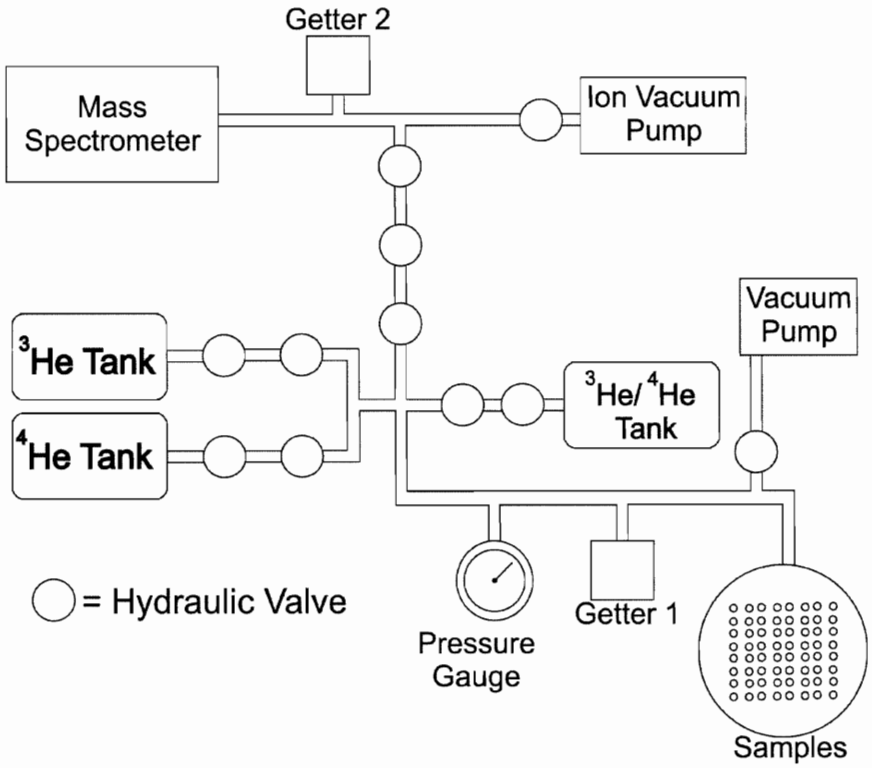

***Figure 3.9**: Dalhousie He mass spectrometer extraction line general layout. Samples are heated on the sample tray and extracted gas passes through a number of hydraulic valves and chambers before reaching the quadrupole mass spectrometer. ^{4}He tank is used to test the percision of the mass spectrometer. The third tank containing ^{3}He/ ^{4}He is used rarely to ensure the amount of spike released from ^{3}He and ^{4}He tanks is well constrained.*

A Neodymium/YAG laser was used to heat samples to 1050+/-15 ˚C when focused on the sample bearing platinum crucibles. Samples undergo two stages of heating; an initial 5 minute stage for primary degassing, and a 5 minute re-heat to ensure the sample has been completely degassed. If the re-heat measurement yields the presence of Helium, it is a good indication of inclusions being present that had not completely degassed in the first heating stage. Common mineral inclusions such as Zircon and Monazite would retain He through the first stage of heating due to their higher Helium retention temperatures (note: no crystal failed the re-heat test in this study).

After gasses are released from the sample they are moved towards the mass spectrometer through a series of hydraulic valves, and chambers (Fig. 3.9). This is done to move the gas as a single unit through the chambers, with the final result being all released He reaching the mass spectrometer as a single pulse. As the gas moves towards the mass spectrometer for analysis, it also goes through a number of filtering processes to leave ultrapure He for measurement. The first filtering process involves freezing all released gases to 8-10 K, and subsequent reheating to mobilize only the inert gasses, He and H, leaving active gases frozen. Freezing occurs once the gas has exited the sample tray into the first chamber. The second filtering process involves two "getters" that remove all hydrogen from the gas solution, leaving only He for analysis.

After the pulse of He reaches the mass spectrometer, the precise amounts of ^{3}He and ^{4}He are measured. Measurements by the mass spectrometer are not taken as amounts of ^{3}He and ^{4}He, rather the $^{3}He/^{4}He$ ratio is measured. Before reaching the mass spectrometer, the samples are spiked with 286 fmol of ^{3}He. The mass spectrometer can precisely and sensitively measure the variance from this ratio with the additional ^{4}He released from the

sample. ^{2}He (as well as Hd (doubly ionized hydrogen), and deuterium (^{2}H)) is also measured in order to avoid high levels that may cause interference.

This entire heating to measurement process is programmed into a computer connected to the mass spectrometry system, allowing the set of 25 samples to be run automatically. The ^{4}He measurements from this study ranged from 1648.99 fmol to 4.82 fmol within 1.5% precision (note: Two measurements of 0.17 fmol and 0.22 fmol were returned that are below the blank measurement will be discussed further in the §4.4).

3.6 Uranium Thorium Samarium Analysis

After the crystals are degassed and He is measured, abundances of parent isotopes ^{238}U, ^{232}Th, and ^{147}Sm were measured with an inductively coupled plasma mass spectrometer (ICP-MS) at the University of Kansas. Measurement of ^{235}U is not done directly because it is assumed to exist in natural isotopic abundance (^{235}U= ^{238}U/137.88; Evans et al. 2005). Farley (2002) describes the process in which U, Th, and Sm isotopes are measured by an ICP-MS. The procedure requires the samples to be dissolved in HNO_3 while still within the platinum crucibles. This solution is also spiked with known amounts of ^{235}U, ^{230}Th, and ^{149}Sm diluted with a known amount of water, and heated in an oven to ensure the sample has been completely dissolved. Finally, the U, Th, and Sm isotope ratios are then measure with the ICP-MS to precisions <1-2% for most samples. Duplicate measurements of all samples were made with slight variation in spike volume and concentration. The amount of U-Th-Sm that is expected ranges from 10's to 1000 ppm.

In order to avoid error associated Pt dissolution, ICP-MS signals of mass 234 were monitored. Dissolution of Pt crucibles may cause the formation of ions $^{194}Pt^{40}Ar^{+}$, $^{195}Pt^{40}Ar^{+}$, and $^{194}Pt^{40}Ar^{+}$ so any increase in the normal abundance of mass 234 (0.0057%) is an indication of Pt interference (Evans et al., 2005). None of the samples were subject to substantial Pt interference.

3.7 F_T Correction

Once rocks have cooled below their closure temperature they begin to retain Helium that has formed as a result of decay from U, Th, and Sm. The alpha-particles produced during decay are released with energies between 4-8 MeV and can travel 11 μm to 34 μm (~20 μm on average) through the solid crystal before coming to rest (Farley et al., 1996). This characteristic allows a possibility for alpha-particles to be ejected from, or injected into crystals. If a parent nucleus is located more than 20 μm from the crystal surface (the maximum stopping distance) the alpha-particle has almost a 100% chance of being retained. On the other hand decays that occur within 20μm of the crystal surface will have a chance of being ejected approaching 50% directly on the crystal surface (Farley, 2002).

Farley et al. (1996) developed a model that can be used to correct for Helium ejection. This model assumes that implantation of alpha-particles is negligible, distribution of parent nuclides U, Th, and Sm is homogeneous, and a perfect hexagonal prismatic crystal habit. Their model shows that measured ages (calculated with equation 3.1) must be divided by an F_T correction factor that is calculated based on the surface area to volume ratio (ß), and the alpha-particle stopping distance that is unique to minerals and parent atoms (U, Th, and

Sm). ß and F_T can be calculated for hexagonal prisms of apatite with the following equations.

$$ß = (2.31L+2R)/(RL) \quad (3.2);$$

Where R is half the distance between opposite apices of the hexagonal crystal face, and L is the length of the hexagonal prism (Fig. 3.6).

$$^{238}U \text{ series: } {}^{U}F_T = 1 - 5.13ß^2 + 6.78ß \quad (3.3);$$

$$^{232}Th \text{ series: } {}^{Th}F_T = 1 - 5.90ß^2 + 8.99ß \quad (3.4);$$

From these two F_T correction factors, a mean correction must be calculated based on the relative amounts of U, Th, and Sm using the following equation.

$$\text{Mean } F_T = {}^{238}a\ {}^{U}F_T + (1 - {}^{238}a)\ {}^{Th}F_T \quad (3.5);$$

where ^{238}a is the fraction of He that is derived from ^{238}U.

The calculations that are involved in the F_T correction dictate which grains are suitable for testing. As noted in § 3.3, grains must not contain inclusions or bubbles, nor be zoned in order for the crystal to have homogeneous distribution of U and Th. Also, grains must be of perfect crystal habit, with equilateral hexagonal prism shape for the modeling parameters to be met, and the variable ß to truly reflect the surface area to volume ratio of the apatite crystal.

3.8 He Age Determination

Measurements were returned as individual ratios of $^{235}U/^{238}U$, $^{230}Th/^{232}Th$, and $^{149}Sm/^{147}Sm$ for each grain, which were then converted to nuclei of the radioactive elements using methods described by Evans et al. (2005) (Appendix A.4). Using the actual amount of ^{238}U, ^{235}U, ^{232}Th, ^{147}Sm nuclei and fmol of ^{4}He, as well as the empirical knowledge of these radioactive elements decay constants, measured He ages can be calculated using equation 3.1. These calculations were carried out in MatLab using an algorithm created by Jose Antinao-Rojas, outputting calculated and corrected He ages for the entire set of samples. Interpretations will be explained in chapter 5 and further discussed in § 6.

3.9 Sources of Error

The (U-Th-Sm)/He is a multi step process that incorporates error from many different sources. Measuring U, Th, Sm and He, incorporates 1 – 3 % uncertainty each that will have an effect on the precision of measured He ages. Calculated F_T corrections for each crystal will also incorporate uncertainty towards the measured He age. The uncertainty involved in the F_T correction is based on uncertainties in the process of grain measurement, and "a conservative estimate on how well typical apatite crystals approximate the idealized hexagonal prism geometry" (Ehlers and Farley, 2003). This estimate of uncertainty drastically increases as crystal dimensions decrease and the magnitude of the F_T corrections increases (Fig. 3.10). For this study the uncertainty associated with the F_T correction was between 2 and ~25 % (Fig. 3.10). All sources of analytical error were summed in quadrature (Eqn. 3.6) to establish the total analytical error ($^{4}He = 8\ ^{238}U\ (e\text{^}(\lambda_{238}t) - 1) + 7\ (^{235}U/137.88)\ (e\text{^}(\lambda_{235}t) - 1) + 6\ ^{232}Th\ (e\text{^}(\lambda_{232}t) - 1) + ^{147}Sm\ (e\text{^}(\lambda_{147}t) - 1)$; Table 3.1 and Table 3.2)

$$\sigma = (U^2 + Th^2 + Sm^2 + He^2 + F_T^2)^{1/2} \qquad 3.6$$

Vertical Transect Sample Uncertainty						
	Uncertainty in Measurements					
Sample #	U	Th	Sm	He	FT	Total Analytical Error
FT07-01-1	1.120	0.524	0.725	1.500	10.815	11.012
FT07-01-2	1.148	0.824	1.252	1.500	11.542	11.791
FT07-01-3	1.123	0.809	1.069	1.500	6.984	7.355
FT07-01-6	1.191	1.209	2.561	1.500	11.170	11.681
FT07-01-9	1.557	1.461	1.732	1.500	15.277	15.595
FT07-02-1	1.272	0.233	1.689	1.500	8.478	8.869
FT07-02-2	0.641	1.740	1.376	1.500	9.545	9.934
FT07-02-3	1.141	1.629	1.047	1.500	4.624	5.356
FT07-02-4	0.649	1.384	0.269	1.500	3.897	4.454
FT07-02-6	1.503	0.566	2.158	1.500	7.370	7.988
FT07-03-2	0.680	0.974	0.780	1.500	4.729	5.160
FT07-03-4	0.579	1.758	0.947	1.500	7.787	8.198
FT07-03-7	1.807	1.523	1.015	1.500	10.815	11.217
FT07-03-8	0.362	1.469	0.997	1.500	11.542	11.779
FT07-03-9	1.184	0.170	1.452	1.500	9.261	9.568
FT07-04-5	1.665	1.409	1.029	1.500	4.948	5.705
FT07-04-6	1.413	1.417	1.086	1.500	3.593	4.510
FT07-04-7	0.579	0.877	0.761	1.500	6.138	6.451
FT07-04-8	0.882	0.726	0.758	1.500	4.523	4.959
FT07-04-9	1.859	0.946	2.757	1.500	5.564	6.720
FT07-05-2	1.271	1.198	0.631	1.500	7.787	8.144
FT07-05-3	0.718	0.966	0.785	1.500	5.063	5.472
FT07-05-4	1.274	0.583	0.478	1.500	6.458	6.793
FT07-05-6	0.712	2.256	1.272	1.500	8.238	8.794
FT07-06-1	0.683	1.181	0.299	1.500	3.454	4.016
FT07-06-2	0.575	0.748	0.367	1.500	4.836	5.164
FT07-06-6	0.523	0.582	0.759	1.500	4.062	4.465
FT07-07-1	1.140	0.377	0.174	1.500	4.062	4.497
FT07-07-2	0.569	0.881	0.352	1.500	3.897	4.319
FT07-07-4	0.459	1.176	0.458	1.500	8.478	8.714
FT07-07-6	2.200	1.086	0.943	1.500	12.341	12.707
FT07-07-7	1.211	0.474	0.982	1.500	7.370	7.695
FT07-73-10	1.020	0.922	1.214	1.500	17.132	17.295
FT07-73-7	0.555	0.492	0.512	1.500	12.203	12.327
FT07-74-1	1.026	0.891	2.280	1.500	26.312	26.488
FT07-74-11	3.077	1.344	1.653	1.500	12.482	13.117
FT07-75-10	0.672	0.655	0.691	1.500	8.728	8.932
FT07-75-11	0.556	0.711	0.143	1.500	17.358	17.447

***Table 3.1**: Uncertainties involved in the measurement (% error) of U, Th, Sm, and He, and F_T correction from the Bruce Mountains vertical sampling transect.*

Horizontal Transect Sample Uncertainties						
	Uncertainty in Measurements					
Sample #	Uranium	Thorium	Samarium	Helium	Ft Correction	Total Analytical Error (%)
FT07-21-3	1.83	3.69	2.20	1.50	9.08	10.32
FT07-21-10	1.12	0.77	2.15	1.50	21.95	22.15
FT07-22-1	5.34	0.56	0.93	1.50	13.07	14.24
FT07-22-4	1.56	0.48	1.66	1.50	6.92	7.46
FT07-22-8	0.94	1.10	0.95	1.50	4.87	5.39
FT07-25-3	0.88	0.98	1.12	1.50	1.70	2.85
FT07-25-5	0.71	0.95	1.75	1.50	4.27	4.99
FT07-25-6	1.29	0.53	2.61	1.50	6.80	7.57
FT07-26-1	1.00	0.85	0.60	1.50	5.14	5.55
FT07-26-8	1.73	0.56	1.55	1.50	5.56	6.24
FT07-27-4	1.39	1.07	1.19	1.50	6.63	7.12
FT07-27-5	0.93	0.76	0.56	1.50	5.52	5.87
FT07-27-6	0.37	0.91	0.80	1.50	4.15	4.59
FT07-28-2	0.86	0.89	0.58	1.50	10.59	10.78
FT07-28-3	1.82	0.44	0.24	1.50	8.81	9.14
FT07-29-4	1.09	0.70	1.96	1.50	11.67	12.00
FT07-29-5	1.40	0.84	1.90	1.50	5.10	5.88
FT07-29-6	5.31	1.18	2.29	1.50	13.38	14.70
FT07-30-2	4.47	1.08	1.99	1.50	9.94	11.23
FT07-30-5	2.06	0.67	1.94	1.50	14.37	14.74
FT07-31-12	1.12	0.47	1.69	1.50	8.73	9.10
FT07-31-13	1.14	0.51	1.09	1.50	6.63	6.99
FT07-32-1	0.99	0.49	1.49	1.50	13.86	14.06
FT07-32-11	0.66	0.61	0.61	1.50	3.82	4.24
FT07-33-2	3.75	0.90	3.17	1.50	14.72	15.62
FT07-33-8	1.10	1.11	1.97	1.50	4.46	5.33
FT07-34-2	2.20	2.86	0.69	1.50	6.46	7.58
FT07-34-10	0.63	0.51	0.64	1.50	3.98	4.38
FT07-35-6	1.28	0.53	2.06	1.50	18.06	18.29
FT07-35-11	1.48	1.15	1.01	1.50	20.15	20.32
FT07-36-1	0.85	0.34	0.95	1.50	14.54	14.68
FT07-36-7	1.89	0.62	0.62	1.50	16.27	16.47
FT07-37-2	1.59	0.50	2.11	1.50	12.48	12.86
FT07-37-7	0.85	0.53	0.57	1.50	5.84	6.14
FT07-39-4	1.13	0.89	1.87	1.50	10.37	10.74
FT07-39-5	0.84	1.20	1.29	1.50	8.90	9.23

Table 3.2: *Uncertainties involved in the measurement(% error) of U, Th, Sm, and He, and F_T correction from the SW-NE horizontal sampling transect.*

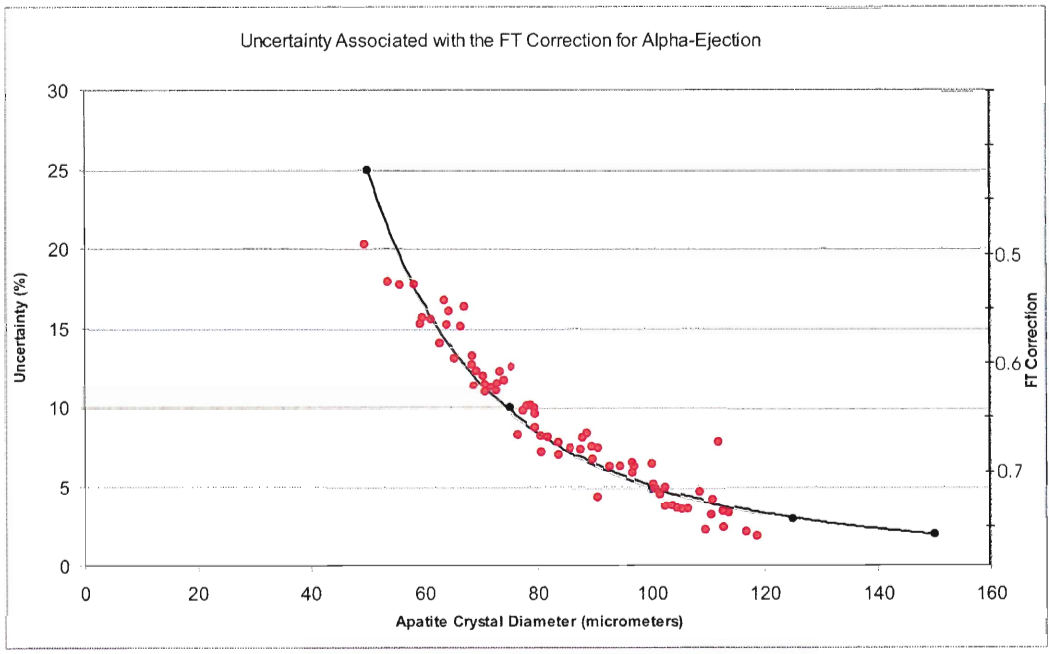

***Figure 3.10**: Approximation of uncertainty plotted and F_T correction against apatite crystal diameter. Crystal radius and corresponding F_T correction (right y-axis) from this study plotted as red points (Data from Ehlers and Farley, 2003)*

There are also many sources of error that can not be accounted for quantitatively. Crystal properties such as rounding, and zoning incorporate random error that affects the accuracy of measured He ages. U-Th-Sm bearing inclusions on the other hand incorporate systematic error in that they will have the general effect of increasing He ages due to increased amounts of radiogenic He. During the interpretation process assuming geothermal gradients can be the source of variable amounts of random error. Assuming a constant geothermal gradient is unrealistic due to the dynamic nature of thermal energy within the earths crust. Also, assuming isotherms are at a constant depth below the surface is a source of random error in that it assumes that topographic features as well as uplift and exhumation have no effect on local geothermal gradients.

4 Results

4.1 Apatite Selection

The apatite selection process was complicated by the quantity and quality of crystals present in the samples. Apatite abundance varied from sample to sample with many of the samples containing a high concentration of the mineral, but in a few samples no suitable apatite crystals were identified. Of the 28 samples that were crushed and mechanically separated, two were completely void of apatite grains that were acceptable for testing (FT07-23 and FT07-24). The other 26 samples displayed a scarcity of grains appropriate for (U-Th-Sm)\He thermochronometry, with the vast majority of apatite crystals being under the size threshold, completely non-symmetrical, mechanically weathered or infested with inclusions. This rarity of ideal apatite crystals necessitated that the largest of the small crystal fraction and most symmetrical of the non-symmetrical grains would be accepted. Also, crystals that held small amounts of inclusions were also accepted as long as the inclusion dimensions were minute compared to the dimensions of the crystals in which they were enclosed. It was shown by Vermeesch et al., (2007) that the amount of additional radiogenic He from small amounts of inclusions that are less than a few percent of the length, width and height of the crystal is negligible. For example a zircon inclusion with 5000ppm of U (upper concentration limit) that is 1% of the length, width and height (1/1,000,000 of the volume) of an apatite crystal with 20 ppm of U will contribute <0.025% of the He that the apatite crystal will. With exceptions in crystal size, symmetry and inclusions, a maximum of 5 grains per sample moved on to the extraction phase, but in many samples only 2 grains from each sample were tested for He, U, Th and Sm (refer to Appendix B for images of apatite crystals).

4.2 SW-NE Horizontal Transect Results

Samples from the SW-NE transect showed an inconsistency in the quantity of apatite crystals that were suitable for testing. Samples FT07-23 and FT07-24 from this sampling transect were completely devoid of suitable apatite grains, so measurements from these sample locations were not taken. Though apatite was present in the 16 remaining samples, limited quantities of high quality crystals were available, so only two He ages were measured from many of the samples. He ages from this sampling transect displayed a wide range (16 ± 2 Ma to 657 ± 71 Ma) (Table 4.1). Two ages of 16Ma (FT07-29-6 and FT07-22-8) in particular dramatically stand out from the rest. During He extraction these crystal had ^{4}He measurements that were less than the blank measurement. The cause of young He ages along the Baffin Bay margin cannot be stated with confidence, but their He age reproduction, and proximity to each other, as well as another anomalously low He age of FT07-22-8 (60 Ma) gives reason to believe they have geologic significance that will be discussed in §5.1. For the purpose of general interpretation of the horizontal transect they were removed due to the fact that the majority of the remaining samples only had two crystals suitable for dating. He ages significantly older than that constrained by the highest elevation sample of the Bruce Mountains (~300 Ma, §4.3) are unlikely, so He ages over 400Ma were removed. With these ages removed the weighted averages and weighted standard deviations were calculated based on the uncertainty associated with each calculated (U-Th-Sm)/He age (Table 4.2, Appendix A.6). Using the weighted mean permits ages with less uncertainty to have more weight when calculating the mean for that sample.

Sample	Lat.	Long.	Elev. (m)	Distance from Margin	Crystal R	U (ppm)	Th (ppm)	Sm (ppm)	He (fmol)	He Age	Mean Ft	Corrected age	Uncertainty	(+/-)σ
FI07-29-4	71.74	73.71	366	0	39	173.00	199.73	246.97	53.79	164	0.62	263	12.00	32
FI07-29-5				0	27	47.90	24.05	109.52	30.25	159	0.72	220	5.88	13
FI07-29-6				0	33	12.71	43.65	42.89	0.22	9	0.58	16	14.70	2
FI07-21-3	71.69	73.84	351	7500	44	76.45	46.93	100.31	16.22	111	0.65	171	10.32	18
FI07-21-10				7500	51	144.13	97.84	88.68	12.56	98	0.54	182	22.15	40
FI07-22-1	71.68	74.04	306	13500	80	5.18	60.48	159.58	0.17	9	0.56	16	14.24	2
FI07-22-4				13500	54	128.58	24.06	111.13	38.40	141	0.68	208	7.46	15
FI07-22-8				13500	44	76.66	127.34	261.53	18.78	43	0.72	60	5.39	3
FI07-23	71.64	74.09	608											
FI07-30-2	71.58	74.25	589	26500	50	15.27	85.67	80.28	4.82	95	0.61	154	11.23	17
FI07-30-5				26500	48	55.32	196.04	132.67	8.96	98	0.56	174	14.74	26
FI07-24	71.50	74.58	487											
FI07-25-3	71.46	74.67	425	46500	45	112.72	89.30	68.43	506.91	327	0.81	404	2.85	12
FI07-25-5				46500	48	70.95	46.96	60.61	67.13	226	0.73	310	4.99	15
FI07-25-6				46500	55	32.98	42.33	50.87	15.95	173	0.67	257	7.57	19
FI07-26-1	71.43	74.76	419	51000	36	134.57	84.36	92.35	150.95	366	0.70	521	5.55	29
FI07-26-8				51000	39	26.85	28.86	73.72	13.52	140	0.70	200	6.24	12
FI07-27-4	71.38	74.82	469	56000	35	234.45	184.37	154.86	226.07	331	0.69	482	7.12	34
FI07-27-5				56000	50	219.76	141.31	101.06	154.09	218	0.70	310	5.87	18
FI07-27-6				56000	33	537.61	404.35	220.96	1648.99	320	0.76	420	4.59	19
FI07-28-2	71.33	75.00	529	65000	37	50.66	182.23	305.37	58.27	406	0.62	657	10.78	71
FI07-28-3				65000	32	50.86	23.14	106.77	11.56	123	0.65	189	2.20	4
FI07-31-12	71.27	75.20	452	75000	40	58.19	181.63	81.41	48.56	209	0.66	318	9.10	29
FI07-31-13				75000	45	142.24	107.08	132.09	102.33	205	0.70	294	6.99	21
FI07-32-1	71.21	75.32	511	82000	32	157.40	291.63	67.30	76.79	225	0.61	372	14.06	52
FI07-32-11				82000	57	93.85	192.82	110.36	228.37	304	0.75	407	4.24	17
FI07-33-2	71.17	75.48	443	90000	32	36.16	107.87	84.05	6.53	134	0.55	242	15.62	38
FI07-33-8				90000	53	73.95	48.77	40.26	120.92	274	0.74	369	5.33	20
FI07-34-2	71.03	75.90	422	111500	45	674.43	480.04	208.23	413.39	234	0.68	344	7.58	26
FI07-34-10				111500	56	235.54	219.85	219.90	368.05	336	0.73	460	4.38	20
FI07-35-6	70.79	76.58	508	147500	29	76.65	139.83	225.01	12.56	158	0.54	292	18.29	54
FI07-35-11				147500	28	132.64	230.95	259.14	38.86	255	0.54	472	20.32	96
FI07-36-1	70.60	77.08	459	175500	32	74.93	365.12	264.55	33.75	183	0.58	317	14.68	47
FI07-36-7				175500	30	84.89	257.48	418.01	23.70	143	0.57	251	16.47	41
FI07-37-2	70.46	77.48	404	197500	34	61.94	67.67	227.35	13.63	128	0.61	209	12.86	27
FI07-37-7				197500	47	76.77	145.24	266.87	72.63	190	0.70	269	6.14	17
FI07-39-4	70.33	77.81	76	216500	37	50.04	81.29	370.72	40.37	385	0.63	616	10.74	66
FI07-39-5				216500	39	67.97	57.86	236.70	22.98	163	0.65	251	9.23	23

***Table 4.1**: Caption on page 58.*

Sample (#)	Distance From Margin	orrected Age (M	Reason for Discard	Uncertainty	Weighted Average	Std Dev.	Elevation	400 m (0.5C/km)	400 m (2.5C/km)
FT07-29-4	0	263		0.12	234	20	366	232	234
FT07-29-5	0	220		0.06					
FT07-29-6	0	16	Anomolously young	0.15					
FT07-21-3	7500	171		0.10	175	5	351	172	174
FT07-21-10	7500	182		0.22					
FT07-22-1	13500	16	Anomolously young	0.14	208	16	306	203	207
FT07-22-4	13500	208		0.07					
FT07-22-8	13500	60	Anomolously young	0.05					
FT07-23				0.00					
FT07-30-2	26500	154		0.11	163	10	589	173	165
FT07-30-5	26500	174		0.15					
FT07-24				0.00					
FT07-25-3	46500	404	Too Old, Inclusions	0.03	289	26	425	290	289
FT07-25-5	46500	310		0.05					
FT07-25-6	46500	257		0.08					
FT07-26-1	51000	521	Inclusions	0.06	200	12	419	201	200
FT07-26-8	51000	200		0.06					
FT07-27-4	56000	482	Too Old	0.07	310	18	469	313	310
FT07-27-5	56000	310		0.06					
FT07-27-6	56000	420	Too Old	0.05					
FT07-28-2	65000	657	Too Old	0.11	189	4	529	196	191
FT07-28-3	65000	189		0.09					
FT07-31-12	75000	318		0.09	305	12	452	307	305
FT07-31-13	75000	294		0.07					
FT07-32-1	82000	372		0.14	372	52	511	378	374
FT07-32-11	82000	407	Too Old	0.04					
FT07-33-2	90000	242		0.16	337	55	443	339	338
FT07-33-8	90000	369		0.05					
FT07-34-2	111500	344		0.08	344	26	422	345	344
FT07-34-10	111500	460	Too Old	0.04					
FT07-35-6	147500	292		0.18	292	54	508	298	294
FT07-35-11	147500	472	Too Old	0.20					
FT07-36-1	175500	317		0.15	286	33	459	289	287
FT07-36-7	175500	251		0.16					
FT07-37-2	197500	209		0.13	250	28	404	250	250
FT07-37-7	197500	269		0.06					
FT07-39-4	216500	616	TO, Inclusions	0.11	251	23	76	234	247
FT07-39-5	216500	251		0.09					

***Table 4.2**: Caption on next page.*

***Table 4.1 (Page 56)**: Complete results from the SW-NE horizontal sampling transect listed in order of distance from the margin (m).*

***Table 4.2 (Page 57)**: Weighted averages from the SW-NE horizontal sampling transect with outliers removed and reasoning for removal. If average is calculated from only one sample, the uncertainty of that sample is stated as the standard deviation.*

He ages from the horizontal transect were normalized to 400 m elevation in order to reflect exposure of paleo-depths and not He ages in relation to contemporary elevation (assuming a 25°C/km, for a cooling rate of 0.5 °C/Ma and 2.5 °C/Ma from Bruce Mountains Transect for the upper Paleozoic, §4.3)(Table 4.2). The youngest He ages were observed from samples within a narrow region adjacent to Baffin Bay (within ~30km) where little land mass exists above sea level and within the eastern limit of the Davis Highland. Average He ages from this highly dissected area range from 163 ± 10 Ma to 234 ± 20 Ma (normalized to 400 m using a 0.5 °C/Ma cooling rate). The oldest ages observed from the horizontal transect occur within the Davis Highlands and Baffin Upland surface immediately SW of the coastal range. Ages within the highest elevated area range from 290 ± 26Ma to 417 ± 56Ma (with the exception of FT07-26 and FT07-28). This trend of increasing He ages gives way to a trend of He ages decreasing at roughly 147-175 km from the eastern margin. In this region near Foxe Basin measured He ages substantially decline to between 289 ± 33 Ma and 234 ± 76 Ma, still notably older than the ages measured on the Baffin Bay coast reflecting the lower amounts of exhumation on the plateau. Interpretations of this systematic trend in ages will be discussed in §5.1.

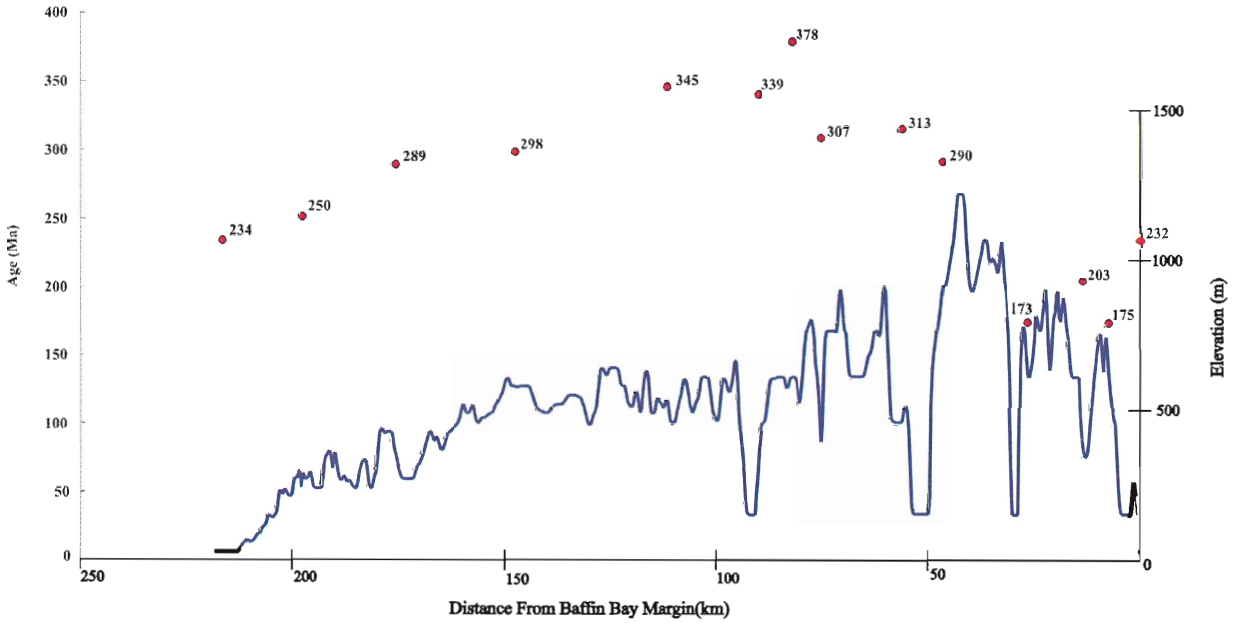

***Figure 4.1**: Topographic profile of the SW-NE horizontal transect from the 250m digital elevation map with weighted average He ages plotted at sample locations (ages normalized to 400 m using 0.5 ºC/Ma from the Bruce Mountains vertical transect). The youngest He ages are located in the front of the rift shoulder where fjord dissection is the greatest, the oldest ages are found within the Baffin Upland Surface and interior of the Davis Highlands, and the He ages furthest from Baffin Bay decline again. (Note: Samples FT07-26, FT-0-028 not plotted)*

4.3 Bruce Mountains Vertical Transect Results

A total of 10 samples was collected from the Bruce Mountains area, ranging in elevation from 40 to 1028 m. He ages through the vertical column range from 139 ± 8 Ma (690m elevation) to 493 ± 55 Ma (805m elevation), but do not show a clear trend of age increasing with elevation as would normally expected in a vertical profile of a column that underwent constant uplift and exhumation (Table 4.3). Reproducibility of (U-Th-Sm)/He ages for the Bruce Mountains vertical sampling in general is quite poor so an attempt was made to discard obvious outliers and crystals that were not ideal for testing. Sample FT07-01 constrained the highest elevated sample He age at ~300 Ma (refer to Table 4.3).

Understanding the He age should decrease with increasing depth down the column, He ages that were older than 300 Ma were removed for interpretation. Using the same rationale, ages younger than 200 Ma were removed because of good constraint of ~275 Ma He age from sample FT07-07. For samples FT07-73, and 74 in which only two apatite grains were dated and one He age was removed (>300 Ma), the uncertainty of He age is stated in place of the standard deviation. Weighted averages and standard deviations again were calculated based on uncertainty calculated in §4.2 (Table 4.4, Appendix A.6).

Table 4.3: *(next page): Complete results from the Bruce Mountains vertical sampling transect in order from most to least elevated.*

Sample #	Elevation	Latitude (N)	Longitude (W)	Crystal r	U(ppm)	Th(ppm)	Sm(ppm)	He (fmol)	He Age	Mean Ft	Corrected Age(Ma)	Uncertainty	(+/-) sigma
FT07-01-1	1028	71.15706	73.74453	36.0	117.29	34.35	158.95	32.20	169	0.64	265	11.01	29
FT07-01-2	1028			35.0	169.85	251.39	197.08	75.00	188	0.63	298	11.79	35
FT07-01-3	1028			43.5	129.90	61.92	224.76	74.80	201	0.69	292	7.35	21
FT07-01-6	1028			35.5	329.32	57.35	150.47	93.10	187	0.63	296	11.68	35
FT07-01-9	1028			31.0	146.25	45.85	231.90	39.20	224	0.59	379	15.60	59
FT07-02-1	884	71.15496	73.77113	40.0	67.04	23.43	47.81	82.80	310	0.69	449	8.87	40
FT07-02-2	884			38.0	226.51	61.09	54.61	158.50	224	0.67	333	9.93	33
FT07-02-3	884			52.0	144.95	51.85	77.52	200.20	255	0.74	343	5.36	18
FT07-02-4	884			56.0	99.35	19.95	37.70	140.40	219	0.76	288	4.45	13
FT07-02-6	884			42.5	13.05	14.20	119.42	6.59	132	0.69	192	7.99	15
FT07-03-2	805	71.15433	73.77365	51.5	298.77	251.57	102.66	549.30	295	0.74	400	5.16	21
FT07-03-4	805			41.5	174.92	36.49	96.64	73.89	166	0.68	243	8.20	20
FT07-03-7	805			36.0	83.33	72.81	157.10	46.37	310	0.63	493	11.22	55
FT07-03-8	805			35.0	247.02	54.19	180.79	74.21	168	0.64	263	11.78	31
FT07-03-9	805			38.5	208.63	61.35	173.53	85.15	224	0.65	343	9.57	33
FT07-04-5	690	71.15363	73.77026	50.5	62.39	34.12	50.37	29.51	101	0.73	139	5.70	8
FT07-04-6	690			58.0	44.55	16.51	113.36	36.41	118	0.76	154	4.51	7
FT07-04-7	690			46.0	92.32	97.18	85.51	59.60	159	0.70	225	6.45	15
FT07-04-8	690			52.5	324.91	279.58	99.73	441.14	213	0.74	287	4.96	14
FT07-04-9	690			48.0	119.15	104.24	59.46	80.90	175	0.71	247	6.72	17
FT07-05-2	562	71.14994	73.7761	41.5	182.62	116.34	322.62	228.46	310	0.69	446	8.14	36
FT07-05-3	562			50.0	112.46	38.86	255.07	75.61	169	0.72	234	5.47	13
FT07-05-4	562			45.0	141.90	382.32	376.84	128.47	192	0.69	280	6.79	19
FT07-05-6	562			40.5	183.39	34.27	306.91	92.95	202	0.68	299	8.79	26
FT07-06-1	484	71.14922	73.76467	59.0	262.50	84.94	184.65	440.65	232	0.77	302	4.02	12
FT07-06-2	484			51.0	234.68	112.81	307.31	319.51	237	0.74	321	5.16	17
FT07-06-6	484			55.0	217.98	64.33	215.04	347.53	297	0.75	397	4.47	18
FT07-07-1	334	71.14992	73.74577	55.0	40.92	292.74	267.84	120.37	200	0.73	273	4.50	12
FT07-07-2	334			56.0	82.71	417.24	264.31	229.64	200	0.74	268	4.32	12
FT07-07-4	334			40.0	199.85	162.81	406.22	155.75	237	0.68	350	8.71	31
FT07-07-6	334			34.0	33.09	23.74	277.37	8.61	117	0.63	186	12.71	24
FT07-07-7	334			42.5	115.05	20.74	277.80	58.91	193	0.69	280	7.70	22
FT07-73-7	210	71.14869	73.73525	29.5	556.28	286.10	437.64	81.91	155	0.62	251	17.30	43
FT07-73-10	210			34.2	784.41	159.73	380.94	221.89	204	0.57	359	12.33	44
FT07-74-1	110	71.14933	73.72135	24.5	275.72	102.08	269.46	21.10	128	0.50	254	26.49	67
FT07-74-11	110			33.8	127.19	67.20	220.85	37.16	237	0.60	393	13.12	52
FT07-75-10	40	71.14858	73.71501	39.5	211.30	203.29	281.84	116.72	187	0.67	279	8.93	25
FT07-75-11	40			29.3	103.41	126.55	456.83	20.80	140	0.57	244	17.45	43

The weighted mean ages display a range of 295 ± 3 Ma to 251 ± 43 Ma (Table 4.4). A general decrease of He age with depth is observed as the highest elevated sample (FT07-01 at 1028m) has a weighted average of 295 ± 3 Ma and the lowest elevated sample has a weighted average of 267 ± 17 Ma. This gives an indication that the entire column of rock within the Bruce Mountains vertical transect cooled through the apatite He closing temperature (~75 °C) from ~250-300 Ma. All samples with the exception of FT07-03 fit this average cooling trend. The interpretations of this trend will be discussed in §5.2.

Sample	Elevation(m)	Corrected He Age (Ma)	Discarded/Reasoning	Uncertainty	Weighted Average	Std Dev	2sigma
FT07-01-1	1028	265	Too Old	0.110	295	3	5
FT07-01-2		298		0.118			
FT07-01-3		292		0.074			
FT07-01-6		296		0.117			
FT07-01-9		379	Too Old	0.156			
FT07-02-1	884	449	Too Old	0.089	288	13	26
FT07-02-2		333	Too Old	0.099			
FT07-02-3		343	Too Old	0.054			
FT07-02-4		288		0.045			
FT07-02-6		192	Too Young	0.080			
FT07-03-2	805	400	Too Old	0.052	251	10	20
FT07-03-4		243		0.082			
FT07-03-7		493	Too Old	0.112			
FT07-03-8		263		0.118			
FT07-03-9		343	Too Old	0.096			
FT07-04-5	690	139	Too Young	0.057	256	27	53
FT07-04-6		154	Too Young	0.045			
FT07-04-7		225		0.065			
FT07-04-8		287		0.050			
FT07-04-9		247		0.067			
FT07-05-2	562	446	Too Old	0.081	266	28	55
FT07-05-3		234		0.055			
FT07-05-4		280		0.068			
FT07-05-6		299		0.088			
FT07-06-1	484	302	Too Old	0.040			
FT07-06-2		321	Too Old	0.052			
FT07-06-6		397	Too Old	0.045			
FT07-07-1	334	273		0.045	273	5	9
FT07-07-2		268		0.043			
FT07-07-4		350	Too Old	0.087			
FT07-07-6		186	Too Young	0.127			
FT07-07-7		280		0.077			
FT07-73-10	210	251		0.173	251	43	87
FT07-73-7		359	Too Old	0.123			
FT07-74-1	110	254		0.265	254	67	134
FT07-74-11		393	Too Old	0.131			
FT07-75-10	40	279		0.089	267	17	34
FT07-75-11		244		0.174			

***Table 4.4**: Bruce Mountains vertical transect weighted average results after outliers have been removed.*

5 Interpretations and Discussion

5.1 Implications of the SW-NE Horizontal Transect He ages

One of the main objectives of thermochronologic study of north-central Baffin Island was to determine how the Baffin Island margin has been evolving since rift flank uplift altered the topography. The strength of the constant elevation transect is that a geothermal gradient does not need to be assumed for interpretation. All He ages observed from the SW-NE transect by far predate the hypothesized initiation of continental rifting (Devonian – late Cretaceous compared to mid Cretaceous – Paleocene as determined by Balkwill et al. (1990) based on the age of the Hassel Formation) indicating that samples from the SW-NE transect had all cooled through the PRZ prior to uplift related to rifting. Increasing elevation during rifting is likely to have increased rates of river incision, changed stream drainage patterns, and caused early formation of the present day topography. Paleo-drainage networks and their affect on the topography and shallow geothermal gradient prior to rifting will be ignored for the purpose of interpretation of the horizontal transect (isotherms are at a constant depth at a given time). This assumption allows He ages to be a direct indication of exhumation and how the Baffin Island rift margin is evolving with exhumation, and not variations in geothermal gradient with dynamic topography.

The distribution of He ages along the vertical and horizontal transects indicate that rift flank uplift has occurred. Landward from the Baffin Bay coastline the youngest ages of the horizontal transect occur within the coastal lowlands and highly dissected flank of the Davis Highlands (~200 Ma), the oldest ages are within the core of the Davis Highlands and Baffin Upland surface (~300-400 Ma), and ages decrease again to comparatively moderate ages located within the Lancaster Plateau and Foxe Plain (~230-300 Ma) (Fig. 5.1). The He

age distribution and relief (incision) indicates that relative to the rest of the transect the greatest amount of exhumation occurred near the Baffin Bay margin. This is consistent with a westward tilting (the northwest rises) of the Baffin crustal block, much like that observed on rift shoulders in similar extensional environments (Australia, Persano et al., 2002; Labrador; Centeno, 2005 and others). This would have caused a rift escarpment to form along the present day Baffin Bay margin. Additional near shore marine seismic data are needed to help define the position and maximum original height of the escarpment.

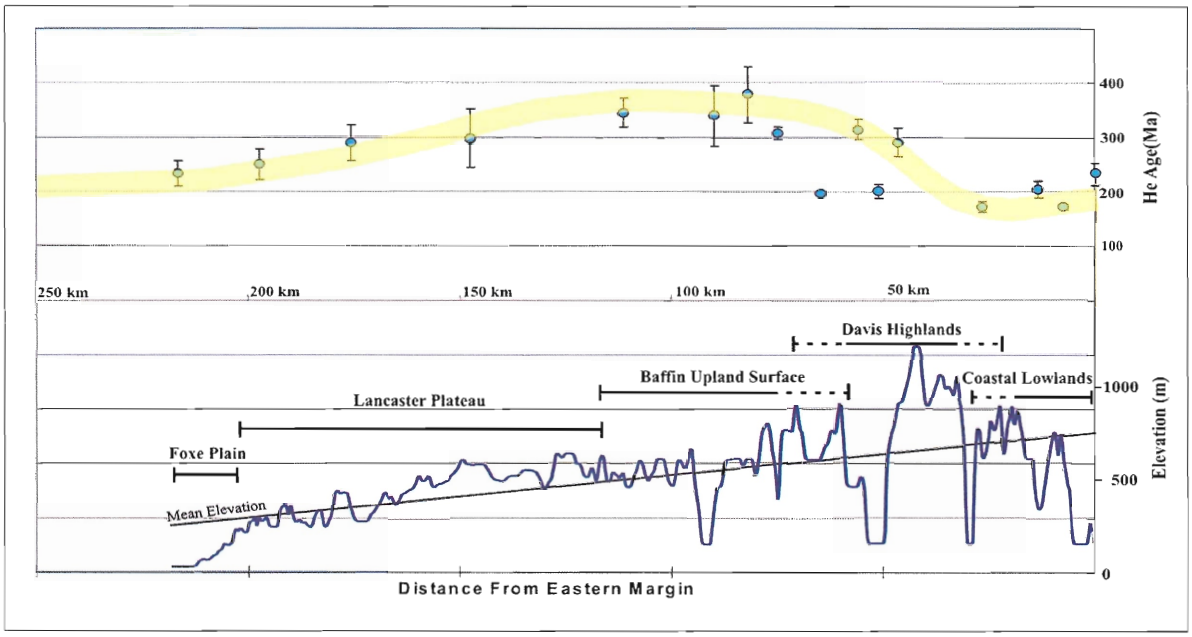

***Figure 5.1**: He ages along the SW-NE rift perpendicular horizontal transect with yellow trend line displaying that younger ages on both margins, and old He ages within the core of the island. The solid blue line below is the topographic profile of the SW-NE horizontal transect from a 250m DEM. The straight black line labeled mean elevation helps to indicate the amount of westward tilting the Baffin crustal block has undergone since initial uplift event (presumably rifting).*

Higher rates of exhumation relative to Davis Highlands are also observed in the Foxe Plains as dictated by the stream power rule (equation 2.1). The similarity of ages from the Foxe Plains to that observed in the area where the rift scarp actively is being eroded, suggests that it too underwent increased erosion rates as a result of rift flank uplift. The two regions of increased erosion are separated by the regional drainage divide located within the core of the Davis Highlands. This pattern of exhumation supports a down wearing or pinned drainage divide model as described by Gallagher et al. (1998) (Fig. 2.3), where the escarpment and distal slope are down worn, similar to that observed on the Great Escarpment in Southeast Australia, and the Ungava Peninsula of Labrador and many others (Persano et al., 2005; Centeno, 2005).

It is interesting that the first four ages from the rift margin decrease landward. This would support an 'escarpment retreat model' (Fig. 2.2) in which the most recent exhumation occurs closest to the base of the modern escarpment as the escarpment migrates landward (Gallagher et al., 1998). This would suggest that the position of the initial escarpment was at least as far as the farthest east sample. In an end-member scarp retreat model, the scarp would have retreat a minimum of 30 km. Assuming that the uplift event occurred just prior or during the deposition of the Hassel Formation in the northern Baffin Bay (~100Ma), this rift scarp would have been migrating towards its current position at a rate of $\geq$0.30 km/Ma. Compared to the Great Escarpment of southeast Australia where 5-10 km/Ma of scarp retreat is documented, this Baffin Island retreat is extremely slow. It is possible that dry climate conditions dominated in the Mesozoic and early Tertiary (Scotese, 2002), and may have contributed to slow scarp retreat rates. However, the distribution of cooling ages, incision,

and relief strongly supporting the downwearing model of rift flank uplift evolution, it is more likely that the scarp retreat was not the principle process along this margin.

The age distribution appears to refute the premise that peneplanation has caused the low relief surfaces that define the physiographic provinces of Baffin Island. Peneplanation assumes that the lowland and upland surfaces had been graded to a common base level (the Ocean), and subsequent uplift of differential magnitudes brought them to their current elevation. If this had occurred, the He ages along the iso-elevation transect would have displayed a gradual younging of He ages from the Foxe Basin to the surfaces of higher elevation where the exhumation was greatest, even in the steady state condition. Instead, the He ages increase toward the higher altitude surfaces refuting this hypothesis.

5.2 Implications of He ages from the Bruce Mountains Vertical Transect

The data from the Bruce Mountains vertical transect display a clear trend of decreasing He age with elevation (Fig. 5.2). This trend has been observed in many other thermochronologic studies conducted on vertical sampling transects (Wolf et al., 1997; Centeno, 2005, Fitzgerald et al., 2006), reflecting the vertical column of rock sequentially cooling through a closing isotherm as it is exhumed. A simple linear trend in the Bruce Mountains vertical transect is indicated (Fig. 5.2) because (i) sample FT07-03 is younger than the majority of deeper samples (this sample has been excluded), and (ii) the imprecision of the other samples preclude higher degree polynomial fits to the data. It is unlikely that thermal induced He diffusion is the cause of younger He ages at higher elevations in the vertical transect because there is no evidence of a thermal event occurring between 200 and

300 Ma and a more recent thermal event, associated with rifting or the Icelandic Plume, would likely have reset the lower elevation samples as well. These events could not have increased the temperature of higher elevation samples without having the same effect on lower samples, as emplacement of igneous material in the region did not occur and they would have had an effect limited to deep crustal depths. Also, if thermal resetting took place it is likely that a trend of decrease He age with crystal size would be observed, because crystals with smaller radius are more susceptible to He diffusion (Farley and Stockli, 2002). Rather a general trend of poor age reproducibility regardless of crystal radius can be observed, with the exception of FT07-01 and to a lesser extent FT07-07 (Fig.5.3).

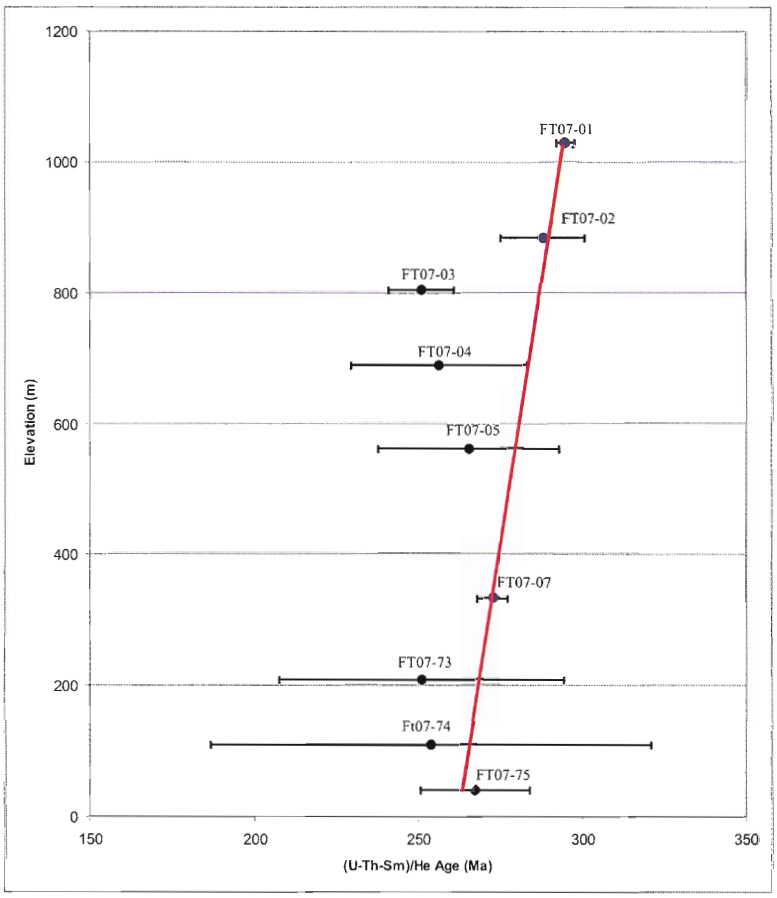

Figure 5.2: *He ages plotted against age from the Bruce Mountains vertical sampling transect. The red line between FT07-01 and FT07-75 depicts the exhumation between these two samples project through the time period of 300-263Ma. (Note: Error displayed as ±2σ)*

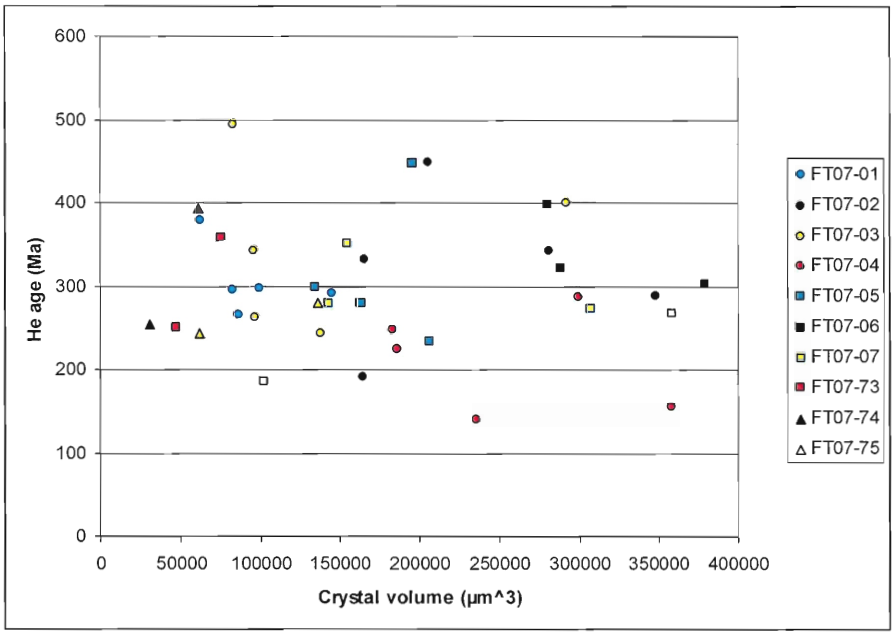

***Figure 5.3**: Distribution of apatite crystal volume (μm^3) with measured He age of the vertical sampling transect. Crystals from each sample site do not show a direct correlation between crystal volume and He age.*

Between the time that FT07-01 and FT07-07 closed to He diffusion, the rocks were cooling at a rate of 0.5-2.2 °C/Ma. Fitzgerald et al. (2006) observed that samples cooling at rates <3 °C/Ma displayed a poor He age reproducibility compared to samples that cooled more rapidly, ranging over 20Ma because closure temperature is controlled by cooling rate (which at slow rates could cause the PRZ to range from 75°C to 40° C). As the samples from the Davis Highlands cooled at a slow rate, it is possible that the extended period of time within the PRZ could be partially responsible for spurious ages of the vertical transect, and poor age reproducibility.

Assuming that the He ages of samples FT07-01 and FT07-07 are directly related to elevation and the time it cooled through ~75 °C, some rough estimates of erosion can be made. A closing temperature of ~75 °C is assigned for all samples for mathematic simplicity

(with a 25°C/km geothermal gradient, 75 °C is at a depth of 3km) and it is the generally accepted average value for closing temperature of the apatite (U-Th-Sm)/He technique (Ehlers and Farley, 2003). Though our samples had an average crystal radius of 45 μm and the closing temperature was slightly lower than this, it will not affect the calculated erosion rate for the vertical transect because the rock column would have cooled through the lower isotherm at the same rate as the 75 °C isotherm. The erosion rate for the vertical transect was calculated by dividing the vertical distance between the two samples by difference in He age between them. The average erosion rate calculated between FT07-01 to FT07-07 is 32 m/Ma (with 2σ for both averaged He ages taken into consideration, erosion rates can range from 18 m/Ma to 87 m/Ma, Table 4.4). This erosion rate fits the time of cooling for most samples relatively well with the exception of FT07-03. In calculating this erosion rate it is assumed that the geothermal gradient is constant over the entire period. Keeping the assumption of a constant 25 °C/km geothermal gradient and a He closing temperature for apatite of 75 °C, an average erosion rate to the present day can also be established. Ignoring the effects of exhumation and topography on isothermal distribution, the region underwent a maximum erosion rate of 13 m/Ma (assuming 0 °C isotherm is located at sea level), and minimum of 10 m/Ma (assuming 0 °C isotherm located at the peak of the vertical transect) (Fig. 5.4). These averaged denudation rates are in the range observed within northern Baffin Bay (Grist and Zentilli, 2004) and the Torngats of Labrador following rift flank uplift (Centeno, 2005).

Average erosion rates calculated from the Permian to present imply that the erosion during the late Paleozoic was in fact higher than normal rates for the region. If it is expected that a short period of rift flank uplift caused accelerated exhumation (approximately 25 Ma in the Torngat Mountains; Centeno, 2005), then erosion rates must have been lower than that

observed rate from the vertical transect for much of the history of the region (Fig 5.2). It is possible to use an inverse modeling approach to further examine the history of the Bruce Mountains exhumation history. Because the Torngat Mountains likely underwent a similar syn and post-rifting climate history and consist of similar lithologies as Baffin Island (Centeno et al., 2005), it is reasonable to assign cooling rates of 30 m/Ma over ~15 Ma during rifting and ~10 m/Ma following (keeping in mind that the crustal root under the Torngat Mountains may have accelerated the cooling rate and shorted the time). Assuming rifting in north-central Baffin Island was contemporaneous with the deposition of syn-rift sediments of the Hassel Formation (110 Ma), erosion rates between 273 Ma (Sample FT07-07) and 110 Ma must have declined to 4-11 m/Ma. These rates were calculated by extrapolating observed erosion rates during the Paleozoic from the vertical transect of this study, to those assumed during and after rift flank uplift adopted from the Torngat Mountains study, completing the exhumation history (Fig. 5.4).

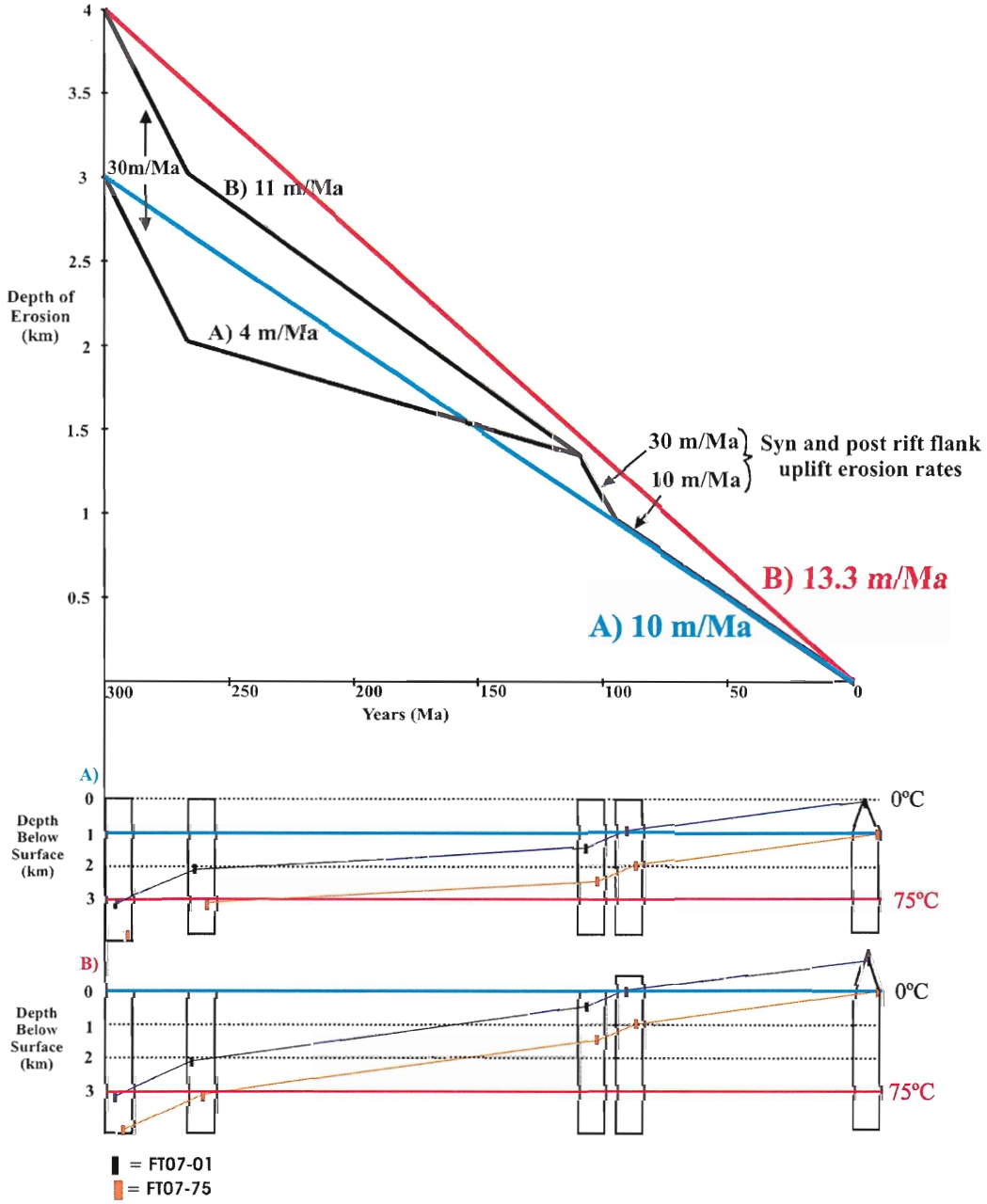

Figure 5.4: *Projected erosion rates between 273 Ma and 110 Ma constrained by Bruce Mountains vertical transect erosion rate (~30 m/Ma) during the Permian, and syn and post-rift rates observed in the Centeno (2005) study in the Torngat Mountains of Labrador estimated to occur at 110 Ma in the north-central Baffin Island region. Plots below display how the average erosion rates of 10 and 13.3m/Ma where calculated, as the paths of highest elevated sample FT07-01 and lowest elevated sample FT07-75 are exhumed assuming 25 ºC/km and that; A) the 0 ºC isotherm is located at the peak of the ridges in the area (~1000m); and B) the 0 ºC isotherm is located at sea level. Erosion rates between a) 4 and b) 11 m/Ma were calculated using these parameters for the Triassic to mid-Cretaceous period.*

The thermal signature of the late Cretaceous - Paleocene rifting has not yet been exhumed above sea level indicating that exceptionally low rates of erosion must have persisted in the region since the Permian. Considering Baffin Island has likely undergone rift flank uplift in the late Cretaceous – Paleocene as indicated by sedimentary records as well is the SW-NE transect of this study, the rate of erosion must have decreased drastically between the Triassic and this event. Low rates of erosion are feasible during this period of time considering the arid climate of the region, and its position within a relative tectonically inactive region between the Permian and Cretaceous creating minimal topography to be denuded (Scotese, 2002).

It is also possible that erosion rates following rift flank uplift occurred were much lower than the assigned rate of 10 m/Ma from the Torngat Mountains. Lacustrine sediments located in a central location on the Baffin Upland surface imply that erosion rates following the Paleocene were relatively low, considering exposed, weak sedimentary lithologies have been preserved. Further implication that Baffin Island was subjected to low erosion rates following rifting were observed by Staiger et al. (2006). They found that during the most recent glaciation, and likely the entire Quaternary glacial period, regions that were covered by ice underwent extremely low exhumation rates (0.4 m/Ma). These factors may point out that erosion rates following the Paleocene rift flank uplift were lower than the value assigned from the Centeno (2005) study, and the erosion rates estimated between the Permian and Cretaceous were slightly higher than 4 - 11 m/Ma (Fig. 5.4)

Assuming the extrapolated erosion history (Figure 5.4) approximates the actual history of the region well, it appears to closely resemble aspects of modeled cooling histories

from both the Devon Island and Kap Trautwine of NW Greenland (Refer to Fig. 5.4, Grist and Zentilli, 2004). The resemblance of Permian cooling between Kap Trautwine and north-central Baffin may suggest that the two regions were proximal prior to the formation of Baffin Bay, and that north-central Baffin Island underwent some degree of uplift related to the formation of the Sverdrup Basin. This agrees with NW directed drainage of rivers from Northern Baffin Island as described by Bird (1967) prior to the formation of Baffin Bay (Fig. 2.6). It is also likely that north-central Baffin Island underwent a very similar heating and accelerated cooling event as that modeled for Devon Island during the initiation of rifting in Baffin Bay during the late Cretaceous. However, the fact that the apatite (U-Th-Sm)/He record on Devon Island recorded the Cretaceous rifting signal indicates that more erosion occurred in this region. This likely due to the supracrustal lithologies of Devon Island (Fig. 2.7) as well as its proximity to the Sverdrup Basin, where it was likely subjected to higher magnitudes of uplift and erosion during the late Paleocene basin formation.

The magnitude of erosion must have been much higher in the southern segment of the Eastern Arctic Rim as well considering the thermal signature of accelerated uplift from the Cretaceous observed within the Torngat Mountains. This too follows Bird's (1967) interpretation of paleo-drainage, where river flow direction in southern Baffin Island and Ungava Peninsula was south and north respectively into the Hudson Straight. This left north-central Baffin Island in the approximate area of the regional drainage divide during much of the Paleozoic. If the present Davis Highlands were the location of the regional drainage divide preceding and following the formation of Baffin Bay, an abnormal low rate of erosion for the Eastern Arctic Rim are very likely to have occurred during that period as well. This

also indicates that the region had some degree of topographic elevation prior to the onset of rift flank uplift.

5.3 Limitations of the apatite (U-Th-Sm)/He technique in north-central Baffin Island

The north-central Baffin Island study area posed a few limitations on the effectiveness of the apatite (U-Th-Sm)/ He thermochronometry technique. One of which was the orthogneiss rocks sampled did not contain the quantity nor quality of optimal apatite crystals that are normally necessary for such a study. Apatite crystals tended to be small, rounded, and contain and a large number of inclusions, all of which factors well known causes of spurious (U-Th-Sm)/He measurements and ages. The number of pristine apatite crystals located within the samples limited the number of crystals from each sample that could be tested, in turn lowering the precision. Small crystal radius and inclusions are factors that strongly depend on the orthogneiss rocks that were sampled also, but grain rounding and abrasion of the outer edge of the crystals may have occurred during physical processing. The effect of crystal inclusions on He age could be minimized by using a more aggressive dissolution process during U-Th-Sm analysis with HF instead of HNO_3, but the non-homogeneity distribution of U, Th, and Sm still breaks a fundamental assumption of the F_T correction (Vermeesch et al., 2007). Zoning of crystals may have also been a factor, but the degree that zoning had an affect on the samples tested can never be known for certain. The amount and style (core concentrated or rim concentrated) of crystal zoning of the general population could be tested for by ion mass spectrometry, electron microprobe, or fission track radiography. There was also an abundance of zircon observed within many of the samples tested, from which high amount of alpha injection may have affected individual

crystals differently depending how the zircon and apatite was distributed within the rock prior to separation.

5.4 Future Work in the Region

As stated in §5.2, low temperature thermochronometric study of the north-central Baffin Island region was unable to identify the presumed period of accelerated exhumation due to rifting and rift flank uplift. Rocks that had cooled through the apatite He closing temperature when the region underwent rift flank uplift are buried at an unknown depth below the surface. These results indicate that the region has been subject to very low rates of erosion. Had the area undergone higher rates and magnitudes of exhumation then the thermal signature may have been exposed within the vertical transect. With this now known it can be acknowledged that current thermochronometers are incapable of constraining the hypothesized time frame that Baffin Island underwent rift flank uplift.

Though the cooling history during and following rift flank uplift is still buried deep below the current sea level, the cooling history prior to that observed can be studied using the same samples that were collected and processed for (U-Th-Sm)/He thermochronology. Using a different thermochronometer on the same samples with a higher closing temperature will reflect when that rock was exhumed through this higher closing temperature, which will have occurred at an older age. Thermochronometric techniques such as apatite fission-track (T_C = ~100°C), zircon (U-Th-Sm)/He (T_C = 180°C) and zircon fission track (T_C = 250°C) could all be applied to the samples already processed with apatite already separated and many samples containing an abundance of zircon (Stockli, 2005). With these chronometers

complimenting the data from this study the cooling history of the rock prior to that displayed by apatite (U-Th-Sm)/He could be attained for individual samples (Fig. 5.5). This procedure is conducted by plotting the closing temperature against measured ages from each thermochronometer, giving the cooling evolution of that sample from the highest closing temperature to the lowest. Using multiple thermochronometers can also be used to validate interpretations that were made for entire sampling transects. A second thermochronometric technique applied to samples from the vertical sampling transect for instance could be used as a second test to support the trend that increased rates of cooling were occurring during the Permian. If the two thermochronometers agree than as it too was subject to accelerated cooling but at a greater depth. If the two cooling histories disagree however it would be evident that one of the techniques was giving an erroneous cooling history (Fig. 5.6)

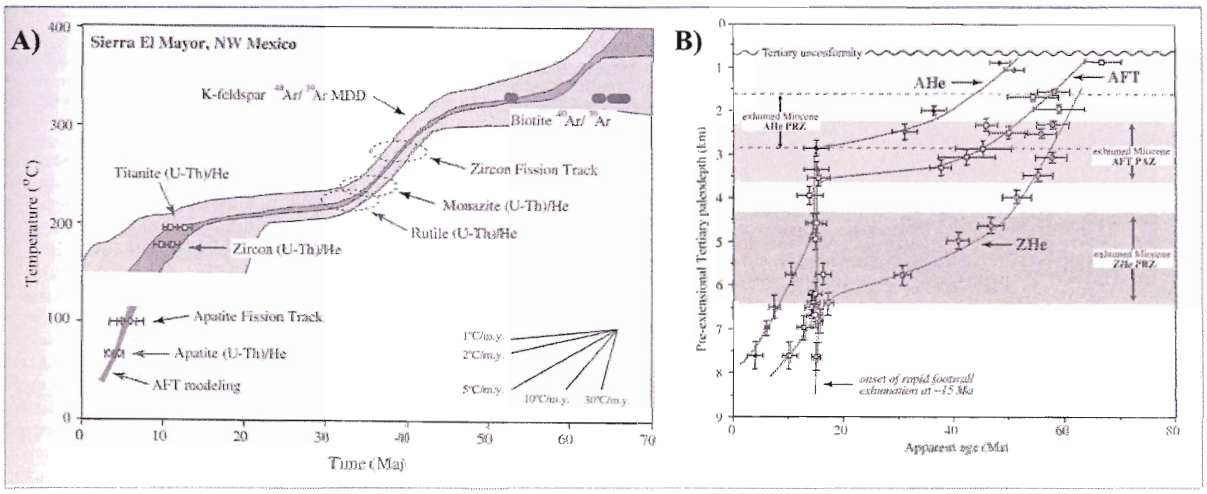

Figure 5.5*: Two examples of how multiple low temperature thermochronometers can be utilized. A) An example of how using multiple low-temperature thermochronometers on a single sample, the cooling history for that sample can be determined. This could be used to determine the cooling history of the samples from this study prior to the ages established by apatite (U-Th-Sm)/He thermochronometry. B) An example of how multiple low-temperature thermochronometers can be used on the same sampling transect to validate observations made with apatite (U-Th-Sm)/He. All thermochronometers display an accelerated cooling rate occurring at ~15 Ma, but at depths corresponding their T_C (Figure from Stockli, 2005).*

6. Conclusions

A main objective of conducting a low temperature thermochronometric study on north-central Baffin Island was to understand how the high elevation passive margin had evolved since its formation. From (U-Th-Sm)/He analysis of 16 samples collected in linear horizontal sampling transect positioned perpendicular to the rifted margin (Fig 1.2), He ages displayed a systematic variation with distance from Baffin Bay that closely resembled the pinned divide model for an uplifted rift flank (Fig. 5.1). This was expected in accordance with many other rifted margins that exhibit similar trends in exhumation (Centeno, 2005; Persano et al., 2002; Brown et al., 2000). A unique feature to this rifted margin is that the rift flank also appears to show some indication that rift scarp retreat is also pushing the escarpment inland as well. Though Gallagher et al.'s (1998) models are only end models, there are very few if any documented occurrences of rift flanks that exhibit both rift scarp retreat and pinned divide denudation trends.

The second main objective for this study was to constrain a period of accelerated cooling that could be related to rifting of Greenland from the North American Craton. In order to accomplish this objective (U-Th-Sm)/He thermochronology of 10 samples from a vertical sampling transect located within the Bruce Mountains was carried out. Results from the vertical transect were found to reflect what was interpreted as an accelerated cooling event during the late Paleozoic. Late Cretaceous ages that were expected to reflect accelerated cooling during continental extension, basin formation, and rift flank uplift were not observed. This is likely because exhumation in the region has not been sufficient enough since rifting, to exhume rocks that were crossing the ~75°C isotherm as rifting was occurring. Low erosion rates could be the result of a number of things, but the resistive Precambrian

lithologies that Baffin Island is composed of, and a low erosive environment for much of the Islands history are likely the main forces.

Further thermochronometry in an attempt to fulfill this second objective are not recommended because rocks that will display a cooling age that reflects rift flank uplift will be buried for many more millions of years. Instead it is suggest that additional thermochronometers such as apatite and zircon fission track and zircon (U-Th-Sm)/He, can be used to analyze already processed samples in order to constrain the cooling history of the Baffin surface prior to the (U-Th-Sm)/He ages that were observed in this study. Using multiple thermochronometers could also be used validated the interpretation that the vertical transect was undergoing a period of accelerated cooling during the late Paleozoic.

References

Andrews, J.T., Guennel, G.K., Wray, J.L., and Ives, J.D. 1971. An Early Tertiary Outcrop in North-Central Baffin Island Northwest Territories, Canada: Environment and Significance. Canadian Journal of Earth Sciences, 9:233-238.

Balkwill, H.R., McMillan, N.J., Maclean, B., Williams, G.L., and Srivastave, S.P. 1990. Geology of the Labrador Shelf, Baffin Bay, and Davis Striat, Chapter 7 In: Geology of the Continental Margin of Eastern Canada, M.J. Keen and G.L. Williams (ed); Geological Survey of Canada, Geology of Canada, no. 2, p. 293-348.

Bethune, K.M., Scammel, R.J. 2003. Geology, geochronology, and geochemistry of Archean rocks in the Eqe Bay area, north-central Baffin Island, Canada: constraints on the depositional and tectonic history of the Mary River Group of northeastern Rae Province. Canadian Journal of Earth Sciences, 40: 1137-1167.

Bird, J.P. The Physiography of Arctic Canada. The John Hopkins Press, Baltimore, Maryland, 1967.

Brown, R.W., Gallagher, K., Gleadow, A.J.W., and Summerfield, M.A. 2000. Morphotectonic evolution on the South-Atlantic margins of Africa and South America. In: Geomorphology and Global Tectonics (Ed by M.A. Summerfield), pp 255-281. John Wiley and Sons, New York.

Centeno, JP. 2005. Exhumation of the Torngat Mountain, northern Labrador, Canada. MSc. Thesis, University of Kansas, Lawrence, Kansas.

Chalmers, J.A., T.C.R. Pulvertaft. Development of the Labrador Sea: a review. From: Wilson, R.C.L., Whitmarsh, R.B., Taylor, B., and Froitzheim, N. 2001. *Non Volcanic Rifting of Continental Margins: a Comparison of Evidence from land and Sea.* Geologic Society, London, Special Publication, 187, 77-105.

Dawes, P.R., Christie, R.I. 1991. Geomorphic regions, Chapter 3 In: Geology of the Innuitian Orogen and Arctic Platform of Canada and Greenland, H.P. Trettin (ed); Geologic Survey of Canada, Geology of Canada, no. 3. p.29-56.

Dunai, T.J. 2005. Forward Modeling and Interpretation of (U-Th)/He Ages. In. Low Temperature Thermochronology: Techniques, Interpretations, and Applications. P.W. Reiners and T.A. Ehlers (eds.). Reviews in Mineralogy and Geochemistry, 58: 259-274.

Eyles, N., 1996. Passive Margin Uplift along the North Atlantic region and its role in Northern Hemisphere late Cenozoic Glaciation. Geology 24 103-106.

Ehlers, T.A. Farley, K.A., 2003. Apatite (U-Th)/He thermochronometry: methods and applications to problems in tectonic and surface processes. Earth and Planetary Science Letters 206 1-14.

Evans, N.J., Byrne, J.P., Keegan, J.T., and Dotter, L.E. 2005. Determination of Uranium and Thorium in Zircon, Apatite, and Fluorite: Application to Laser (U-Th)/He Thermochronology. Journal of Analytical Chemistry, 12:1159-1165.

Farley, K.A. 2002. (U-Th)/He Dating: Techniques, Calibrations, and Applications. In: Porcelli, D., Ballentine, C.J., and Wieler, R. (eds.) Noble gases in geochemistry and cosmochemistry. Reviews in Mineralogy and Geochemistry, 47: 819-843.

Farley K.A., Stockli, D.F. 2002. (U-Th)/He Dating of Phosphates: Apatite, Monatite, and Xenotime. In: Phosphates: Geochemical, Geobiological, and Materials Importance. M.J. Kohn, J. Rakovan, and J.M. Hughes (eds.). Reviews in Mineralogy and Geochemistry, 48: 559-578.

Farley, K.A., Wolf, RW., and Silver, LT. 1996. The effects of long alpha –stopping distances on (U-Th)/He ages. Geochimica et Cosmochimica Acta 60: 4223-4229.

Fitzgerald, P.G., Baldwin, S.L., Webb, L.E., and O'Sullivan, P.B. 2006. Interpretations of (U-Th)/He single grain ages from slowly cooled crustal terranes: A case study from the Transantarctic Mountains of southern Victoria Land. Chemical Geology, 225: 91-120.

Funck T., Lounden, K.E. 1999. Wide-angle seismic transect across the Torngat Orogen, northern Labrador: Evidence for a Proterozoic crustal root. Journal of Geophysical Research, 104:7463-7480.

Gallagher, K., R. Brown. Denudation and Uplift at Passive margins: the record on the Atlantic Margin of Southern Africa, Phil. Trans. R. Soc. Lond. A, 357, 835-859, 1999.

Gallagher, K., Brown, R., and Johnson, C. 1998. Fission-track analysis and its applications to geological problems. Annual Review of Earth and Planetary Sciences, 26: 519-572.

Grist, A.M., Zentilli, M. 2004, Aspects of the thermal history of the eastern margin of Canada based on apatite fission track and (U-Th)/He thermochronology. Dalhousie Ph.D Thesis. Copyright by Alexander M.Grist.

Grist, A.M., Zentilli, M. 2005. The thermal history of the Nares Strait, Kane Basin, and Smith Sound region in Canada and Greenland: constraints from apatite fission-track and (U-Th-Sm)/He dating. Canadian Journal of Earth Science, 42:1547-1569.

Hanson, K., Reiners, P.W. 2006. Low Temperature thermochronology of the southern East Greenland continental margin: Evidence from apatite (U-Th)/He and fission track analysis and implications for intermethod calibration. Lithos, 92: 117-136.

Japsen, P., Bonow, J.M., Green, P.F., Chalmers, J.A., Lidmar-Bergstrom, K. 2006. Elevated, passive continental margins: Long-term highs or Neogene uplifts? New evidence from West Greenland, Earth and Planetary Science Letters, 248:330-339.

Jackson, G.D. Berman, R.G. 2000. Precambrian metamorphic and tectonic evolution of Northern Baffin Island, Nunavut, Canada. The Canadian Mineralogist 38: 399-401.

Johns, S.M., Young, M.D. 2006. Bedrock geology and economic potential of the Archean Mary River group, norther Baffin Island, Nunavut. Geologic Survey of Canada, Current Research, 2006-C5.

Kooi, H., C. Beaumont. Escarpment on high-elevation rifted margins: Insights derived from a surface processes model that combines diffusion, advection, and reaction, Journal of Geophysical Research, 99, 129-209, 1994.

Mancktelow, N.S., Grasemann, B. 1997. Time-dependant effects of heat advection and topography on cooling histories during erosion. Tectonophysics, 270: 167-195.

Persano, C., Finley, M.S., Bishop, and P., Barford. 2002. Apatite (U-Th)/He age constraint on the development of the Great Escarpment on the southeastern Australian passive margin. Earth and Planetary Science Letters, 200:79-90.

Saalmann, K., Tessensohn, F., Piepjohn, K., von Gosen, and W., Mayr, U. 2005. Structure of Paleogene sediments in east Ellesmere Island: Constraints on Eurekan tectonic evolution and implications for the Nares Strait problem. Tectonophysics, 406:81-113.

Scotese, C.R. 2002. Paleoamap Project, wensite:www.scotese.com.

Skaarup, N., Jackson, H.R., and Oakey, G. 2006. Margin Segmentation of Baffin Bay/ Davis Strait, eastern Canada based on seismic reflection and potential field data. Marine and Petroleum Geology, 23:127-144

Spotila, J.A., Bank, G.C., Reiners, P.W., Naeser, C.W., Naeser, N.D., and Henika, B.S. 2004. Origin of the Blue Ridge escarpment along the passive margin of Eastern North America. Basin Research, 16:41-63.

Srivastava, S.P., Arthur, M.A. Tectonic Evolution of the Labrador Sea and Baffin Bay: Constraint imposed by regional geophysical and drilling results from leg 105. From: Srivastava, S.P., Arthur, M., Clement, B. et al. 1989. Proceedings of the Ocean Drilling Program, Scientific Results, Vol. 105.

Staiger. J.W., Gosse, J. Little, E.C., Utting, D.J., Finkel, R., Johnson, J.V., and Fastook, J. 2006. Glacial erosion and sediment dispersion from detrital cosmogenic nuclide analysis of till. Quaternary Geology 1:29-42.

Stock, J.D., Montgomery, D.R. 1999. Geologic constraints on bedrock river incision using the stream power law. Journal of Geophysical Research, 104: 4983-4993.

Stockli, D.F. 2005. Application of Low-Temperature Thermochronometry to Extensional Tectonic Settings. In. Low Temperature Thermochronology: Techniques, Interpretations, and Applications. P.W. Reiners and T.A. Ehlers (eds.). Reviews in Mineralogy and Geochemistry, 58: 411-448.

Vermeesch, P., Seward, D., Latkoczy, C., Wipf, M., Gunther, and D., Baur, H. 2007. Alpha-Emitting mineral inclusions in apatite, their effect on (U-Th)/He ages, and how to reduce it. Geochimica et Cosmochimica Acta, 71:1737-1746.

Wolf, R.A., Farley, K.A., and Silver, L.T. 1997. Assessment of (U-Th)/He thermochronometry; the low-temperature history of the San Jacinto Mountains, California. Geology, 25: 65-68.

Young, M.D., Sandeman, H., Berniolles, F., and Gertzbein, P.M. A preliminary stratigraphic and structural geology framework for the Archean Mary River Group, northern Baffin Island Nunavut. Geological Survey of Canada, Current Research, 2004, C-1.

Appendix A: Equations Used in Study

1. River incision determined by stream powere rule:

$$\varepsilon = KA^m S^n \qquad (2.1)$$

where S is slope, A is drainage area, K is a constant, and n and m are positive exponents which along with K reflect rock resistance and other environmental attributes of individual rivers (e.g. Stock and Montgomery, 1999).

2. Equation used to determine the He age from amount of He, U, Th, and Sm nuclei:

$$^4He = 8\ ^{238}U\ (e^{\wedge}(\lambda_{238}t) - 1) + 7\ (^{235}U/137.88)\ (e^{\wedge}(\lambda_{235}t) - 1) + 6\ ^{232}Th\ (e^{\wedge}(\lambda_{232}t) - 1) + {}^{147}Sm\ (e^{\wedge}(\lambda_{147}t) - 1)) \qquad (3.1);$$

where $\boldsymbol{\lambda}$ is the decay constant for the parent atoms ($\boldsymbol{\lambda_{238}} = 1.551 \times 10^{-10}\ y^{-1}$, $\boldsymbol{\lambda_{235}} = 9.849 \times 10^{-10}\ y^{-1}$, $\boldsymbol{\lambda_{232}} = 4.948 \times 10^{-11}\ y^{-1}$, $\lambda_{147} = 6.539 \times 10^{-12}$) and **t** is the amount of time He has been accumulating in the mineral (years) (Farley, 2002).

3. Ft Correction equations:

$$ß = (2.31L+2R)/(RL) \qquad (3.2);$$

Where ß is the surface area to volume ratio, R is half the distance between opposite apices of the hexagonal crystal face, and L is the length of the hexagonal prism:

$$^{238}U \text{ series: } {}^{U}F_T = 1 - 5.13ß^2 + 6.78ß \qquad (3.3);$$

$$^{232}Th \text{ series: } {}^{Th}F_T = 1 - 5.90ß^2 + 8.99ß \qquad (3.4);$$

$$\text{Mean } F_T = {}^{238}a\ {}^{U}F_T + (1 - {}^{238}a)\ {}^{Th}F_T \quad (3.5);$$

4. Determination of U-TH-Sm nuclei from ratios for He age determination (Evans et al., 2005);

Determining # of ^{238}U Atoms from $^{235}U/\ ^{238}U$ (Isotopic Ratio):

RU_{sa} = Isotopic ratio of the spiked sample (measured);

RU_{sp} = Isotopic ratio of calibrated spike (calibrated);

RU_{min} = Isotopic ratio of the mineral in nature (0.0072);

$RU_{standard}$ = Isotopic ratio of standard solution (calibrated);

RU_{sst} = Isotopic ratio of spiked standard solution (measured);

U_{ust} = Total # of ^{238}U atoms in the unspiked standard solution;

U_{sp} = Total # of ^{238}U atoms in spike;

Uc_{st} = Concentration of ^{238}U in the calibrated standard solution, ng/mL;

UV_{st} = Volume of ^{238}U of standard solution added, μL;

$^{238}U_{atoms}$ = # of ^{238}U in the sample;

$$^{238}U_{atoms} = {}^{238}U_{sp} * (RU_{sa} - RU_{sp})/(RU_{min} - RU_{sa})$$

$^{238}U_{sp}$ = # of ^{238}U in the spike;

$$^{238}U_{sp} = {}^{238}U_{ust} * (RU_{st} - RU_{sst})/(RU_{sst} - RU_{sp})$$

$^{238}U_{ust}$ = # of moles in the unspiked standard

$$^{238}U_{ust} = (Uc_{st}/238 * UV_{st}\ (10^3))*((1/RU_{st})/((1/RU_{st}) + 1))$$

Determining # of Th and Sm atoms from isotopic ratio:

RX_{sa} = Isotopic ratio of the spiked sample (measured);

RX_{sp} = Isotopic ratio of calibrated spike (calibrated);

RX_{sst} = Isotopic ratio of spiked standard solution (measured);

X_{ust} = Total # of X atoms in the unspiked standard solution;

X_{sp} = Total # of X atoms in spike;

Xc_{st} = Concentration of x in the calibrated standard solution, ng/mL;

XV_{st} = Volume of X of standard solution added, μL;

x = molecular weight of X (Th = 232, Sm = 149)

X_{atoms} = # of X in the sample;

$X_{atoms} = Abs(X * (RX_{sp} - RX_{sa})/(RU_{sa})$

X_{sp} = # of X in the spike;

$X_{sp} = X_{ust} * (RX_{sst})/(RX_{sp} - RX_{sst})$

X_{ust} = # of moles in the unspiked standard

$X_{ust} = (Xc_{st}/x * XV_{st} (10^3))$

5. Adding up uncertainties in quatrature

$$\sigma = (U^2 + Th^2 + Sm^2 + He^2 + F_T^2)^{1/2} \qquad 3.6;$$

6. Weighted Average

X= weighted mean

A= corrected He age

U=uncertainty

$X=(A_1*1/U_1 + A_2*1/U_2 + A_3*1/U_3 \ldots\ldots..)/ (1/U_1 + 1/U_2 + 1/U_3 .....)$

σ = weighted standard deviation

$\sigma = (1/U_1 (A_1 - X)^2 + 1/U_2 (A_2 - X)^2 + 1/U_3 (A_3 - X)^2 ...)/(1/U_1 + 1/U_2 + 1/U_3 ...)$

Appendix B: Images of Apatite Crystals analyzed for (U-Th-Sm)/He

Images of each crystal tested for the north-central Baffin Island Study. Images were taken with the Zeiss Axioplan binocular microscope at magnification varying 200-400x in order to observe crystal habit. (Sample number followed by crystal radius (μm) is displayed on image)

Horizontal Transect (From NE-SW)

FT07-29

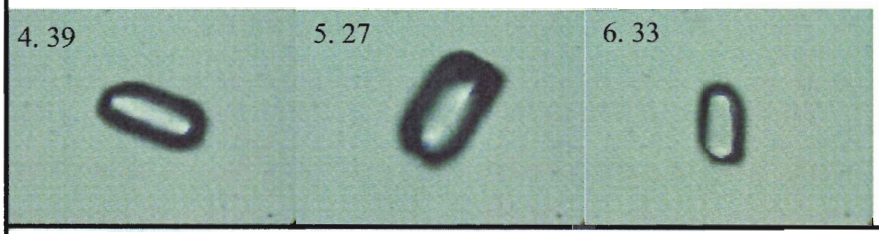

FT07-21

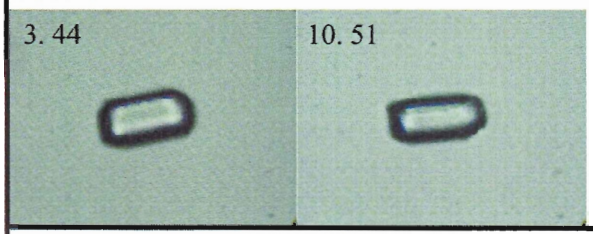

FT07-22

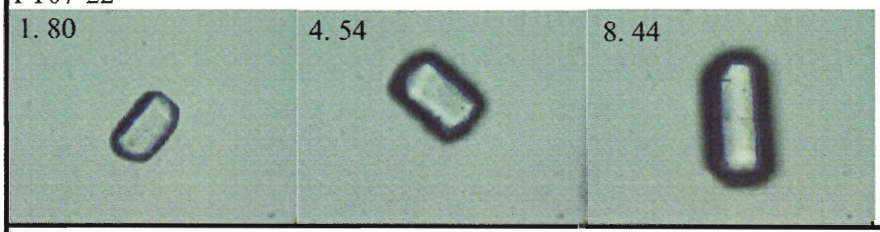

FT07-30

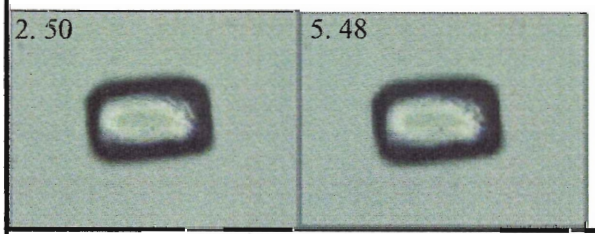

FT07-25

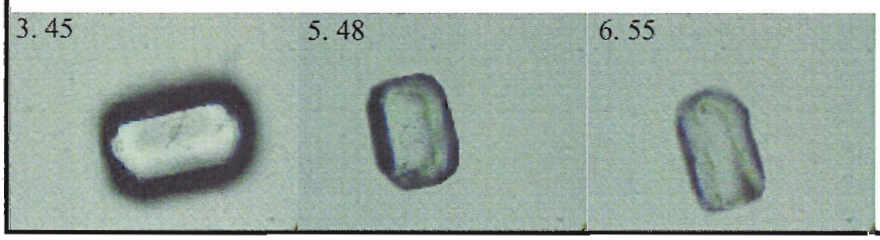

FT07-26

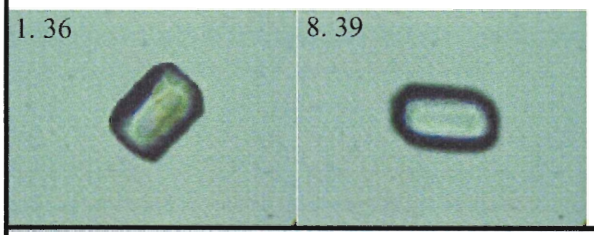

FT07-27

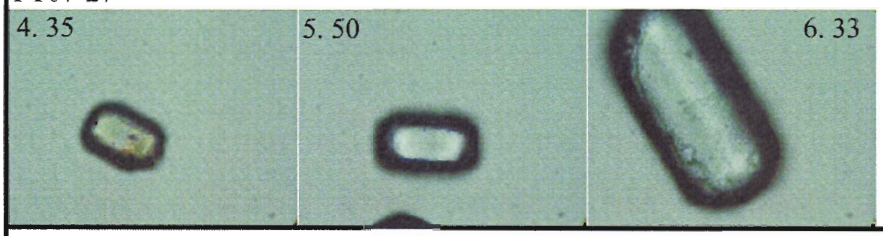

FT07-28

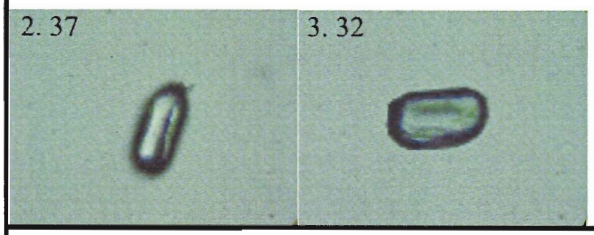

FT07-31

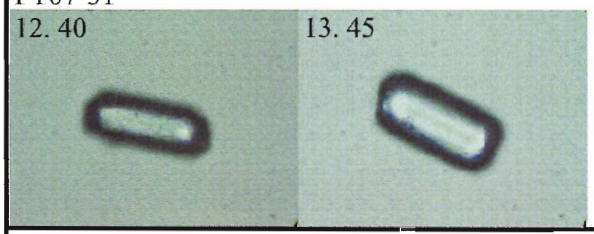

FT07-32

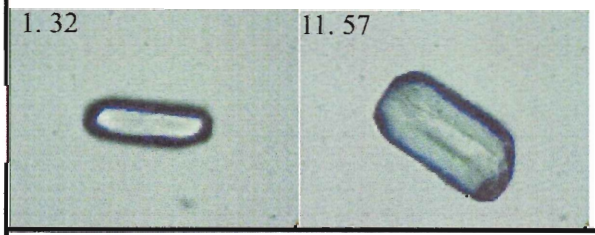

Ft07- 33

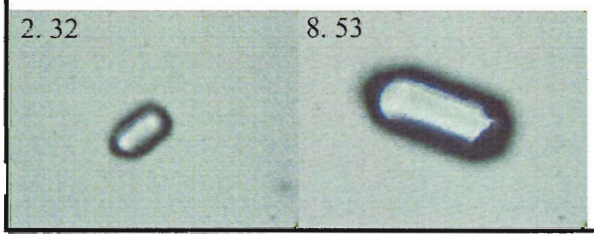

FT07-34

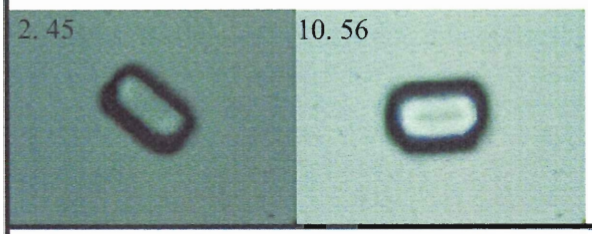

FT07-35

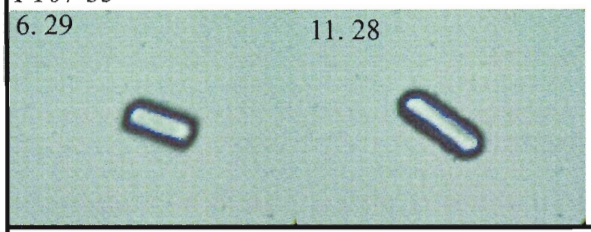

FT07-36

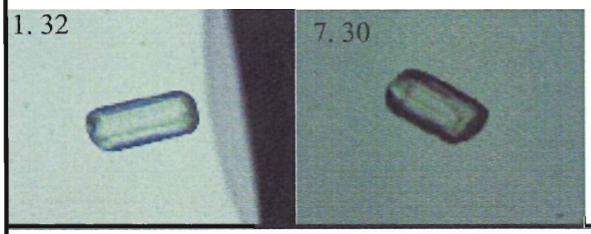

FT07-37

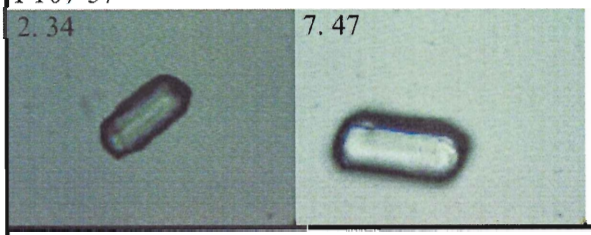

FT07-39

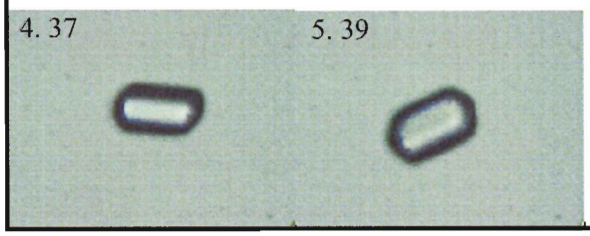

Continued on next page with Vertical Transect

Vertical Transect (From Highest elevation to lowest)

FT07-01

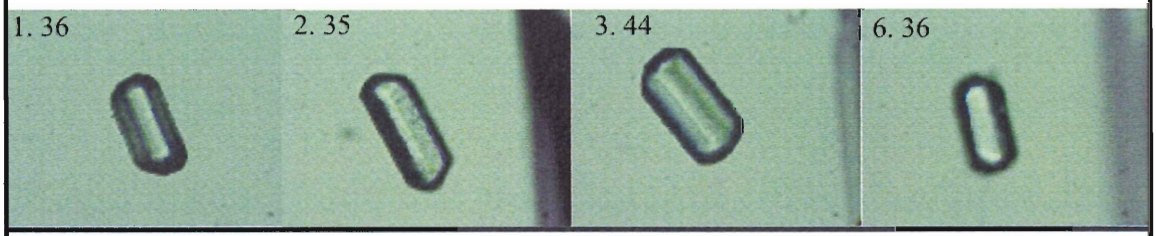

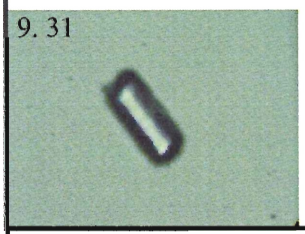

FT07-02

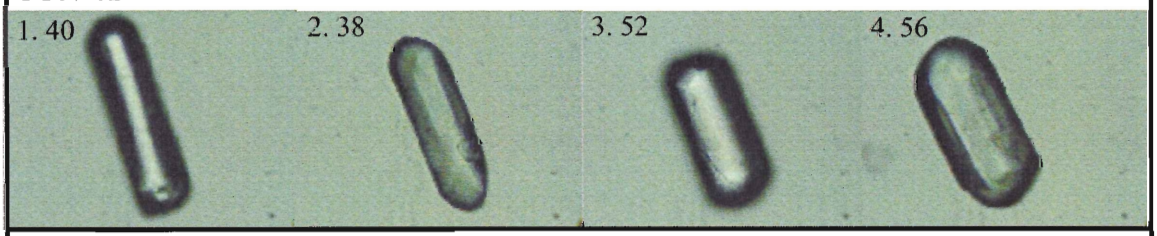

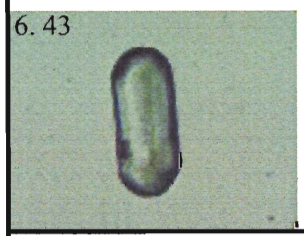

FT07-03

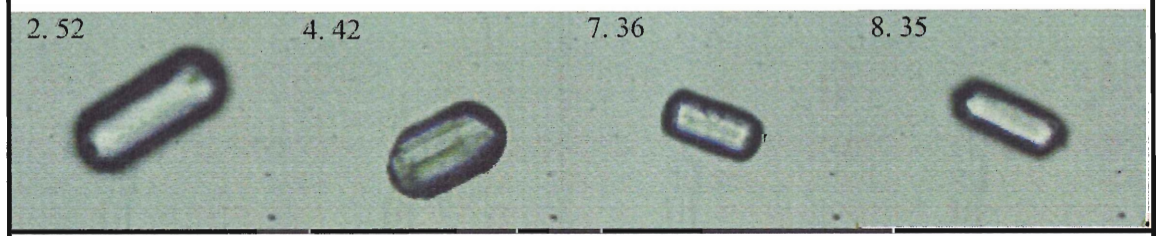

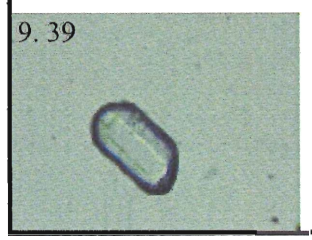

FT07-04

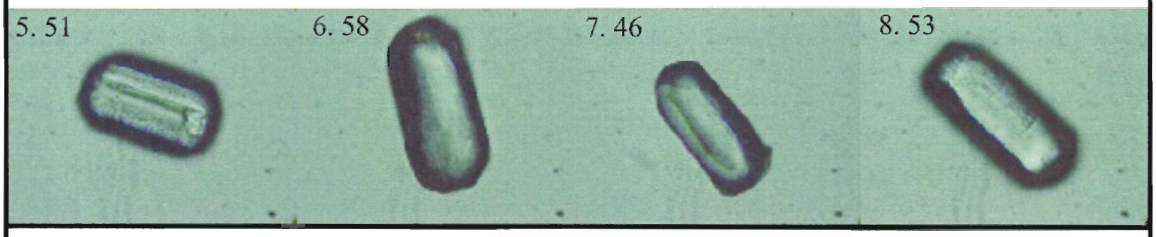

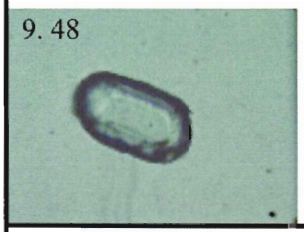

FT07-05

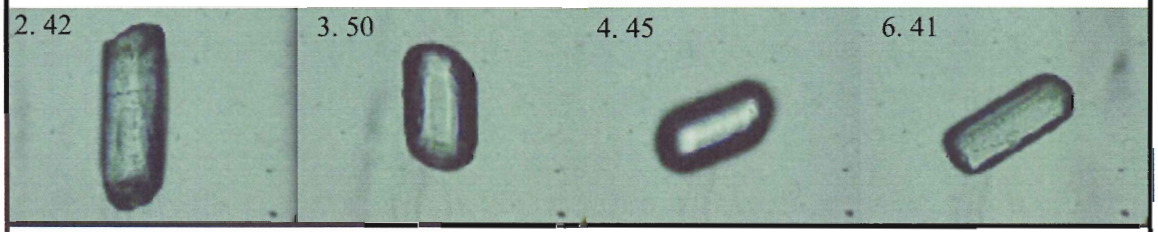

FT07-06

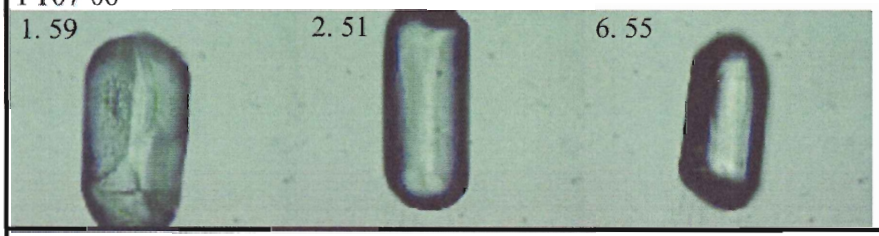

FT07-07

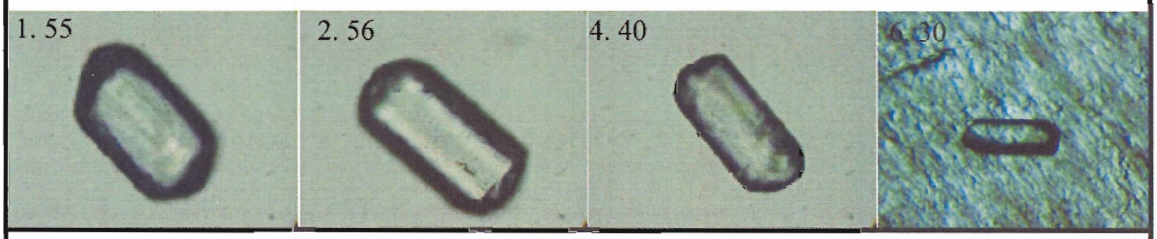

FT07-73

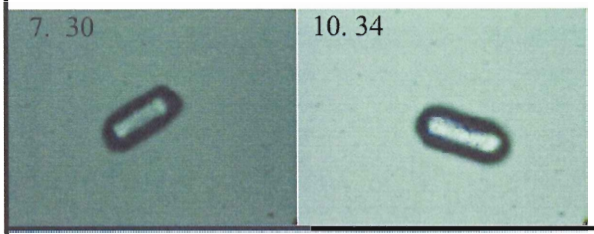

FT07-74

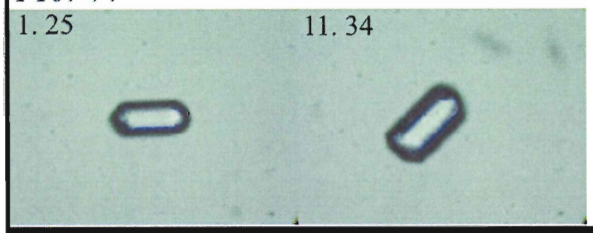

FT07-75